NON-LINE-OF-SIGHT IDENTIFICATION AND MITIGATION FOR INDOOR LOCALIZATION USING ULTRA-WIDEBAND SENSOR NETWORKS

by

Bruno Jorge de Carvalho e Silva

Submitted in partial fulfillment of the requirements for the degree
Philosophiae Doctor (Computer Engineering)

in the

Department of Electrical, Electronic and Computer Engineering
Faculty of Engineering, Built Environment and Information Technology

UNIVERSITY OF PRETORIA

November 2020

SUMMARY

NON-LINE-OF-SIGHT IDENTIFICATION AND MITIGATION FOR INDOOR LOCALIZATION USING ULTRA-WIDEBAND SENSOR NETWORKS

by

Bruno Jorge de Carvalho e Silva

Supervisor:	Dr. G.P. Hancke
Co-Supervisor:	Prof. G.P. Hancke
Department:	Electrical, Electronic and Computer Engineering
University:	University of Pretoria
Degree:	Philosophiae Doctor (Computer Engineering)
Keywords:	Localization, non-line-of-sight, ranging, ultra-wideband, wireless sensor networks

With the advent of Industry 4.0, indoor localization is central to many applications across multiple domains. Although impulse-radio ultra-wideband (IR-UWB) enables high precision time-of-arrival (TOA) based ranging and localization for wireless sensor networks, there are several challenges, including multi-user interference and non-line-of-sight (NLOS) conditions. NLOS conditions occur when the communication path between receiver and transmitter is obstructed, and these conditions are frequent indoors due to walls and other obstructions. To maintain location accuracy and precision similar to line-of-sight (LOS) conditions, identification and mitigation of these NLOS conditions is crucial. For identification and mitigation methods to be implemented in sensor networks, they must be of low complexity to minimize their influence on localization requirements.

This thesis investigates NLOS identification and mitigation for IEEE 802.15.4a IR-UWB sensor networks. The objective of this thesis is to improve location accuracy in NLOS conditions for IR-UWB sensor networks. A comprehensive review of the state-of-the-art in NLOS identification and mitigation is conducted, and limitations of these methods with regards to the use of multiple channels, dependence on training data, mobility and complexity (particularly for applications with time constraints) are

highlighted. This thesis proposes identification and mitigation methods that address the limitations found in state-of-the-art methods.

A distance residual-based method for NLOS identification is proposed. Compared to conventional NLOS identification which relies on knowledge of LOS and NLOS channel statistics, or analysis of the standard deviation of range measurements over time, this identification method does not rely on these parameters.

A NLOS classification method that distinguishes between through-the-wall and around-the-corner conditions using channel statistics extracted from channel impulse responses is proposed. Unlike most methods in literature that focus on distinguishing between LOS and NLOS, this method classifies NLOS conditions into through-the-wall and around-the-corner, therefore providing more context to the location estimate, and consequently enabling mitigation methods to be used for specific types of NLOS conditions.

A through-the-wall ranging error mitigation method that relies on floor plans is proposed. A novel model for through-the-wall TOA ranging is proposed and experimentally evaluated. The conventional through-the-wall TOA ranging model in literature requires many parameters which cannot be calculated in realistic scenarios. Compared to through-the-wall TOA ranging models found in literature, the proposed model relies on information from floor plans to reduce the number of unknown parameters in the model. The results show that NLOS errors caused by through-the-wall propagation are significantly mitigated with the proposed method, resulting in location accuracy which approaches the LOS case.

A NLOS mitigation method which corrects location estimates affected by random ranging errors is proposed. This method relies on geometric constraints based on the fact that biases introduced by NLOS conditions in TOA range measurements are positive. The method is evaluated for cases where NLOS ranges are identifiable and cases where they are not identifiable. For the latter case, the results show that the proposed method significantly outperforms state-of-the-art optimization-based mitigation methods in terms of execution time, while retaining similar performance in terms of location accuracy.

ACKNOWLEDGEMENTS

It has been a long journey that would have not been possible without support. I would like to thank:

- Dr. Hancke and Prof. Hancke for giving me the opportunity to complete my doctorate under their supervision. Your guidance and support have been invaluable.
- The Centre for Connected Intelligence for sponsoring my studies.
- Mari Ferreira and the staff in the department for their assistance and patience with my many requests.
- My friends and colleagues in the Advanced Sensor Networks group for all the tips and insightful discussions about research.
- My parents for all their sacrifice to provide a good education, and my siblings for their patience and support, particularly over these last few years.

LIST OF ABBREVIATIONS

ATC	Around-the-corner
CDF	Cumulative distribution function
CIR	Channel impulse response
COOP	Cooperative
COTS	Commercial off-the-shelf
CSI	Channel state information
DDP	Detected direct path
DP	Direct path
EM	Electromagnetic
GDOP	Geometric dilution of precision
GPS	Global Positioning System
IOT	Internet-of-Things
IR-UWB	Impulse-radio ultra-wideband
LBS	Location-based services
LLS	Linear least squares
LLSE	Linear least squares estimation
LM	Levenberg–Marquardt
LOS	Line-of-sight
LP	Linear programming
LQI	Link quality indicator
LR	Logistic regression
LRT	Likelihood ratio test
LSE	Least squares estimation
MCU	Microcontroller
ML	Maximum likelihood
MLE	Mean location error
MPC	Multipath component
MSE	Mean-squared error
NBC	Naïve Bayes classifier
NLOS	Non-line-of-sight
NLLS	Non-linear least squares

PDP	Power delay profile
PHY	Physical layer
PR	Precision
PRF	Pulse repetition frequency
QP	Quadratic programming
RBF	Radial basis function
RC	Recall
RF	Radio-frequency
RFE	Recursive feature elimination
RMS	Root mean square
RMSE	Root mean square error
RSSI	Received signal strength indicator
RWGH	Residual weighting
RX	Receiver
SDP	Semidefinite programming
SDS-TWR	Symmetric double-sided two-way ranging
SFD	Start frame delimiter
SOCP	Second-order cone programming
SPI	Serial peripheral interface
SSDR	Sum of the squares of distance residuals
SVM	Support vector machine
TOA	Time-of-arrival
TOF	Time-of-flight
TTW	Through-the-wall
TWR	Two-way ranging
TX	Transmitter
UDP	Undetected direct path
UWB	Ultra-wideband
V2V	Vehicle-to-vehicle
WPAN	Wireless personal area network
WSN	Wireless sensor networks

TABLE OF CONTENTS

CHAPTER 1 INTRODUCTION

1.1 PROBLEM STATEMENT

1.1.1 Context of the problem

The global positioning system (GPS) was originally conceived for navigation purposes by the United States Department of Defense in 1978, and made available to public use in the 1980s. Similar systems include Russia's Global Navigation System (GLONASS) and China's Beidou, which launched in 2011 [1]. With advances in technology, receivers for these systems have been integrated into smartphones and similar devices. There are many applications in wireless sensor networks that require localization across various application domains, including smart cities and industry [2],[3]. Projections indicate that the indoor location market will grow to 17 billion USD by 2025 [4].

GPS receivers, however, are too expensive to be deployed in sensor networks [5], and have limited capability indoors due to poor reception caused by signal attenuation. Unlike GPS, where signals transmitted from satellites to receivers outdoors reach receivers mostly through line-of-sight paths, radio propagation indoors often occurs through non-line-of-sight paths due to the presence of walls and other obstructions.

Many low cost and low power localization alternatives exist for sensor networks, including the use of received signal strength (RSSI), time-of-arrival (TOA) or angle of arrival (AOA) [6]. Since wireless localization systems estimate distances using properties of signals such as amplitude or phase, these are also affected by NLOS conditions, which in turn affect the accuracy and precision of distance estimates, particularly in the case of RSSI, which is prone to interference and multipath. This is typical

of many sensor networks and is not suitable for many use cases where very precise localization is required.

The need for precise localization in sensor networks motivated an amendment to the IEEE 802.15.4 standard to include an IR-UWB physical (PHY) layer [7] to measure distances using TOA for high precision localization in Wireless Personal Area Networks (WPANs). UWB uses very narrow pulses (<1 ns) for communication, which makes it possible to resolve and timestamp the first path of arrival precisely.

With UWB, very precise distances can be measured between devices at low power, making it ideal for wireless sensor networks, especially with the recent availability of IR-UWB IEEE 802.15.4a devices, which can timestamp signals with picosecond resolution [8]. This high precision, however, is often achieved only in line-of-sight (LOS) conditions, where an unobstructed direct path (DP) between transmitter and receiver exists. In NLOS conditions, the receiver often fails to detect the first path or detects a delayed first path. In both cases, a positive bias is introduced into the ranging measurement, which translates to a location error for which the magnitude is dependent on the severity of the NLOS condition. To maintain the high location accuracy and precision required in many applications, it is necessary to identify these NLOS conditions and mitigate the adverse impact these conditions have on localization. NLOS identification is done to determine whether a channel is LOS or NLOS and NLOS mitigation is done to correct, or mitigate, the impact of the NLOS condition on location accuracy.

To address this problem, several approaches for NLOS identification and mitigation have been proposed in literature [9], [10]. For identification, state-of-the-art methods rely on channel statistics. For mitigation, state-of-the-art methods are typically based on optimization [11]. Although the NLOS problem is well understood and many methods have been proposed, the focus is usually to minimize the location error at the cost of increased complexity. Increasingly more complex algorithms are used for both identification and mitigation. For UWB sensor networks, however, many mitigation approaches are not ideal because they are either too complex for resource-constrained devices, or assume that the NLOS error distribution is known. Furthermore, proposed methods often do not leverage all properties of UWB sensor networks.

1.1.2 Research gap

Most NLOS identification and mitigation techniques in literature aim to improve location accuracy at the cost of complexity. To be suitable to UWB sensor networks, these methods should have low complexity and support both static and mobile sensor networks. An analysis of how suitable NLOS identification and mitigation algorithms are to sensor networks should take the following aspects into consideration:

Complexity: whereas locations in LOS conditions can be determined using trilateration (which is typical done using fast algorithms), NLOS identification and mitigation incurs additional processing delays. Firstly, to have minimal impact on the location update rate, these methods should be of low complexity to execute close to real-time. State-of-the-art mitigation methods are based on convex optimization which requires specialized solvers [11], [12]. Secondly, if on-device identification and mitigation is required, algorithms should be able to execute on resource-constrained devices with minimal processing delay to avoid a significant impact on the location update rate. Recently, with identification and mitigation using deep learning, the tendency is to evaluate increasing complex identification and mitigation techniques that require more training data and produce very good results using raw channel impulse response (CIR) samples without feature extraction [13]. For resource-constrained devices in sensor networks which do not have the capability to process this data on the device, this poses a problem since the device has to transmit the data to a location engine for post-processing using frames with small payloads. Therefore, collecting channel statistics on the devices and transmitting them over the network to a base station for processing is not ideal, particularly in very large sensor networks. Recent trends like edge computing encourage computation to be done on the devices themselves; however, to facilitate this, both identification and mitigation algorithms should be of low complexity.

Mobility: many applications in sensor networks require either static or mobile networks. Ideally, identification and mitigation methods should support both scenarios.

Deployment Environments: sensor networks can be deployed in a variety of environments, including harsh industrial environments or residential environments, and characteristics for these environments differ. Identification and mitigation techniques should be suitable for different environments.

Channel diversity: many NLOS identification algorithms rely on statistics extracted from UWB channels. IEEE 802.15.4a IR-UWB compliant devices expose the CIR for received frames, therefore channel statistics can be extracted from these CIRs to characterize LOS and NLOS channels. Given the large difference between center frequencies in UWB channels [7], it is plausible that significant differences in characteristics between channels are observed, therefore extracting channel statistics from multiple channels may result in better performance than extracting statistics from a single channel.

Many approaches have been proposed in literature, yet most approaches do not explicitly consider the aspects mentioned above nor leverage specific properties of UWB sensor networks. The majority of related work in NLOS identification and mitigation focuses mainly on classification accuracy (for identification) and improved location accuracy (for mitigation). Many methods have been proposed for wireless sensor networks, but they do not consider these aspects cohesively. NLOS identification and mitigation techniques should support the multitude of use cases and applications. To this end, this thesis investigates the state-of-the-art of identification and mitigation while taking these requirements into consideration. Methods which focus on classification and improving location accuracy while addressing these specific requirements are required.

1.2 RESEARCH OBJECTIVE AND QUESTIONS

The objectives of this work are:

- To provide an overview of the state-of-the-art NLOS identification and mitigation methods, and their suitability to IEEE UWB 802.15.4a sensor networks.
- To develop approaches for NLOS identification which are applicable to both static and mobile networks, leverage the channel diversity of UWB, and have low complexity.
- To develop approaches for NLOS mitigation which do not use any training data, are applicable to both static and mobile networks, are cooperative and have low complexity.

The research questions are:

- What are the limitations of current NLOS identification and mitigation methods with regards to their specific use in Ultra-wideband sensor networks?
- Can features from channel impulse responses from multiple channels improve NLOS identification accuracy in comparison to features from a single channel?
- How can techniques that require only limited, or no site-specific training data, for NLOS mitigation be developed?
- How can the ad-hoc/cooperative nature of UWB sensor networks be leveraged for NLOS mitigation?

1.3 APPROACH

The methodology followed for the proposed research is described below.

Literature review, identification of research problem and formulation of research questions: a literature survey was conducted to determine the state-of-the-art in NLOS identification and mitigation. This served as a starting point to identify the research problem and subsequent formulation of research questions.

Formulation of hypothesis: based on the knowledge acquired from the literature review and identified research gaps, the following hypotheses were formulated:

- Channel statistics from multiple channels in 802.15.4a IR-UWB sensor networks can improve identification accuracy of NLOS conditions,
- NLOS conditions can be detected with high accuracy without relying on channel statistics,
- Location errors in indoor localization caused by NLOS can be significantly mitigated without relying on channel statistics,
- Including node-to-node ranges in the localization process can further mitigate location errors caused by NLOS.

Analysis and experimentation: evaluation of state-of-the-art NLOS identification and mitigation methods served as a starting point for experimentation to determine the limitations of these methods with reference to the research questions and hypothesis. This was in the form of simulations and subsequent experimental evaluations in different indoor environments using IEEE 802.15.4a compliant IR-UWB sensor nodes.

Hypothesis verification: Novel NLOS identification and mitigation techniques that address limitations of state-of-the-art methods and answer the research questions were developed to verify the stated hypothesis and that the objectives of the research were met. The proposed methods were evaluated through simulations and experimental measurement campaigns, and compared to state-of-the-art techniques.

Contribution: the research output was published in the form of journal articles and a thesis, where guidelines for further research were given.

The detailed steps for the proposed research are listed below:

- Investigated state-of-the-art NLOS identification and mitigation methods,
- Compared methods according to how suitable they are to UWB sensor networks,
- Collected data from UWB sensor nodes through measurement campaigns in various indoor environments, which included range measurements and channel impulse responses from two channels defined in the IEEE 802.15.4a standard with a large difference in center frequencies.

1.4 RESEARCH GOALS

The main goal of this research is to develop NLOS identification and mitigation methods which improve localization in NLOS conditions. To this end, the state-of-the-art will be investigated and novel identification and mitigation methods that are suitable to IR-UWB sensor networks (taking into consideration location accuracy/precision, complexity, mobility and channel diversity) will be proposed.

1.5 RESEARCH CONTRIBUTION

A comprehensive review of the state-of-the-art in NLOS identification and mitigation is presented in Chapter 2. This review is presented from a perspective of IR-UWB sensor networks. Challenges particular to harsh industrial environments - which often present more issues than conventional indoor environments such as residential and office environments - are also discussed.

A NLOS identification method that does not rely on channel statistics nor range measurement statistics is proposed in Chapter 3. The method relies on a classifier trained with distance residuals (instead of channel statistics) from LOS and NLOS conditions. Since residuals are calculated at the localization level and are therefore agnostic to the wireless standard used in the PHY layer, this approach is not limited to UWB localization. Given that these distance residuals are calculated at the localization level, individual NLOS are not identifiable as they are in cases where NLOS identification is performed at the ranging level. The proposed method addresses this limitation by supporting identification of individual NLOS ranges for cases where certain criteria are met.

A NLOS classification method to classify NLOS conditions into TTW or ATC is proposed in Chapter 4. Both types of NLOS conditions occur often in indoor localization and their identification is crucial for the application of specific mitigation methods for each type of condition. This method relies on channel statistics extracted from two UWB channels: one channel in the low-band (3244–4742 MHz) and one channel in the high-band (5944–10234 MHz). In general, channel statistics from the channel in the high-band result in higher classification accuracy. When channel statistics from both channels are combined, high classification accuracy is achieved with less channel statistics, leading to less complex classifiers. Although this method requires channel statistics, the data is collected from two sites, but the results are not biased towards any of the sites. The results are supported by measurement campaigns.

A mitigation method for TTW NLOS conditions based on a novel TTW TOA ranging model and information from floor plans is proposed in Chapter 5. This TTW TOA ranging model has less parameters than the conventional TTW TOA ranging model and does not rely on the knowledge of incidence angles or other parameters that require a detailed characterization of the environment. The model is experimentally evaluated and integrated into localization using a NLLS estimator. All results show that NLOS conditions caused by TTW are significantly mitigated with the proposed method,

yet knowledge of channel statistics and models for NLOS errors are not required. The results are supported by measurement campaigns.

Three variants of a NLOS mitigation method that does not rely on floor plans nor channel statistics are proposed in Chapter 6. This method relies on geometric constraints - that arise due to the fact that the biases created by NLOS conditions are by definition positive - to estimate a more accurate location in comparison to a LLS estimator. The method is evaluated for the case where NLOS ranges are not identifiable and the case where they are identifiable. The first case is compared to state-of-the-art SDP based localization and it is found that it results in similar location accuracy, but its execution time is much faster, making it more suitable for applications that require a fast update rate. Furthermore, the proposed method does not require any specialized optimization solvers that are challenging to implement in resource-constrained devices. For the latter case, the method is extended to leverage node-to-node LOS ranges to further constrain the region where the estimated location lies, leading to a more accurate location estimation than the non-cooperative approach.

1.6 RESEARCH OUTPUTS

Journal articles:

B. J. Silva and G. P. Hancke, "IR-UWB-Based Non-Line-of-Sight Identification in Harsh Environments: Principles and Challenges," *IEEE Transactions on Industrial Informatics*, vol. 12, no. 3, pp. 1188-1195, June 2016.

B. J. Silva and G. P. Hancke, "Ranging Error Mitigation for Through-the-Wall Non-Line-of-Sight Conditions", *IEEE Transactions on Industrial Informatics*, vol. 16, no. 11, pp. 6903-6911, Nov. 2020.

B. J. Silva, D. Boshoff and G. P. Hancke, "Classification of Non-Line-of-Sight Conditions for Ultra-Wideband Using Multiple Channels", *IEEE Transactions on Industrial Informatics*, submitted for publication.

Conference papers:

B. J. Silva, R. Dos Santos and G. P. Hancke, “Towards non-line-of-sight ranging error mitigation in industrial wireless sensor networks," in *Proceedings of the 42th Annual Conference of the IEEE Industrial Electronics Society (IECON)*, Florence, Italy, 2016, pp. 5687-5692.

B. J. Silva and G. P. Hancke, “Characterization of non-line of sight paths using 802.15.4a,” in *Proceedings of the 18th IEEE International Conference on Industrial Technology (ICIT)*, Toronto, Canada, 2017, pp. 1436-1440.

B. J. Silva and G. P. Hancke, “An Approach to Improve Location Accuracy in Non-Line-of-Sight Scenarios using Floor Plans,” in *Proceedings of the 17th IEEE International Conference on Industrial Informatics (INDIN)*, Helsinki, Finland, 2019, pp. 1715-1718.

B. J. Silva and G. P. Hancke, “Around-the-Corner or Through-the-Wall? Classification of Non-Line-of-Sight Conditions,” in *Proceedings of the 18th IEEE International Conference on Industrial Informatics (INDIN)*, Warwick, UK, 2020, pp. 142-145.

B. J. Silva and G. P. Hancke, “Non-line-of-sight identification without channel statistics,” in *Proceedings of the 46th Annual Conference of the IEEE Industrial Electronics Society (IECON)*, Singapore, 2020, pp. 4489–4493.

1.7 THESIS OVERVIEW

Chapter 2 presents an overview of the state-of-the-art of NLOS identification and mitigation. The concepts required to understand the content of the following chapters are introduced in Chapter 2, including localization requirements and challenges.

In Chapter 3, a NLOS identification method based on distance residuals is proposed. The method is evaluated via simulations and shown to detect NLOS conditions with high accuracy. Unlike many identification methods in literature, this method does not rely on channel statistics.

In Chapter 4, a NLOS classification method to classify NLOS conditions into through-the-wall or around-the-corner conditions is proposed. The method is evaluated via measurement campaigns using commercial-off-the-shelf (COTS) UWB devices.

In Chapter 5, a novel TOA ranging model for through-the-wall NLOS conditions is proposed and evaluated experimentally. Based on this model, a NLOS mitigation method for through-the-wall propagation is proposed.

In Chapter 6, a localization method for improved localization in the presence of random NLOS ranging errors in proposed. Three variants of the method are proposed: mitigation where NLOS conditions are identifiable; mitigation where NLOS are identifiable and node-to-node ranges are available; and mitigation where NLOS conditions are not identifiable.

The thesis is finally concluded in Chapter 7, where guidelines for future research are given.

CHAPTER 2 LITERATURE STUDY

2.1 CHAPTER OVERVIEW

This chapter introduces the concepts of ranging and localization in NLOS conditions. An overview of the state-of-the-art of NLOS identification and mitigation is provided. Localization requirements - accuracy, update rate, scalability, robustness and privacy - are discussed, including how the first two requirements are the most affected by the introduction of NLOS identification and mitigation into the localization process. The need for identification and mitigation methods that do not rely on training data, have low complexity and support both static and mobile scenarios is highlighted. In Section 2.2, requirements and challenges for localization using UWB sensor networks are discussed in detail. In Section 2.3, several aspects of UWB sensor networks are discussed, with focus on time-of-arrival based ranging in LOS and NLOS conditions. In Section 2.4, several localization methods are discussed and compared. The impact of NLOS conditions on optimization based localization is also discussed. In Section 2.5, a comprehensive comparison of several NLOS identification and mitigation methods is presented. Finally, a summary of the chapter is provided in Section 2.6.

2.2 LOCALIZATION USING UWB WIRELESS SENSOR NETWORKS

2.2.1 Description of localization systems

A UWB localization system consists of the following core components [14]:

Tags: these are static or mobile sensor nodes for which locations must be estimated.

Anchors: these are static nodes with known locations that serve as references to tags, such that the tags' locations are computed relative to the anchors.

Location Engine: where the range measurements are processed and a location is estimated based on the ranging measurements. The location engine can be coupled to the user interface of the system.

For large scale localization systems, a backbone network is used to transport range measurements to a server which hosts the location engine where location estimates are computed.

2.2.2 Application domains

Localization is critical to many applications in wireless sensor networks. Some of these applications are described below. The aim here is not to present an exhaustive overview, but to present a brief overview that provides some context on the importance on accurate/precise localization.

Smart Cities: smart transportation requires real-time location information about busses and other means of transportation for fleet management and can be used for user alerts, for instance. Vehicle-to-vehicle (V2V) networks also require localization [15]. Construction can also benefit from localization to track progress of welding and inspection [16].

Industrial Automation: there are many places like warehouses, where knowing the precise location of products is crucial for logistics [17]. Robot navigation is another application where UWB is used [18]. Inertial measurement units (IMUs) are susceptible to drift and camera-based localization is processing intensive. UWB is an ideal alternative because it is wireless but has higher location accuracy than WiFi. An important use case in industrial environments is safety monitoring, where proximity is used to detect whether an operator is at a safe distance from a machine. Typically, different warning levels are used depending on how close an operator is [19]. In underground mining, in particular, localization is used for a variety of use cases, including personnel tracking, vehicle tracking, and collision avoidance [20].

Healthcare: of particular importance to assisted living is elderly monitoring [21]. It is important to monitor the location of the elderly to provide emergency care when needed. One important use case in elderly monitoring that uses localization is geofencing, which can be used, for instance, to track whether a person has left a house or not, or whether they have entered specific areas of the household. Behavior monitoring of people with dementia can also be done through localization [22].

2.2.3 Requirements

Several requirements that must be met for indoor localization [23] - [24]. These requirements include:

Location Accuracy: how close to the true locations the estimated locations are. For some applications, particularly for safety applications in the industrial domain, high accuracy and precision are expected.

Update Rate: depending on the use case, the localization system should be able to provide many location estimates per second. Navigation, for instance, must be done close to real-time and therefore requires a high update rate.

Scalability: positioning systems should have good scalability to support scenarios with a high tag density. Of particular importance, especially for TOA based systems, is channel access. State-of-the-art TOA positioning systems use Two-Way Ranging (TWR) algorithms, which requires bi-directional messages between tag and anchor. It is difficult to avoid collisions between these bi-directional messages as tag density increases.

Availability: although the requirements for non-critical application domains like smart homes do not have to be strict, high availability is required in many use cases in industrial applications [25]. It is crucial that localization systems provide a location estimate when needed and that location estimates are reliable. For instance, proximity systems used in the detection of personnel near mobile machines in underground mines, must be reliable and have high availability, as a failure in these systems can easily result in a fatality, particularly for use cases where data is tightly coupled to space and time, therefore rendering intermittent data useless.

Robustness: localization must meet quality of service (QoS) requirements even in harsh environments and be robust to failure.

Privacy: certain use cases like personnel tracking in industry require privacy. Although personnel tracking is useful in the case of accidents to help coordinate evacuations, continuous real-time tracking of personnel can violate privacy. It is important that only authorized entities have access to this

information and a certain level of anonymity is achieved. The work in this thesis focuses primarily on the first two requirements - location accuracy and update rate - as these are the most affected by the introduction of NLOS identification and mitigation techniques in the localization process. Table 2.1 lists localization specific requirements for various applications based on information from [23].

Table 2.1. Application requirements.

Category	**Applications**	**Availability**	**Update Rate**	**Privacy**	**Location Accuracy**
Marketing	- Advertising - Proximity Based Rewards	Low to Medium	0.1 Hz	High	10 m
Navigation and Tracking	- Asset Tracking - Personnel Tracking - Robot Navigation	High to Very High	10 Hz	High	1 m
Location Based Information Retrieval	- Proximity Searching - Way-finding	Medium	1 Hz	Medium to High	10 m
Safety and Security	- Emergency Services - Ambient Assisted Living - Security	Very High	1 Hz	Low to Medium	10 m

2.2.4 Challenges

There are several challenges in wireless localization. The industrial domain, in particular, poses more challenges than conventional indoor environments due to dynamic and harsh propagation environments. Challenges include:

Cost: large localization systems with many tags and anchors are costly, particularly with regards to installation. Deployment of wireless localization systems requires infrastructure, and often a backbone which provides a connection to the location engine. For instance, in underground mines which span

several kilometers, it is challenging to achieve cost efficient coverage. Applying simple deployment strategies can reduce installation cost [24].

Interference Management: wireless communication systems may interference with localization systems since both use wireless infrastructure. It is important to have good mechanisms in place to ensure coexistence among these wireless systems [24].

Interoperability and Standardization: in many domains, particularly in the industrial domain, localization systems are supplied as part of full networking solutions that cannot be decoupled from the vendor's infrastructure. This limits the interoperability. Standards will enable anchors, tags and other core components from different vendors to be equipped with standard software and hardware interfaces so that these components can coexist, even if they are from different vendors.

NLOS Propagation: NLOS conditions arise mainly due to propagation characteristics, which are fundamental to understand since many NLOS identification methods rely on the channel statistics which are affected by propagation. A discussion of propagation characteristics is important because any aspect that affects the CIR at the receiver influences the determination of the DP of arrival, which is an essential requirement for accurate TOA ranging. A wide range of IR-UWB ranging/localization investigations have been conducted in indoor scenarios, but the results of those studies are not directly applicable to industrial scenarios since channel characteristics are different. Some propagation aspects which can influence ranging performance are discussed below, with industrial halls and mine tunnels as examples.

Industrial Halls: Experimental characterization of IR-UWB propagation in industrial environments has revealed some differences to the widely accepted Saleh–Valenzuela model [26]. In conventional indoor environments, communication in LOS mainly results in a dominant MPC, i.e. first path, and decreasing subsequent MPCs. In industrial scenarios, the propagation characteristics differ (in comparison to indoor office or residential environments) due to abundant scatterers and reflections from metallic surfaces. The channel model for an industrial channel [27] based on measurement campaigns conducted in industrial halls showed that although MPC clusters are observed, the clusters did not exhibit a single exponential delay, and the decay time constants were different for each cluster. It was concluded that neither cluster power decay nor ray powers are purely exponential; therefore, a model with the ray

power decay as a linear function of excess delay and the cluster power decay as the exponential decay of the peak power of the received clusters is proposed in [27].

Underground Mines: Unlike indoor facilities where the walls are smooth, walls in mines have very rough surfaces which result in scattering and can vary in dielectric properties. In some cases, it has been shown that the number of MPCs rapidly decays in tunnels, resulting in relatively short delay spreads (i.e., the time difference between the first MPC and last MPC) in comparison to conventional indoor environments [28]. In contrast to above-ground channels, propagation in underground tunnels occurs in modes and is dependent on the dimensions and cross-sectional shape of the tunnel as well as wavelength. In contrast to propagation in industrial halls, mine tunnels are low reflective [28] (although this property can change in the presence of heavy machinery), with observed delay spreads in the region of 10 ns in LOS and 30 ns in NLOS in confined environments [29]. Knowledge of the delay spread in specific environments is important, particularly for NLOS identification, where delay spread can be used as a channel statistic.

Propagation is mainly affected by four phenomena: refraction, diffraction, reflection, and scattering. Refraction occurs when an electromagnetic (EM) wave travels from a medium into another medium with a different refractive index; diffraction is the bending of EM waves incident on an object with sharp edges; reflection is caused by EM waves that are incident on a structure with a size much larger than the incident waves wavelength (which in turn causes multipath); and scattering occurs when an EM wave is incident on an object with a size in the order of one wavelength or less. When wireless signals propagate through walls, refraction causes an additional delay and pulse distortions, which are dependent on the pulse shape, where the degree of pulse distortion varies with bandwidth [30].

The most prominent effect on communication performance in industrial environments can be attributed to reflections from metallic structures such as machinery and pipes. These typically result in specular and dense multipath [31], which can be detrimental to communication as well as ranging performance since MPCs might not be resolvable in such instances. Furthermore, machines in the vicinity of wireless networks cause EM interference. Studies have shown that interference in industrial scenarios can be caused by machinery, cranes, motors, and combustion engines [32]. Taking these effects into consideration, it is evident that UWB antennas must have high fidelity so that the pulse shape is not highly distorted to such an extent that the ranging accuracy is affected. Although UWB has high penetration ability, experiments have revealed that refraction, diffraction, and other propagation effects

distort the pulse shape, consequently affecting the ranging accuracy [30]. In summary, many scatterers and metallic reflectors result in multipath and NLOS scenarios due to obstructed DPs. Additionally, there is significant interference in industrial environments and this narrow and wideband interference, in turn, influences UWB communications [33]. The following example illustrates the importance of considering NLOS propagation in industrial environments. Early work based on IEEE 802.15.4a channel models used log-normal distributions for channel statistics such as Kurtosis [34]. Figure 2.1 shows the distribution of Kurtosis for a NLOS channel in the Heavy Machinery Laboratory at the University of Pretoria, extracted from CIRs obtained using IEEE 802.15.4a IR-UWB devices [35]. It is evident that the Kurtosis follows a multi-modal distribution instead of a log-normal distribution.

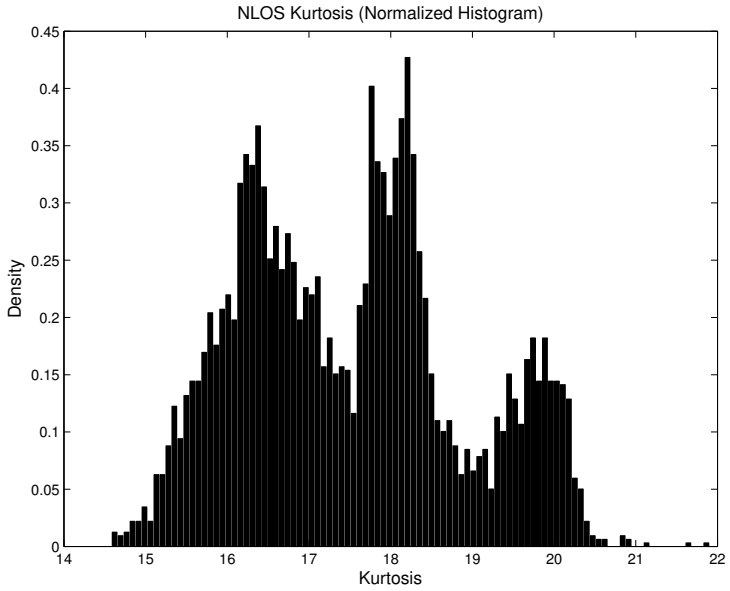

Figure 2.1. Example of Kurtosis distribution for a NLOS channel in an industrial environment. Taken from [36], © 2016 IEEE.

2.3 ULTRA-WIDEBAND SENSOR NETWORKS

The main difference between conventional sensor networks and UWB sensor networks is the use of a IR-UWB PHY in the latter. Whereas conventional sensor networks typically use RSSI for ranging and localization, UWB sensor networks rely on TOA ranging which targets applications that require high ranging and location accuracy. The IEEE 802.15.4a standard defines methods to achieve high precision ranging for Wireless Personal Area Networks (WPANs). It supports TOA ranging in three different bands: the sub-GHz, 3244–4742 MHz (low) and 5944–10234 MHz (high) bands [7] at different data rates. In contrast to common narrowband and wideband wireless - which use continuous

waves - communication in UWB is done with very narrow pulses derived from Gaussian monocycles [37].

There are several advantages to using narrow pulses for communication. Firstly, the use of narrow pulses results in a very high resolution in the time domain, enabling the receiver to resolve multipath components much better then narrowband and wideband communication systems. Secondly, this high time resolution enables the reliable detection of the first arriving path since it can be distinguished from other multipath components. Detecting the first arriving path is essential to achieve precise ranging. Given these properties, IR-UWB is currently the ideal option for wireless sensor networks that target applications which require accurate localization.

2.3.1 Time-of-arrival ranging

The process of determining the distance between two nodes is called ranging. The range can be determined with any parameter that is dependent on the distance between two nodes. Good examples in literature for radio-frequency (RF) devices include RSS and TOA.

The work in this thesis focuses on TOA specifically because this is the standard method used in IEEE 802.15.4a UWB sensor networks [38]. In TOA ranging, the time it takes for a signal to propagate between transmitter and receiver is measured and then converted to distance. Since EM waves propagate approximately at the speed of light, the distance d between two nodes is calculated as:

$$d = c(t_1 - t_0) \tag{2.1}$$

where t_0 is the timestamp at the transmitter, t_1 is the timestamp at the receiver, and $c \approx 3 \times 10^8$ m/s. The difference $t_1 - t_0$ is the time elapsed between transmitter and receiver, where t_0 and t_1 are precise timestamps recorded at the PHY layer of the transmitter and receiver, respectively. For RF waves propagating in free space, a 1 nanosecond propagation time corresponds to approximately 30 centimeters in distance. Therefore, to obtain good ranging accuracy, these timestamps must be determined with picosecond resolution. The IEEE 802.15.4a standard [38] defines guidelines to achieve high precision timestamping in standard compliant devices. For (2.1) to yield good ranging accuracy,

both nodes must have a common timebase, which is achieved through clock synchronization prior to the ranging measurement. However, clock synchronization in the nanosecond range is challenging in UWB devices. Alternatively, TWR - which removes the need for clock synchronization - can be used. In TWR, nodes exchange multiple messages and timestamps are determined for each message. The message exchange for this procedure is illustrated in Figure 2.2, showing an example of Symmetric Double Sided Two-Way Ranging (SDS-TWR), which is a reliable variant of TWR.

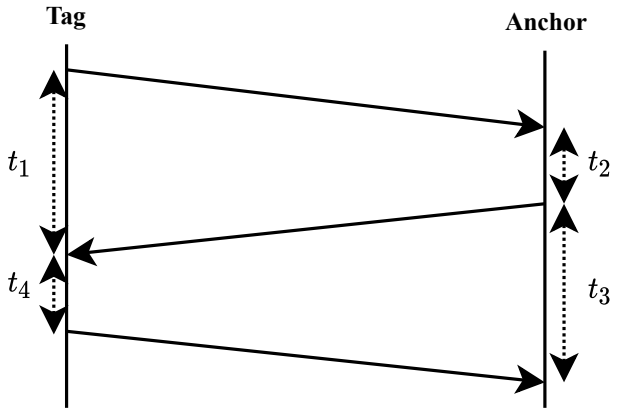

Figure 2.2. Symmetric double sided two-way ranging.

The two-way range between two IR-UWB devices (tag and anchor in this case) is computed as follows. The tag transmits a frame and timestamps the TX time. The anchor receives this frame, timestamps the RX time, processes the frame, and generates a response frame. When the response frame is transmitted to the tag, the anchor timestamps the TX time. The anchor then calculates t_2, which is the time elapsed between the RX and TX timestamps. The tag receives the response frame from the anchor and timestamps the RX time. The tag is now able to compute t_1 from this RX timestamp and the TX timestamp from the very first frame transmitted to the anchor. Calculation of t_3 and t_4 follow the same procedure. Since t_1, t_2, t_3, and t_4 are known, the propagation time is computed by:

$$t_{TWR} = \frac{(t_1 - t_2) + (t_3 - t_4)}{4} \tag{2.2}$$

The distance d_{TWR} is then calculated from (2.2) with $d_{TWR} = c \times t_{TWR}$. In real scenarios, there is always noise associated with the hardware. Therefore, ranges measured by real hardware are given by:

$$\hat{d} = d + n = c(t_1 - t_0) + n \tag{2.3}$$

where n is Gaussian distributed noise with distribution $\mathcal{N}(\mu, \sigma^2)$.

2.3.2 Line-of-sight and non-line-of-sight conditions

There is a distinct difference between LOS and NLOS propagation. In LOS propagation, there is an unobstructed direct path between transmitter and receiver, while in NLOS propagation, the path is obstructed [39]. Figure 2.3 illustrates the difference between LOS and NLOS propagation, where p_3 is a LOS path, and p_1 and p_2 are NLOS paths.

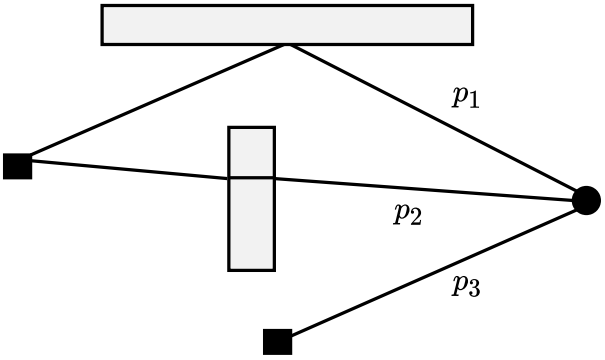

Figure 2.3. Illustration of LOS and NLOS paths.

There are at least three propagation phenomena that are associated with NLOS conditions:

Diffraction: diffraction is the bending of EM waves around sharp objects. The wave becomes a secondary source at the intersection with the object.

Refraction: differences in refractive indices between air and the material obstructions are made of, cause the signal to be refracted as it propagates through the obstruction. Depending on the refractive index, the signal changes direction and propagation time as the wave propagates through the obstruction [40]. A good example of propagation through a wall is path p_2, illustrated in Figure 2.3.

Reflection: in this case, there is an obstruction transmitter and receiver therefore the direct path is completed attenuated and not detectable at the receiver. Given the capability of UWB to resolve

multipath components, the receiver can still detect attenuated multipath components reflected off surfaces and walls in the near vicinity. An example of such a path is p_1 in Figure 2.3.

Although these phenomena are described separately, they can in many cases occur simultaneously. It is also noted that these phenomena are frequency dependent. Considering the three phenomena discussed above, it is evident that the distances for the detected paths are longer than the true paths. It is well known that the propagation speed of EM waves depends on the conductivity, permeability and permittivity of the medium the wave propagates in [41]. The calculation in (2.3) assumes propagation in free space, where c is dependent on the air's permittivity. Since materials have different refractive indices, the propagation speed in different mediums is less than c by a factor dependent on the relative permittivity of the medium [39]. Therefore, using (2.3) to compute the distance in a NLOS condition caused by refraction, results in a larger distance than the true distance. Similarly, the reflected path in Figure 2.3 is also longer than the true path. The difference in length between the true path and the NLOS path is known as ranging - or NLOS - bias. Therefore, in cases where the range is obstructed by any of the phenomena described above, the measured range between two nodes is then given by:

$$\hat{d} = d + b + n = c(t_1 - t_0) + b + n \tag{2.4}$$

where b is the positive ranging bias and the other terms are in defined in (2.3). NLOS identification deals with detecting ranges from NLOS conditions which are corrupted by a positive bias b. NLOS mitigation reduces the impact of b such that the estimated distance between two nodes are as close as possible to the true distance.

2.4 LOCALIZATION METHODS

The most common approach to determine a tag's location is through trilateration. In trilateration, each anchor is represented by a circle, where the center is the anchor's location and the radius is the measured range between tag and anchor. The tag is then the single intersection point of the circles defined by the anchors. Solving the trilateration problem analytically is only possible if the range measurements between anchors and tags are perfect, and the resulting tag's location is a single point of intersection between three circles. However, range measurements in sensor networks are noisy,

resulting in no single point of intersection. A tag's location $\mathbf{x} = [x, y]^T$ is determined by solving the following system of equations:

$$\begin{aligned} \sqrt{(x-x_1)^2+(y-y_1)^2} &= d_1 \\ \sqrt{(x-x_2)^2+(y-y_2)^2} &= d_2 \\ &\vdots \\ \sqrt{(x-x_N)^2+(y-y_N)^2} &= d_N \end{aligned} \tag{2.5}$$

where N is the number of anchors and $[x_i, y_i]^T$ are the anchor locations. This system can be solved in the least squares sense by minimizing the following function:

$$\hat{\mathbf{x}} = \min_{\mathbf{x}} \sum_{i=1}^{N} (d_i - \|\mathbf{x} - \mathbf{a}_i\|)^2 \tag{2.6}$$

where $\|\mathbf{x} - \mathbf{a}_i\| = \sqrt{(x-x_i)^2+(y-y_i)^2}$. This is the range-based least squares (R-LS) approach [42]. A variant of this approach is to square the terms in (2.6), resulting in the alternative form:

$$\hat{\mathbf{x}} = \min_{\mathbf{x}} \sum_{i=1}^{N} \left(\|\mathbf{x} - \mathbf{a}_i\|^2 - d_i^2 \right)^2 \tag{2.7}$$

where the terms are the same as in (2.6). Note that the expression in (2.7) is the squared-range-based least squares (SR-LS) discussed in [42]. Like (2.6), (2.7) is also non-convex but a global solution can be computed efficiently.

Figures 2.4(a) and 2.4(b) show the contour plots for the objective functions in (2.6) and (2.7) for LOS location estimates. The anchor locations are $(x_1, y_1) = (0, 0)$, $(x_2, y_2) = (0, 10)$ and $(x_3, y_3) = (10, 10)$. It is observed that the true location (indicated by the red dot) is close to the estimated location (indicated by the white dot), with location errors of 0.23 m and 0.21 m, respectively. It is noted that for LOS conditions, the range measurement d_i is noisy but it contains no significant bias, i.e. for LOS conditions the range is given by (2.3). The objective functions in (2.6) and (2.7) can be minimized using several algorithms. Some of these algorithms are discussed below.

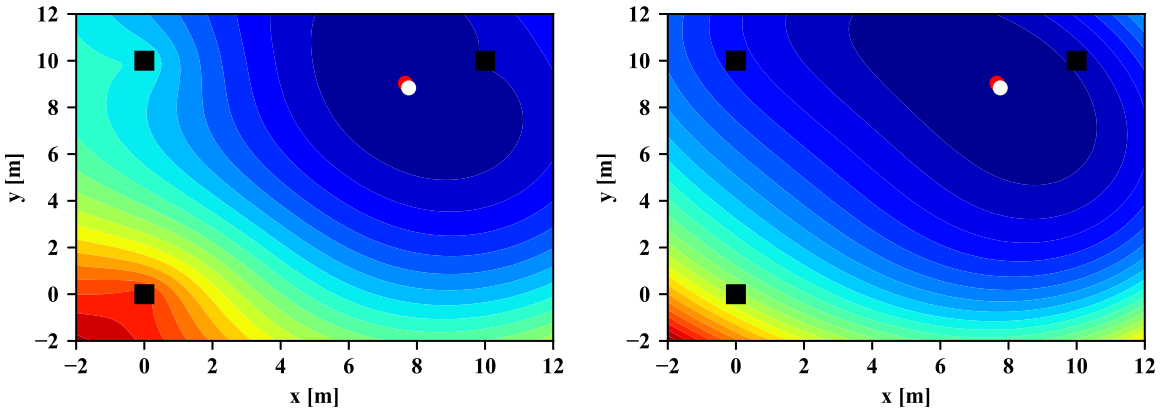

(a) R-LS **(b)** SR-LS

Figure 2.4. Contour plots in LOS conditions for objective functions.

Gradient Descent: This a first order optimization algorithm to find the minimum of a function using first derivatives. The main advantage of Gradient Descent (GD) is its simplicity and low complexity. GD is used for both linear and non-linear least squares problems. GD does not require a matrix inversion, unlike some of the algorithms described below. The time complexity for each iteration is $O(nm)$, where m is the number of variables and n is the number of anchors. One limitation is that a good initial point is necessary to arrive at the global minimum.

Linear Least Squares: the system in (2.5) is linearized through algebraic manipulation, resulting in a closed-form solution [43]. The linear least squares (LLS) solution is given by matrix A:

$$A = \begin{bmatrix} 2(x_n - x_1) & 2(y_n - y_1) \\ 2(x_n - x_2) & 2(y_n - y_2) \\ \vdots & \vdots \\ 2(x_n - x_{n-1}) & 2(y_n - y_{n-1}) \end{bmatrix} \tag{2.8}$$

and a matrix **b**:

$$\mathbf{b} = \begin{bmatrix} r_1^2 - r_n^2 - x_1^2 - y_1^2 + x_n^2 + y_n^2 \\ r_2^2 - r_n^2 - x_2^2 - y_2^2 + x_n^2 + y_n^2 \\ \vdots \\ r_{n-1}^2 - r_n^2 - x_{n-1}^2 - y_{n-1}^2 + x_n^2 + y_n^2 \end{bmatrix} \tag{2.9}$$

where the tag's location $\mathbf{x}$ is calculated as:

$$\mathbf{x} = (\mathbf{A}^T\mathbf{A})^{-1}\mathbf{A}^T\mathbf{b} \tag{2.10}$$

where the terms are the same as in (2.5). The main advantage of this approach is that, unlike GD, no initial guesses are required. However, this approach requires matrix calculations - which include multiplications and Cholesky decomposition - to solve (2.10), resulting in a time complexity of $O(nm^2 + m^3)$.

Non-Linear Least Squares: common iterative algorithms to solve non-linear least squares (NLLS) problems include Gauss-Newton (GN) and Levenberg-Marquardt (LM). Unlike gradient descent, which requires the learning rate to be set, Gauss-Newton does not. Gauss-Newton is also a gradient descent method, but with a higher rate of convergence than GD. Levenberg-Marquardt is another algorithm to solve NLLS problems. Like GD and GN, it is iterative, but is uses a damping factor that is adjusted in each iteration to minimize the residual [44]. The sequential LM algorithm based on QR factorization has a complexity of $O(nm^2 + km^3 + knm + km^2)$ where k is the number of damping parameters [45]. LM may converge faster than gradient descent and it is also more robust to the initial guess than Newton type methods. Table 2.2 summarizes details of the methods discussed above.

2.4.1 Impact of NLOS conditions on localization

For TOA ranging, there is a positive bias b present in the range measurement, therefore the ranges are noisy and biased as modeled by (2.4). In this case, the objective function in (2.7) may result in location estimates with large location errors. The contour plots in Figures 2.5(a) and 2.5(b) show the locations estimates for the same true location in Figures 2.4(a) and 2.4(b), but with two positive biases b_1 and b_2 of 1.5 meters and 2.0 meters, respectively. In this case, the location errors are 1.81 m for

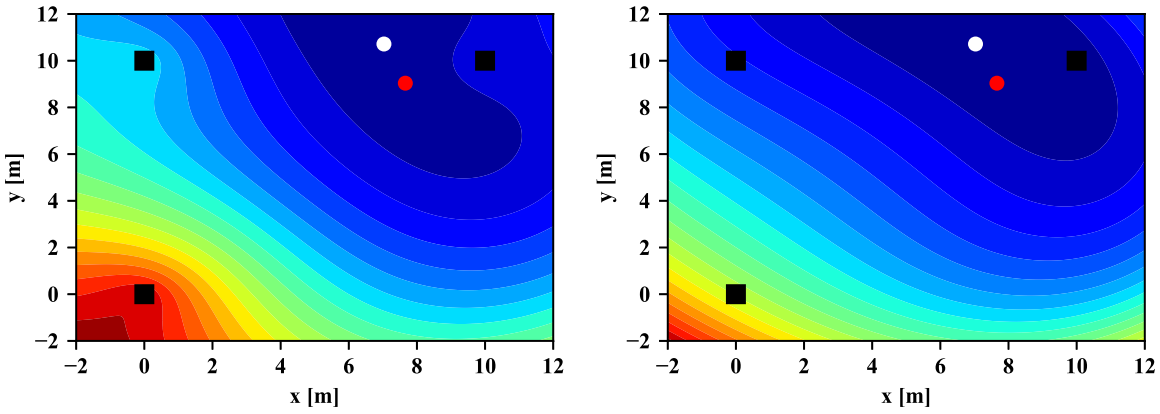

(a) R-LS **(b)** SR-LS

Figure 2.5. Contour plots in NLOS conditions for objective functions.

R-LS and 1.79 m for SR-LS. It is observed that although the optimal solution is (correctly so) at the minimum of the objective function, this minimum is far from the true location because the ranges have been corrupted by positive biases. In other words, the minimum has been 'shifted' to another point. These location errors occur because (2.7) considers the bias b to be part of the distance measurement, therefore the impact of these biases is not mitigated in the location estimate. In order to mitigate the impact of the biases, the biases have to be included in the objective function:

$$\hat{\mathbf{x}}, \hat{\mathbf{b}} = \min_{\mathbf{x},\mathbf{b}} \sum_{i=1}^{N} \left(\|\mathbf{x} - \mathbf{a}_i\|^2 - (d_i - b_i)^2 \right)^2, \quad \text{s.t.} \quad b_i \geq 0 \tag{2.11}$$

where b_i is the bias for the NLOS range between the tag and anchor i, and the other terms are the same as in (2.7). Since the biases are unknown, they must be estimated along with the tag's location. However, the system in (2.11) is underdetermined and non-convex, therefore estimating these biases is not trivial.

2.5 NLOS IDENTIFICATION AND MITIGATION METHODS

There are several techniques for NLOS identification and mitigation in literature. The first group of methods discussed here does not rely on channel statistics extracted from channel impulse responses.

Table 2.2. Summary of localization algorithms.

Algorithm	Details	Time Complexity
GD	- Initial guess required - Iterative algorithm - Prone to local minima	$O(nm)$ per iteration
LLS	- Closed form - Not iterative	$O(nm^2+m^3)$
NLLS (LM)	- Initial guess required - Iterative algorithm - More complex than GD and LLS	$O(nm^2+km^3+knm+km^2)$ per iteration

These methods rely only on range measurements between anchors and source node, i.e. tag. The advantage of these methods is that since they do not rely on channel statistics, they do not require LOS and NLOS channel characterization.

2.5.1 Mitigation using distance residuals

The residual weighting (Rwgh) algorithm for NLOS mitigation using distance residuals was proposed in [46]. It targets NLOS mitigation when range measurements by NLOS are not identifiable and no channel statistics are available. The algorithm compares distance residuals for locations estimated with different sets of anchors, and it leverages the fact that distance residuals are larger in the presence of NLOS ranges. It was shown that Rwgh performs better than just choosing the location estimate with the minimum residual error. Rwgh requires more than three ranges, therefore it not suitable for scenarios with three anchors only, which is the minimum number of anchors required to estimate a 2D location. Most of the research that followed the work in [46] focused on reducing the high computational complexity of the Rwgh algorithm. A performance comparison of several distance residual algorithms for TOA localization was conducted in [47]. The compared algorithms were: Rwgh, Lower-Computational-Cost Residual Weighting (LCC-Rwgh), Iterative Minimum Residual (IMR) and Select Residual Weighting (SRwgh). It was shown that the algorithms are mostly similar with regards to computational complexity and location accuracy. One common limitation of residual-based algorithms is the inability to identify individual NLOS ranges since it does not rely on channel statistics

and the residuals are computed at a localization level. Several challenges for NLOS identification using residual based algorithms were discussed in [48]. However, no explicit NLOS identification algorithm using residuals was proposed, particularly one that can identify individual NLOS ranges.

2.5.2 Identification using distribution of range measurements

NLOS identification without using channel statistics was initially studied in [49]. This work showed that a NLOS channel can be identified by using the time history of range measurements with a simple hypothesis test. The test relies on the prior knowledge of the standard deviation of the measurement noise, and the fact that the presence of NLOS errors increases the standard deviation of the measurements significantly [49]. The standard deviation of range measurements $\hat{\sigma}_m$ is compared to the known standard deviation of range measurements in LOS conditions σ_m. This is motivated by the fact that NLOS conditions introduce positive biases into the range measurements, therefore it is expected that if there are only LOS ranges, then $\hat{\sigma}_m \approx \sigma_m$. There are two possible hypotheses:

$$\begin{aligned} H_0 &: \hat{\sigma}_m = \sigma_m \\ H_1 &: \hat{\sigma}_m > \sigma_m \end{aligned} \tag{2.12}$$

where the LOS hypothesis H_0 is rejected for large values of $\hat{\sigma}_m$ exceeding σ_m. Although the approach proposed in [49] does not require previous channel statistics or NLOS error models, it does require prior knowledge of the standard deviation of measurement noise.

In [50], the ranging error distribution was used. In this approach, a binary hypothesis test is formulated to classify a series of ranging measurements in LOS or NLOS through different likelihood-ratio tests (LRT) tests, depending on whether the statistics (mean and variance) for ranges in LOS and NLOS are known or unknown [50]. The premise is that a high variance in range measurements is observed when there are NLOS errors.

It is noted that these methods can perform poorly indoors since some NLOS conditions are as stable as LOS conditions, particularly if NLOS conditions are caused by TTW propagation. Therefore, no significant difference between the standard deviation of LOS vs NLOS is observed in this case [51]. A

natural progression to using the history of range measurement is the use of tracking filters, discussed further in Section 2.5.4.

2.5.3 Optimization

Linear Programming: LP for NLOS localization was proposed in [52]. With reference to (2.5), the non-linear equations in x and y that define the node's location are first linearized. This linear system of equations is then used to formulate a linear program where the objective function is linear, and NLOS ranges are used to define the feasible region, where the circular constraints are relaxed to square constraints. It is noted that the NLOS ranges are not used in the objective function to determine the location, they are only used to define the feasible region. The results show that this approach improves the location accuracy in the presence of NLOS ranges when compared with to the conventional least squares estimator.

Quadratic Programming: The work in [53] investigated a quadratic programming approach. A joint location and bias estimation scheme using constrained optimization in the form of a Sequential Quadratic (SQ) program was proposed. The complexity of the proposed approach is reduced using a Taylor expansion LP algorithm. In the formulation of the approach, the N unknown biases are assumed to be the same so that the number of unknowns is reduced. This can lead to reduced performance if the true values of the biases are very different from each other. The proposed estimator was evaluated for cases where the NLOS error statistics are known and the case where they are unknown. It was shown that in all cases, the proposed approach significantly outperforms localization using the LS estimator.

Semidefinite Programming: The work in [54] investigated convex relaxation for NLOS mitigation. Second-order cone relaxation (SOCR) and semidefinite relaxation (SDR) based optimization to mitigate NLOS biases were evaluated. The source location and an additional parameter that is related to NLOS errors is estimated. Since the formulated problem is non-convex, it is solved by relaxation and obtaining an equivalent convex semidefinite program (SDP) or second-order cone program (SOCP). Like the approach described in [53], this method also substituted the unknown bias errors by one single unknown bias which acts as a balancing parameter. An upper bound is determined for this parameter and is used as a constraint to the optimization problem. The formulated optimization problem is still

non-convex, therefore it is relaxed into an SDP problem that is convex and can be solved using interior point methods. The proposed method is evaluated for both cases where the NLOS status is perfectly known and the case when it is not. The results show that this approach outperforms LP and QP based approaches, particularly in scenarios where the NLOS status is unknown and most anchors have NLOS links to the source node. For sparse NLOS environments, QP is shown to outperform the proposed approach.

The work in [55] proposed a NLOS mitigation technique based on convex SDP optimization. Compared to QP, Huber and Least Median Squares estimators, this SDP formulation outperforms them in mild and severe NLOS conditions, in terms of location accuracy. However, a small percentage of cases do not converge, resulting in infeasible cases. A soft minimum approach to address this infeasibility issue is proposed in [56], where an additional variable term is introduced into the optimization problem. This approach eliminates the infeasibility issue and slightly outperforms the method in [55] in terms of location accuracy.

2.5.4 Tracking filters

In the case of mobile localization, i.e. tracking, the error variance that is affected by the transition from LOS to NLOS (and vice versa) during movement can be leveraged. This is a property exploited by Particle and Kalman filters [57] for NLOS identification. With Kalman filters, mitigation can be accomplished by either using biased Kalman Filters or discarding successfully identified NLOS measurements, among other approaches. In [58], a biased Kalman filter for mitigation and a sliding window for identification is proposed. For identification, the standard deviation of measurements is calculated over the sliding window and it is passed through a binary hypothesis test to determine whether the measurement originates from a LOS or NLOS condition. For mitigation, TOA measurements are smoothed with a Kalman filter and positive NLOS errors are mitigated when NLOS conditions are detected. The assumption is that the standard deviation of TOA measurements in NLOS is larger than in LOS. Since the Kalman filter is used to estimate the state vector of a mobile target from measured TOA, and the filter design assumes transitions between LOS to NLOS over the target's trajectory, this approach is ideal for mobile scenarios.

The approach in [59] uses K-means clustering with a modified Extended Kalman Filter (EKF) to

identify NLOS conditions. The standard deviation of range measurements is assumed to belong to one of two classes. For the class without NLOS errors, i.e. LOS, the values are assumed to part of a cluster with a center very close to zero and for the class with NLOS errors, the values are assumed to be part of a cluster with a center larger than zero, and the calculated standard deviation is assigned to one of the clusters. The NLOS range measurements are then reconstructed into LOS by smoothing with a polynomial fit. This approach is shown to outperform approaches using only a conventional EKF. Similar approaches using Unscented Kalman Filters (UKF) have also been proposed [60]. Most, if not all, of these approaches rely on motion models and a motion sensor, therefore they are mostly only suitable for mobile scenarios.

2.5.5 Channel statistics

The channel statistics based approach relies on range measurements and on previously recorded channel statistics, or metrics, to determine whether a channel is LOS or NLOS. This approach to NLOS identification leverages the fact that LOS channels typically exhibit different characteristics to NLOS channels, and these characteristics can be distinguished by statistics extracted from CIRs. In the IEEE 802.15.4a standard, the CIR is provided at the PHY layer for every received frame [38].

In contrast to Zigbee and similar low power wireless technologies, which typically only provide RSSI and Link Quality Indicator (LQI), IR-UWB radios make it possible to characterize the channel using many metrics. Although the use of channel statistics, or metrics, has been extensively investigated in literature, this discussion focuses only on the statistics relevant to IR-UWB, and those which can be extracted from the CIR in IEEE 802.15.4a devices.

Skewness: skewness reflects the asymmetry of a probability distribution. Positive, or negative, skewness values indicate asymmetry, with negative values indicating data being skewed to the left and positive values indicating data being skewed to the right. Zero skewness indicates complete symmetry, e.g. normal distribution.

Kurtosis: kurtosis is the ratio of the fourth order moment to the variance [61]. It indicates whether a probability distribution is ‘heavy tailed’ or ‘light tailed’ compared with the normal distribution. High kurtosis values are associated with heavy tails and low kurtosis values are associated with light

tails, therefore kurtosis is indicative of how peaky the data distribution is compared to a normal distribution.

Maximum Path Amplitude: CIR amplitudes in LOS channels are generally higher that CIR amplitudes in NLOS channels.

Delay spread: the delay spread indicates the time dispersion of a communication channel and it is an indicator of how much multipath there is in the channel. It is determined from the power delay profile (PDP) of the channel, and variants include mean excess delay, RMS delay spread and excess delay spread. In contrast to kurtosis and skewness, which indicate amplitude characteristics, the delay spread indicates the multipath spread of the channel.

Rise Time: the difference in delay between the strongest path and first path [62]. For strong LOS channels, where the first path is the strongest path, the rise time is expected to be close to zero, and it is expected to increase in magnitude for NLOS conditions. For IR-UWB, this is measured in nanoseconds.

Received Signal Strength: this is the signal strength measured at the receiver for every received frame. It is well known that LOS channels exhibit higher RSS than NLOS channels.

First Path Power: in LOS channels, most of the energy in the CIR is concentrated in the first path, and the subsequent multipath components do not contain much energy. In NLOS channels, depending on the severity of the NLOS conditions, the energy is more distributed across the CIR.

2.5.6 Statistical approach

When multiple statistics are available, one of the simplest ways to identify NLOS conditions is to use a binary hypothesis test. A general framework for NLOS identification with a binary hypothesis test is as follows. Probability distributions for the metric in question are available (through statistical characterization) for LOS and NLOS channels, which have been determined from data collected in a measurement campaign. For any new received measurements, the goal is to determine whether the measurement is from a LOS or NLOS channel. Two hypotheses H_0 and H_1 are considered. For NLOS

identification, the null hypothesis H_0 is LOS, and the alternative hypothesis H_1 is NLOS. Then, the decision of where a metric (or statistic) m_1 is LOS or NLOS, is done with a LRT as follows [34]:

$$\frac{P_{los}(m_1)}{P_{nlos}(m_1)} \underset{H_1}{\overset{H_0}{\gtrless}} 1 \tag{2.13}$$

where the null hypothesis H_0 (LOS) is selected if the result of (2.13) is greater than 1, and the alternative hypothesis H_1 (NLOS) is selected otherwise. $P_{los}(m_1)$ and $P_{nlos}(m_1)$ are the probability distribution functions of the statistic m_1 for LOS and NLOS, respectively. Instead of directly using the joint distributions, a sub-optimal approach for NLOS identification is to use k metrics by assuming that the metrics are independent:

$$\left(\frac{P_{los}(m_1)}{P_{nlos}(m_1)} \times \frac{P_{los}(m_2)}{P_{nlos}(m_2)} \times \cdots \times \frac{P_{los}(m_k)}{P_{nlos}(m_k)}\right) \underset{H_1}{\overset{H_0}{\gtrless}} 1 \tag{2.14}$$

where m_1 to m_k are the channel statistics extracted from the CIR. Another example of early work on this approach is [63]. This work showed that UWB exhibits significant differences in statistics between LOS and NLOS channels for TOA, RSS, and RMS delay spread. A binary hypothesis test was formulated and models for the three statistics were determined from experimental data. It was shown that LOS and NLOS was identified with high accuracy.

For mitigation, an Hypothesis Testing Regressor (HTC) was proposed in [64]. This regressor incorporates a log-propagation model, and the regression step relies on distance power loss coefficient and ranging noise. More recently, machine learning has gained more popularity for NLOS classification than the conventional statistical approach.

2.5.7 Machine learning

In machine learning, NLOS identification is modeled as a classification problem. In some aspects, the machine learning approach is similar to the statistical approach discussed above, with the main difference being that no actual statistical characterization, i.e. determining the distribution of the statistics under LOS vs NLOS, is necessary, therefore no assumptions are made about the underlying statistical models [62].

This step of determining the PDFs is substituted by a training step using labeled data (in the case of supervised learning) from measurement campaigns. The trained model is then able to predict whether a channel is LOS or NLOS.

The work in [65] extracted features from received UWB waveforms and used a Support vector Machine (SVM) and Gaussian Processes to determine the a posteriori distribution of the range data based on the training data. Features extracted from the UWB waveforms included energy, maximum amplitude, rise time, RMS delay spread, mean excess delay and kurtosis. The work in [64] followed a similar approach, but only statistically characterized received signal strength over a time period. Metrics included the mean, standard deviation, kurtosis, skewness and Rician K factor, which were used in both NLOS identification and mitigation. For NLOS classification, a SVM, a Gaussian Process Classifier, and a binary hypothesis testing classifier were used. For NLOS mitigation, the regression variants of the classifiers were used. This work also showed that using models from a site different to where the training data was collected can lead to poor accuracy [64]. The work in [66] used an artificial neural network (ANN) to identify NLOS conditions caused by undetected direct paths (UDP). Features included RSS and RMS delay spread. Kernel-based machine learning methods, where the features extracted from received signals are projected into a nonlinear orthogonal high dimensional space, were also proposed for UWB [67]. The use of projection is motivated by the fact that in the high-dimensional space all information available in the CIR can be exploited.

Ensemble Classifiers: A Random Forest (RF) based classifier was investigated in [68] using mean, standard deviation, skewness and kurtosis of the CIR magnitude samples as features. The running time of the RF classifier is reduced to at least 50% compared to a least-squares SVM.

Adaptive Boosting (AdaBoost) was also investigated for NLOS localization in [69]. AdaBoost is an algorithm which combines the outputs of classifiers and the weighted sum of the outputs of the weak learners is the output of the 'boosted classifier'. The learners in [69] are: two weak learners based on thresholds for a strongest path and TOA, respectively, and three LRTs for each feature used: kurtosis, mean excess delay and RMS spread delay. These weak learners are combined into a boosted learner, and it is shown that the classifier outperforms SVM-based classifiers in terms of prediction time and classification accuracy.

Deep Learning: The work in [13] uses raw CIR traces to train convolutional neural networks (CNNs).

The main motivation to use raw CIR traces is the fact that feature extraction does not capture the CIR's full information. The results show that this approach outperforms approaches which extract features from CIRs. Typically, CNNs expect 2D data, therefore the dimensionality of the CNN is reduced to accept 1D CIR traces, which reduces the computational complexity. Compared to multilayer perceptron (MLP) and SVMs, the results show that the CNN outperforms both in terms of classification accuracy. The work in [70] compared three different architectures for CNNs used for NLOS identification: Residual Network (ResNet), Encoder and Fully Convolutional Network (FCN). Similar to [13], no feature extraction was done. It was found that the three networks outperform SVMs – with both linear and RBF kernels - significantly in terms of classification accuracy. The results also show that the method generalizes well to unknown environments. Encode outperforms ResNet and FCN, but only by a very small margin.

From a on-device computation perspective, these approaches have an advantage over methods that extract features, since the latter requires feature extraction from the CIR. On the other hand, the CNN requires more computations than a linear classifier like a SVM with a linear kernel.

Unsupervised Learning: unlike supervised learning that requires labeled data for classification, unsupervised learning does not. Recent unsupervised learning algorithms have been used for NLOS classification. The identification method in [71] relies on an Expectation Maximization Gaussian Mixture Model (EM-GMM) model for classification. The model relies on three features: mean excess delay, RMS delay spread and number of paths which contain more than 85% energy of the received signal. LOS and NLOS features are used to model a GMM. To discriminate LOS and NLOS signals, the GMM parameters - mean vectors, covariance matrices and mixing coefficients – must be estimated. This is done using the Expectation Maximization algorithm [71]. Compared to SVMs, the algorithm has a faster execution time, but has a lower classification accuracy.

Typically, the NLOS identification problem is modeled as a binary classification problem to predict whether a channel is LOS or NLOS. This requires labeling data from both LOS and NLOS conditions. A One-Class SVM for NLOS identification proposed in [72] only requires training with LOS. The results show that the performance is lower than SVMs. This kind of classifier classifies NLOS samples as 'outliers' since it is only trained to identify LOS conditions.

In machine learning, NLOS mitigation is modeled as a regression problem. Similar to NLOS identification, channel statistics are extracted from LOS and NLOS channels, but are used to train regression models instead of classification models. The work in [65] collected several impulse responses for NLOS and LOS links to train a Least Squares Support Vector Machine (LS-SVM) regressor to estimate the NLOS ranging error. The work in [64] followed a similar approach but used a Least Square Support Vector Machine Regressor (LS-SVMR), a Gaussian Process Regressor and a Hypothesis testing Regressor. The work in [73] used a Relevance Vector Machine.

2.5.8 Fuzzy logic

The fuzzy inference approach also requires channel statistics, but since it is a rule-based method, there is no training step. The fuzzy inference system in [74] uses three channel statistics from the CIR: RSS, first path power strength and rise time. The output is an estimate of the ranging error according to the rule set of the fuzzy inference system. Estimation of this error allows correction of NLOS ranges. Each parameter is labeled as very low, low, medium, high and very high according to the severity of NLOS condition. For instance, for a severe NLOS condition with a high ranging error, the rise time is high, and both RSS and first path power strength are low. The performance of the method is evaluated for both Gaussian and Triangle member functions, and it was found that it has good performance. Note that this method does not require prior knowledge of LOS or NLOS. Compared with other mitigation methods, this is less complex since although it relies on channel statistics, there is no training step required like in machine learning algorithms.

2.5.9 Identify-and-discard

The simplest form of NLOS mitigation is to discard any ranges identified as NLOS. However, this is not viable in cases where only three range measurements are available, since a minimum of three range measurements are required to estimate a 2D location. Secondly, if only NLOS range measurements are available, then it is not possible to estimate the location if all range estimates are discarded.

2.5.10 Overview of NLOS identification and mitigation methods

Figure 2.6 shows the categories of NLOS approaches described above.

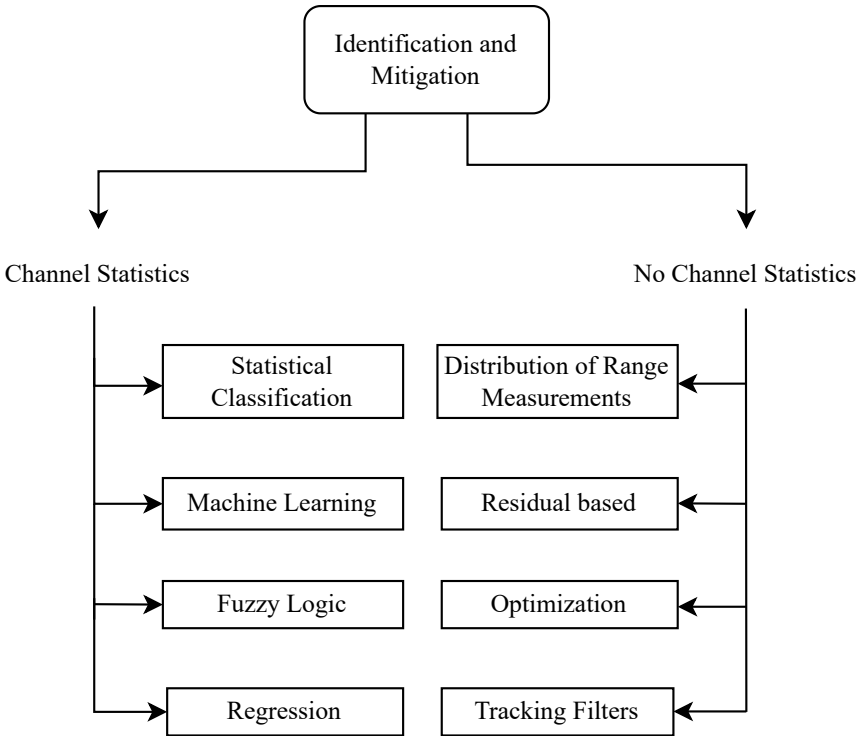

Figure 2.6. Summary of NLOS Identification and Mitigation Methods.

Table 2.3 summarizes some of the properties of the NLOS mitigation approaches discussed above. Note that complexity here does not only refer to time complexity, but also to whether specialized solvers are required. For machine learning - since it is assumed that training is done offline - only the inference complexity is considered. For SVMs with a linear Kernel, for instance, this is $O(n)$, where n is the number of features, while for Random Forests it is $O(np)$, where p is the number of decision trees. Three levels for complexity are defined: Low refers to localization algorithms that only require square roots, multiplication, division, addition and subtraction operations; Medium refers to the algorithms that also rely on matrices; and High refers to algorithms which also require specialized solvers, such as the case of localization using SDP [12]. The Type column refers to whether the algorithm relies on range measurements or requires location estimates.

2.6 CHAPTER SUMMARY

This chapter presented on overview of the state-of-the-art of NLOS identification and mitigation, and introduced ranging and localization concepts for localization in NLOS conditions. Several requirements for indoor localization, and how these are affected by NLOS conditions, were discussed. Key concepts

Table 2.3. Summary of NLOS identification and mitigation methods.

Category	**Channel Statistics Required?**	**Complexity**	**Type**	**Mobility Required?**
Machine Learning	Yes	- Medium to High (depends on classification/regression algorithm) - Linear classifiers are easily implemented but CNNs require specialized libraries	Range	No
Fuzzy Logic	Yes	- Low, since it is a rule-based method - Fast	Range	No
Residual Based	No	- Simple implementation, but high time complexity due to computation of combinations of anchor sets	Location	No
Optimization	No	- High computational complexity, particularly for SDP-based methods which require specialized solvers	Location	No
Tracking Filters	No	- Low to Medium. Kalman filters have simple implementation but particle filters are more complex - Fast	Range and Location	Yes

regarding ranging and localization necessary to understand the work in Chapters 3-6 were also introduced. Differences between localization methods were discussed, and a comprehensive discussion of state-of-the-art of NLOS identification and mitigation methods was presented. It was concluded that novel methods that do not rely on channel statistics nor distribution of range measurements, and have low computational complexity, have to be investigated.

CHAPTER 3 NON-LINE-OF-SIGHT IDENTIFICATION WITHOUT CHANNEL STATISTICS

3.1 CHAPTER OVERVIEW

This chapter proposes a NLOS identification method based on distance residuals. The concept of distance residuals in LOS and NLOS conditions is first described, and subsequently used to develop a NLOS identification method. Since residual based NLOS identification is done at the localization layer, individual NLOS ranges are not readily identifiable. The proposed method enables identification of individual NLOS ranges where the number of LOS ranges exceeds the number of NLOS ranges by at least three. In Section 3.2, the motivation for the work in this chapter is given, and the context of the work is described. Section 3.3 explains the concept of distance residuals and how they are used for NLOS identification. The calculation of distance residuals in 2D explained in detail. Section 3.4 discusses the simulation setup. In Section 3.5, the simulation results are discussed. The proposed method is evaluated for various numbers of anchors and random tag locations. Concluding remarks are given in Section 3.6. Finally, a summary of the chapter is provided in Section 3.7.

3.2 INTRODUCTION

Accurate localization is useful for a number of applications in industry [75], [76], [77]. Ideally, low power technologies such as Bluetooth [78], [79] or Ultra-wideband are used for localization, but several challenges exist [14]. In particular, NLOS propagation causes ranging errors and reduces location accuracy significantly [36], [80]. To improve location accuracy in NLOS conditions, NLOS

identification is an intermediate step in many NLOS mitigation techniques [81]. However, most of the NLOS identification methods investigated in literature rely on channel statistics. Although statistics based NLOS identification has been extensively researched, some limitations exist with the application of these methods in sensor networks. Firstly, this approach requires measurement campaigns, where statistics have to be collected for different types of environments since statistics extracted from a dataset collected in a residential environment, for instance, might not be suitable for NLOS identification in a harsh industrial environment. Secondly, statistics extracted from RF channels cannot be directly applied to positioning systems that are not RF based since the communication channels are fundamentally different. Therefore, a shift towards NLOS identification approaches that do not rely on channel statistics is beneficial.

In this chapter, an alternative method for NLOS identification that requires no channel statistics is investigated. Distance residuals are obtained at the localization level and not at the ranging level, therefore they are agnostic to the wireless technology in PHY layer. Such an approach provides several benefits over the conventional statistics based approach. Firstly, for standards like IEEE 802.15.4a where channel statistics can be extracted from exposed channel impulse responses, these features have to be extracted and NLOS identification has to be done on the device since it is not feasible to send the information to a central location engine, especially in large scale sensor networks. Secondly, statistics have to be characterized for different environments, which require measurement campaigns that can be impractical. Therefore, a method that is able to identify NLOS on the device but does not require additional statistics other than ranging data is preferable. The goal of this work is to investigate such a method. Similar to statistics based NLOS identification, the method investigated in this chapter uses machine learning, but instead of relying on statistics extracted from LOS and NLOS channels, it relies on distance residuals. It is shown that the difference in NLOS classification accuracy between the convex-hull region enclosed by the anchors and outside this convex-hull region is small. It is also shown that similar to the statistics based method, individual NLOS ranges can be identified.

3.3 PROPOSED METHOD

3.3.1 Distance residuals

Given a sensor network with N anchors and a node, i.e. tag, the measured distance between the i-th anchor and node, is given by:

$$\hat{d}_i = d_i + b_i + n_i \tag{3.1}$$

where d_i is the true distance between anchor i and the node, b_i is the NLOS ranging bias caused by an obstruction between the node and anchor i, and n_i is ranging noise with Gaussian distribution $\mathcal{N}(0, \sigma^2)$. The 2D location of a node can be determined by solving the following system of equations for the node's location $[x\ y]^T$:

$$(x_i - x)^2 + (y_i - y)^2 = \hat{d}_i^2, i = 1, ..., N \tag{3.2}$$

where (x_i, y_i) is the fixed and known location of the i-th anchor and $\hat{d}_i$ is the measured distance between the node and the i-th anchor in (3.1). The node's location can be estimated by minimizing the following objective function:

$$\hat{x}, \hat{y} = \min_{x,y} \sum_{i=1}^{N} ((x_i - x)^2 + (y_i - y)^2 - \hat{d}_i^2)^2 \tag{3.3}$$

According to (3.1), the distance measurement $\hat{d}_i$ includes noise n_i and a positive bias b_i due to NLOS conditions. The distance residual δ is given by:

$$\delta_i = l_i - \hat{d}_i \tag{3.4}$$

where l_i is the Euclidean distance between anchor i and the tag's location estimated in (3.3), and $\hat{d}_i$ is the measured distance between anchor i and tag given in (3.1). The sum of the squares of distance residuals (SSDR) is given by [48]:

$$\Delta = \sum_{i=1}^{N} \delta_i^2 \tag{3.5}$$

where N is the number of anchors and δ_i is calculated in (3.4). Figure 3.1 illustrates residuals for NLOS ranges. The tag's location is estimated using (3.3). The measured distance d_i is the radius of the circle centered at anchor i. In the ideal case where all ranges are LOS and have no ranging noise, the tag's location is a single point of intersection of the three circles illustrated in Figure 3.1, resulting in a value of zero for all residuals δ_i.

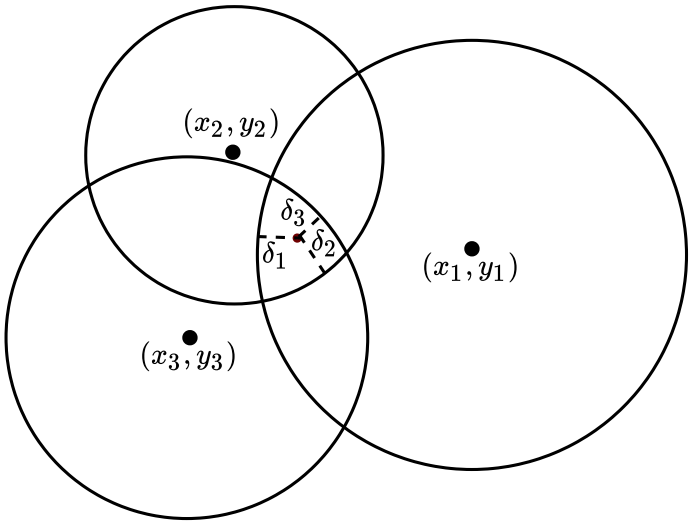

Figure 3.1. Distance residuals: NLOS conditions. Taken from [82], © 2020 IEEE.

3.3.2 Classification

In literature, NLOS identification methods that use machine learning typically rely on features extracted from received signals or channel impulse responses [62]. In this work, the following features are considered:

SSDR: the sum of the squares of distance residuals Δ defined in (3.5).

Mean and standard deviation: the mean and standard deviation of all N distance residuals per location estimate.

Maximum: the largest distance residual among all N distance residuals per location estimate. These features are extracted from the simulation for 3 to 8 anchors (see Section 3.4 for more details) for both LOS and NLOS. The correlations between features are shown in Table 3.1. Since all features are highly correlated and therefore redundant, only the SSDR is selected. Motivated by the fact that only a single feature is used, a Naïve Bayes Classifier is used to classify location estimates into LOS or NLOS.

Table 3.1. Correlation matrix for features.

	SSDR	**Mean**	**Std. Dev.**	**Maximum**
SSDR	1.0	0.90	0.67	0.86
Mean	0.90	1.0	0.77	0.96
Std. Dev.	0.67	0.77	1.0	0.92
Maximum	0.86	0.96	0.92	1.0

3.3.3 Identification of individual NLOS ranges

It is noted that channel statistics based NLOS identification methods work at ranging level, where NLOS identification is done per ranging measurement. With distance residuals, identification is done at the localization level, therefore it is known that at least one of the ranges is NLOS, but no information about which specific ranges are NLOS is provided. However, in some cases, it is possible to determine which ranges are NLOS if these criteria are met: there are more than three anchors, i.e. $N > 3$, and there are at most $N-3$ NLOS ranges. Consider an example with four anchors where $N = 4$. Given four anchors, there are four possible sets of three anchors: $S_1 = \{1,2,3\}$, $S_2 = \{1,2,4\}$, $S_3 = \{1,3,4\}$ and $S_4 = \{2,3,4\}$, where the integers in each set denote anchors 1 to 4. The four SSDRs corresponding to each set are computed as follows:

$$\begin{aligned} \Delta_{123} &= \delta_1^2 + \delta_2^2 + \delta_3^2 \\ \Delta_{124} &= \delta_1^2 + \delta_2^2 + \delta_4^2 \\ \Delta_{134} &= \delta_1^2 + \delta_3^2 + \delta_4^2 \\ \Delta_{234} &= \delta_2^2 + \delta_3^2 + \delta_4^2 \end{aligned} \tag{3.6}$$

Assuming that d_1 is the only NLOS range, and that d_2, d_3 and d_4 are all LOS ranges, Δ_{234} will be classified as LOS since none of its ranges are NLOS, and the remaining SSDRs will be classified as NLOS. Table 3.2 shows the predictions for different NLOS ranges, assuming only one range is NLOS and the classifier has a prediction accuracy of 100% for each SSDR.

Table 3.2. Predictions if only one range is NLOS.

NLOS Range	Δ_{123}	Δ_{124}	Δ_{134}	Δ_{234}
d_1	NLOS	NLOS	NLOS	LOS
d_2	NLOS	NLOS	LOS	NLOS
d_3	NLOS	LOS	NLOS	NLOS
d_4	LOS	NLOS	NLOS	NLOS

Therefore, if only one of the four ranges is NLOS, it is possible to identify which range it is by classifying the four SSDRs and selecting the corresponding NLOS range according to Table 3.2. It is noted that in cases where there is more than one NLOS range, all four SSDRs will be classified as NLOS since all sets of anchors have at least one NLOS range. This is the basis of the algorithm to identify individual NLOS ranges described in Figure 3.2. In summary, the identification of individual NLOS ranges is done by calculating all SSDRs using (3.6), and then classifying them into LOS or NLOS using a Naïve Bayes classifier. Because in practical scenarios the NLOS classification accuracy is not 100% (see Table 3.4), there can be incorrect predictions, which ultimately affect how accurately individual NLOS ranges are identified.

3.4 SIMULATIONS

The anchor locations for the simulation are shown in Figure 3.3. The simulations were carried out for different sets of anchors, ranging from 3 to a total of 8 anchors. Table 3.3 shows each set of anchors and their respective 2D coordinates. For each set of anchors, 2000 location estimates with LOS ranges and 2000 location estimates with at least one NLOS range and at most $N-1$ NLOS ranges are generated. This is done for Region I and Region II, resulting in a total of 8000 location estimates.

Region I is the region enclosed by the anchors, i.e. the convex-hull, bounded by the inner square in Figure 3.3. The region bounded by the outer square (but excluding Region I) is defined as Region II. It is expected that classification accuracy is higher in Region I because the assumption of inconsistent

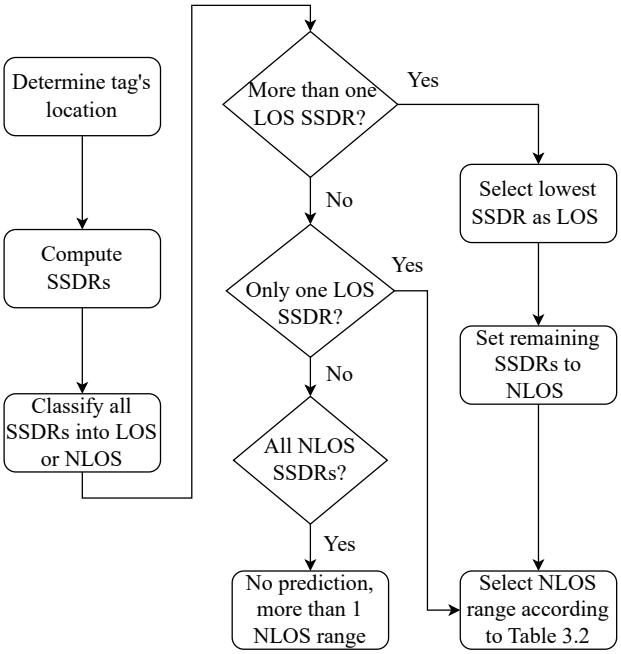

Figure 3.2. Description of algorithm to identify individual ranges for four anchors. Taken from [82], © 2020 IEEE.

localization does not always hold in Region II [48], which can lead to a large number of NLOS estimates being incorrectly classified as LOS. Hence, the two regions are separated to determine the classification accuracy for each region.

For LOS locations, the bias b in (3.1) is set to 0 for all ranges. For NLOS locations, the bias is assumed to be larger than the ranging noise so that it can be differentiated from it. Therefore, bias b_i is generated from an uniform distribution with values that lie in the interval $5\sigma < b_i < 3.5$. The ranging noise is Gaussian distributed with $\mu = 0$ and $\sigma = 0.15$ m. These are appropriate values for TOA based technologies such as UWB and acoustic positioning. These values are listed in Table 3.3. The SSDRs are calculated from the LOS and NLOS locations generated in the simulation, and then used to train the classifier. The data is split into training (60%) and testing (40%) sets.

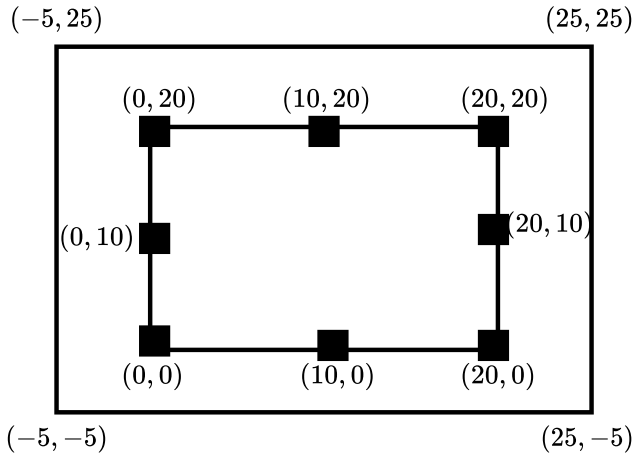

Figure 3.3. Anchor locations for simulations. Taken from [82], © 2020 IEEE.

Table 3.3. Simulation parameters.

Parameter	Values
Set 1 (3 anchors)	$(0,0),(0,20),(20,20)$
Set 2 (4 anchors)	$(0,0),(0,20),(20,20),(20,0)$
Set 3 (5 anchors)	$(0,0),(0,20),(20,20),(20,0),(20,10)$
Set 4 (6 anchors)	$(0,0),(0,20),(20,20),(20,0),(20,10),(10,20)$
Set 5 (7 anchors)	$(0,0),(0,20),(20,20),(20,0),(20,10),(10,20),(0,10)$
Set 6 (8 anchors)	$(0,0),(0,20),(20,20),(20,0),(20,10),(10,20),(0,10),(10,0)$
Bias b distribution	$\mathcal{U}(0.75, 3.5)$
Noise n distribution	$\mathcal{N}(0.0, 0.15^2)$

3.5 RESULTS AND DISCUSSION

3.5.1 Classification

Two metrics are used to evaluate the performance of the classifier:

Classification Accuracy: sum of true positives and true negatives, divided by the total number of instances.

F1 Score:

$$\mathbf{F1} = \frac{2 \cdot \mathbf{PR} \cdot \mathbf{RC}}{\mathbf{PR} + \mathbf{RC}} \tag{3.7}$$

where precision (**PR**) is the ratio of true positives to the sum of true and false positives, and recall (**RC**) is the ratio of true positives to the sum of true positives and false negatives. Table 3.4 shows the classification results for Region I and Region II.

Table 3.4. Classification accuracy and F1 Score for NLOS identification in Region I (top) and Region II (bottom).

Number of Anchors	**3**	**4**	**5**	**6**	**7**	**8**
Classification Accuracy (%)	97.24	98.71	99.09	99.16	99.29	99.33
F1 Score (%)	96.76	98.63	99.03	99.10	99.24	99.35
Classification Accuracy (%)	88.48	97.28	98.86	98.80	98.07	99.29
F1 Score (%)	88.25	97.31	98.89	98.63	98.11	99.25

When only three anchors are used, the classification accuracy for Region II is significantly lower than the classification accuracy in Region I. This is because the low number of anchors can easily lead to NLOS location estimates with consistent localization, where the biases cause NLOS location estimates that geometrically resemble LOS location estimates. However, as the number of anchors increases, the probability of consistent localization in Region II decreases because there are more NLOS biases present, therefore increasing the classification accuracy in Region II.

For Region I, the classification accuracy improves slightly as the number of anchors increases, as shown in Figure 3.4. This is because the SSDR increases with increased number of anchors, i.e. the SSDRs add up, resulting in a greater distinction between LOS and NLOS. Figure 3.5 shows a scatter plot of location errors and SSDR for eight anchors, and it is observed that all NLOS location estimates have a SSDR larger than 0.5.

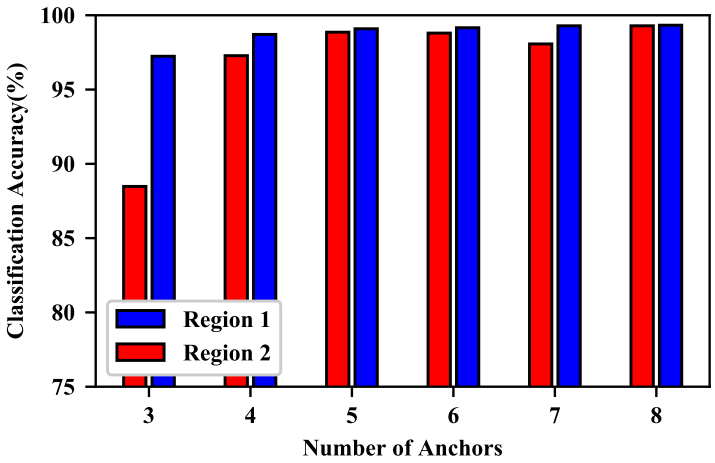

Figure 3.4. Classification accuracy for different number of anchors. Taken from [82], © 2020 IEEE.

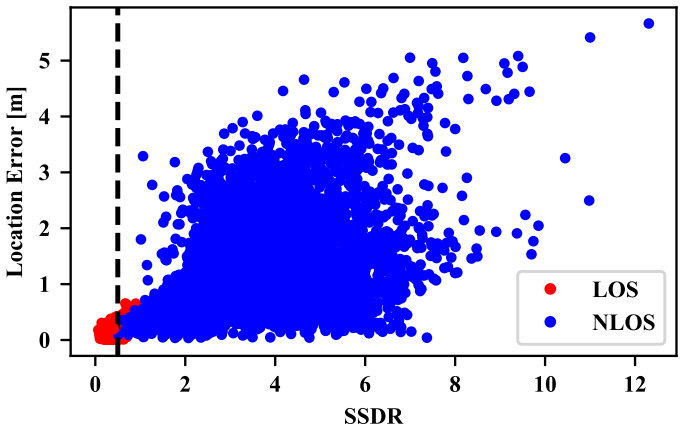

Figure 3.5. Location errors vs SSDR in Region I for eight anchors. Taken from [82], © 2020 IEEE.

3.5.2 Identification of individual NLOS ranges

For individual NLOS range identification, the classification accuracy is defined as the number of instances where the correct bias is correctly identified, divided by the number of total instances. This was tested for four anchors. The classification accuracies are 76% and 69% for Region I and Region II, respectively. These classification accuracies are relatively low because all four SSDRs for the four sets of anchors described in Table 3.2 have to be correctly classified into LOS or NLOS. However, as the results in Table 3.4 show, the prediction accuracy of the classifier used to classify SSDR into LOS or NLOS is not perfect. Therefore, if any of the SSDRs are not correctly classified, then an incorrect bias is selected, affecting classification accuracy considerably.

3.6 CONCLUSION

The use of distance residuals for NLOS identification was investigated in this chapter. The motivation for this approach is that unlike other approaches in literature, it does not rely on channel statistics. Via simulations, it was shown that the sum of the squares of distance residuals can be used to identify the presence of NLOS ranges and in some cases, identify which specific ranges are NLOS. For future work, the approach will be evaluated using experimental datasets and identification of individual ranges for more than four anchors will also be evaluated. It is also of interest to investigate the performance of this approach for RSS based positioning systems, which often rely only on RSS and have no access to other PHY parameters.

3.7 CHAPTER SUMMARY

This chapter proposed a NLOS identification method based on distance residuals. The method was evaluated via simulations and it was shown that NLOS location estimates are detected with high accuracy.

Section 3.2 motivated and described the context of the work presented in the chapter. Section 3.3 introduced the concept of distance residuals, and how they are used for NLOS identification. Section 3.4 explained the simulation setup. In Section 3.5, the proposed method was evaluated via simulations and it was found that the proposed method can identify NLOS conditions with high accuracy without knowledge of channel statistics. When specific criteria are met, individual NLOS ranges can also be identified. Concluding remarks were given in Section 3.6.

CHAPTER 4 CLASSIFICATION OF NLOS CONDITIONS USING MULTIPLE CHANNELS

4.1 CHAPTER OVERVIEW

This chapter proposes a NLOS classification method for through-the-wall (TTW) and around-the-corner (ATC) conditions. The method is evaluated experimentally, and the results show that these two types of NLOS conditions can be distinguished with high accuracy using features extracted from multiple channels.

Section 4.2 motivates and explains the context of the work in the chapter. Section 4.3 explains the characteristics of NLOS conditions caused by TTW and ATC propagation. Section 4.4 describes the experimental setup and protocol. Section 4.5 discusses the classification results. The conclusion is given in Section 4.6. Finally, a summary of the chapter is given in Section 4.7.

4.2 INTRODUCTION

Localization is required for many use cases in a variety of applications. Although accurate and precise localization is possible in LOS conditions, it is still a challenge in NLOS conditions. In industrial environments, specifically, NLOS identification is important. Various NLOS identification and mitigation algorithms have been investigated for industrial environments [83], [84] for productivity and safety purposes.

Typical NLOS conditions in many indoor and industrial scenarios are often caused by ATC propagation conditions which occur often in underground tunnels and warehouses where there is limited visibility. The direct path is often attenuated to such an extent that the receiver cannot detect it, therefore the range between transmitter and receiver is estimated based on a reflected path, resulting in large ranging errors [39]. A typical use case in these scenarios is collision avoidance, where failure to detect these conditions can result in fatalities because the system can indicate a large distance between transmitter and receiver due to ATC propagation, when in fact they are much closer. In such cases, the quality of ranging estimates degrades according to the severity of the NLOS condition, particularly if the direct path between transmitter and receiver is not detectable.

Another type of NLOS condition that is predominant in indoor scenarios is caused by TTW propagation, where the direct path is obstructed, but still detectable at the receiver. In this case, ranging errors are caused by the difference in relative permittivity between air and the wall, and are introduced in the distance estimate when the measured TOF is converted from time to distance. Ranging errors caused by TTW are usually smaller than ATC, and are typically proportional to the thickness of the wall. It is of interest to distinguish between these two types of NLOS conditions, since it can enable the selection of an appropriate NLOS error mitigation strategy for each case. For instance, a technique that mitigates errors caused specifically by TTW propagation requires identification before mitigation [80]. Similarly, the ability to identify ATC conditions can aid localization in scenarios like intersections in underground mining tunnels. Several papers in literature have focused on the NLOS identification problem. This work focuses on classifying the type of NLOS condition into one of two predominant NLOS conditions in indoor scenarios: ATC or TTW. The work in [80] discussed TTW NLOS conditions, but focused on the mitigation aspect only, and not on the identification of TTW NLOS conditions. Multipath statistics have been analyzed in indoor scenarios, and it has been highlighted that the magnitude of ranging errors depends on the severity of the NLOS condition, particularly in cases where the direct path is not detectable [39]. To investigate this further, a measurement campaign in a variety of ATC and TTW scenarios was performed. The contributions of this chapter are:

- The results show that TTW and ATC NLOS conditions can be differentiated with high accuracy using machine learning classifiers. The results are supported by experimental data obtained from measurement campaigns using IEEE 802.15.4a compliant UWB devices,
- The impact of channel selection on classification accuracy is investigated. This is motivated by the fact that TTW and ATC conditions have propagation properties which can manifest

differently depending on the channel's center frequency. In particular, the results show that higher classification accuracy is obtained when using features extracted from a channel with a higher center frequency and that extracting features from multiple channels enables less complex classifiers,

- The results show that high classification accuracy is achievable with linear classifiers which have low inference complexity. This encourages the use of simpler machine learning classifiers, which is an important step towards real-time NLOS classification in resource-constrained edge devices.

The proposed method exploits the fact that UWB channels have large differences in center frequencies between the low and high bands. This allows more detailed characterization of propagation conditions due to diversity, and can therefore improve NLOS classification. Features are extracted from two channels (one in the low band and one in the high band) and feature selection is used to train better classifiers with less features than the case where only a singular channel is used.

4.3 THROUGH-THE-WALL VS AROUND-THE-CORNER PROPAGATION

This section discusses differences in propagation between ATC and TTW conditions to provide more context about the features described in Section 4.4.

4.3.1 Through-the-wall

In TTW scenarios, RF waves are affected by refraction (as illustrated in Figure 4.1), and NLOS ranging errors are in the order of the wall's thickness [39]. RF waves are refracted because of the difference in permittivity between the wall's material and air. This refraction results in a larger propagation time of the wave through the wall in comparison to air, and its impact on the measured TOF is dependent on frequency. Since the IEEE 802.15.4a standard supports channels in the sub-GHz, 3244–4742 MHz (low) and 5944–10234 MHz (high) bands [7], measured ranges in TTW scenarios under different channels can be different, particularly if the channels' center frequencies are far apart. Figure 4.2 shows measured NLOS ranging biases for Channel 2, which has a center frequency of 3.9 GHz, and Channel 5, which has a center frequency of 6.5 GHz. These measurements were taken for a wall with a thickness of 35 cm, and were collected with a fixed transmitter TX and a mobile receiver RX, with

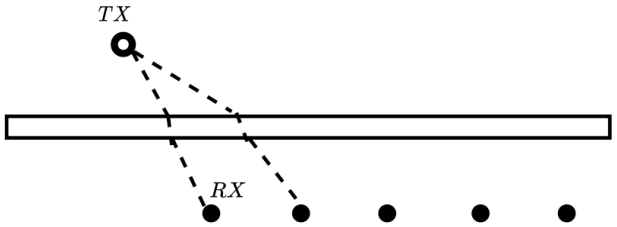

Figure 4.1. TTW Scenario: 2D plan view of a wall obstructing the communication path between an anchor TX and multiple tags RX.

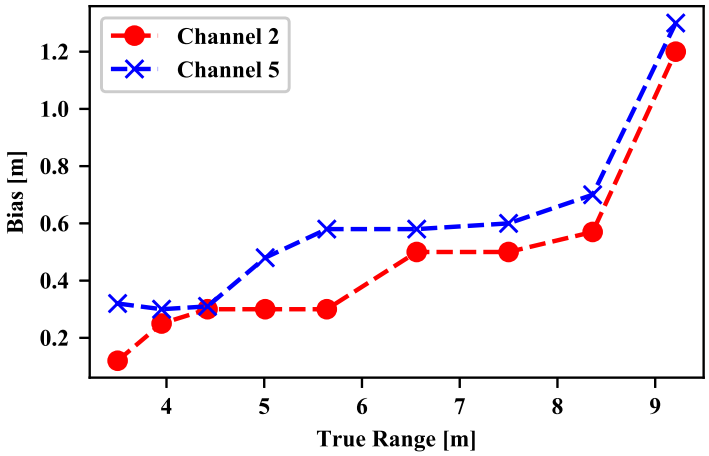

Figure 4.2. NLOS ranging biases for Channel 2 and 5 for a TTW scenario.

locations as illustrated in Figure 4.1. It is evident that the NLOS biases are mostly similar, with a maximum difference of less than 50 cm between the two channels.

4.3.2 Around-the-corner

In ATC scenarios, reflections are the dominant form of propagation. In cases where the transmitter and receiver are close, such as in the path between TX and RX illustrated in Figure 4.3, it is possible that ranging occurs through the wall, if the receiver is relatively close and is able to detect the attenuated direct path. However, if the transmitter and receiver are farther apart, as illustrated by the second path between TX and RX in Figure 4.3, the direct path between them is obstructed and only reflections are detected at the receiver. It is evident that the reflected paths are longer than the true distance between the nodes, especially if the distance between walls is large. Because propagation characteristics of RF waves are dependent on frequency, different reflected paths can be detected on different channels.

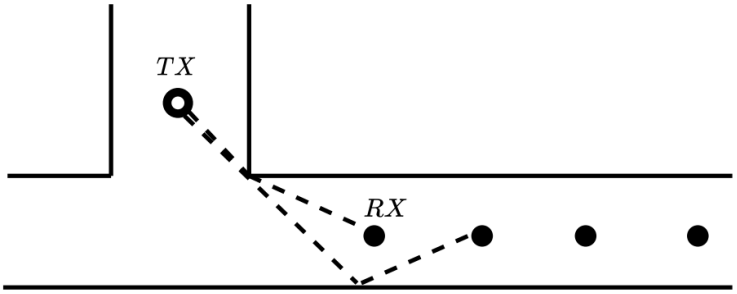

Figure 4.3. ATC Scenario: 2D plan view of a typical ATC scenario between an anchor TX and multiple tags RX.

Furthermore, since RF waves with lower frequencies propagate for longer distances, it is possible that in ATC scenarios, ranging occurs through the wall for the lower frequency channel and through a reflected path (if the direct path has been completely attenuated) for the higher frequency channel, again resulting in a large difference between NLOS ranging biases. In both cases, larger differences in NLOS ranging biases between channels are observed. Measurement results for NLOS biases in a typical ATC scenario are shown in Figure 4.4. It is seen that the difference in biases in Figure 4.4 is much larger than the difference in Figure 4.2. This is due to the fact that the higher attenuation in Channel 5 results in undetected direct paths between TX and RX, therefore ranging is done via reflected paths. Ranging in Channel 2, however, is still possible via attenuated direct paths.

The CIR shown in Figure 4.5 demonstrates more differences between TTW and ATC conditions. Due to the higher attenuation in ATC scenarios, it is expected that the maximum amplitude of the CIR will generally be lower than TTW scenarios, particularly if the ATC condition is severe. Additionally, in ATC scenarios where the first path is very attenuated but still detectable, the path with the maximum amplitude (a reflected path) is typically observed later compared to the first path. In contrast, the first path for the majority of TTW conditions is the same as the maximum path, since all paths are attenuated by the wall. Therefore, by extracting features of CIRs from different channels, it is possible to leverage all these characteristics to improve NLOS classification accuracy.

4.3.3 Through-the-wall and around-the-corner in industrial environments

ATC scenarios occur often in industrial environments. In underground mines, for instance, they often occur in tunnel intersections. Since RF waves do not propagate through rock, ranging in these cases is

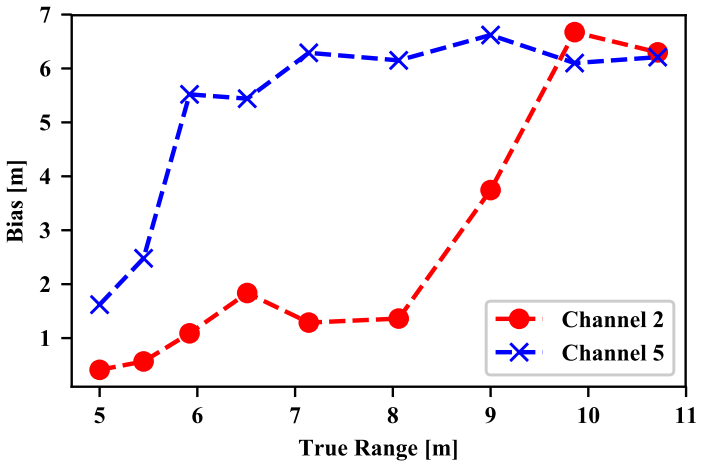

Figure 4.4. NLOS ranging biases for Channel 2 and 5 for an ATC scenario.

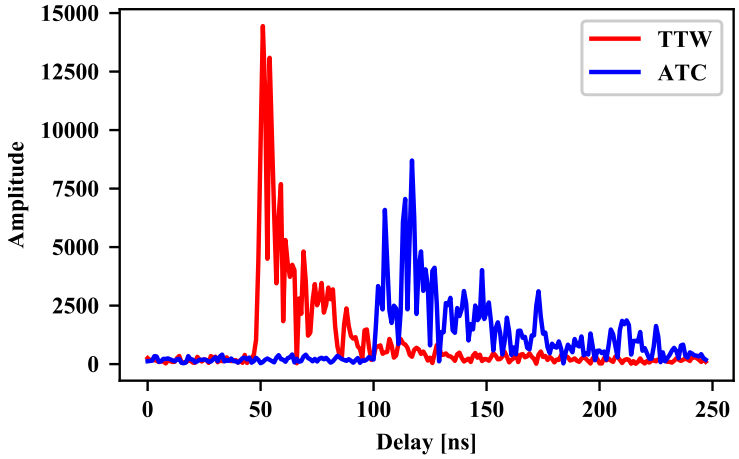

Figure 4.5. Comparison of TTW and ATC CIRs.

done mostly via reflections. Another good example is propagation in warehouses. Forklifts, and other mobile equipment, often have to navigate between shelves and RF waves can be affected by reflection from metal and by absorption by material such as paper [85], which completely attenuates the direct path. For both examples mentioned above, it is important to detect these ATC conditions, particularly in cases where ranging and localization are used for safety applications. TTW and ATC classification can also improve navigation of drones used in surveillance, which often require high accuracy localization. Since GPS is not reliable indoors, UWB localization with TTW and ATC classification can improve localization for drones in NLOS conditions.

4.4 DESCRIPTION OF EXPERIMENTS

4.4.1 Experimental setup and protocol

There have been studies on NLOS identification that extracted channel statistics from IEEE 802.15.4a channel models. Although this approach offers good insight into NLOS, a measurement campaign using real UWB devices is motivated by the fact that it is more realistic to characterize these two types of NLOS conditions using real channel measurements. The measurement campaign was conducted in two buildings at a university campus. The first is a building with lecture halls and offices built several decades ago. In this building, the measurements were conducted in an underground floor with narrow corridors and relatively low ceilings. The second building is a modern building - built less than a decade ago - with large lecture halls, very high ceilings and large corridors. Two different buildings where selected to avoid the data being biased towards any specific building. In each building, measurements were conducted for 2 TTW and 2 ATC scenarios. All TTW measurements were taken over solid walls, with a thickness of at least 25 cm. Since only ranging measurements are required, two EVB1000 evaluation boards equipped with DW1000 UWB radios were used: one configured as a tag *RX* and the other configured as an anchor *TX*. Both devices were mounted on tripods, with their antennas fixed at a height of 1.2 meters. Both were configured with the parameters listed in Table 4.1. A Raspberry Pi was connected to the tag and configured as a wireless access point to wirelessly connect to a laptop to save all received data for posterior offline analysis.

For each scenario, the anchor was kept at a fixed location and the tag was moved to different *RX* locations (about one meter apart from each other) for TTW and ATC scenarios, as illustrated in Figure 4.1 and 4.3, respectively. For each scenario, measurements were collected for at least 8 *RX* locations. The tag locations were selected such that CIRs for different incidence angles between anchor and tag are logged.

For each *RX* location, around 150 CIRs per channel were collected at the tag. Channel 2 and Channel 5 were selected as the radios are calibrated for these two channels by default, and since there is a difference of over 2 GHz between the two channels, it is expected that this is a sufficient difference in center frequency to observe the characteristics discussed in Section 4.3. In some cases where the receiver struggled to decode incoming packets due to the obstructions between transmitter and receiver,

less than 150 CIRs packets were logged. The complete dataset from the measurement campaign consists of 19520 channel impulse responses, of which 47% are in the TTW category and 53% are in the ATC category. The data was pre-processed by removing the mean and scaling to unit variance, and subsequently used to train the classifiers described in Section 4.4.3. The dataset was split into training (60%) and testing (40%) sets. Figure 4.6 shows one of the TTW conditions and Figure 4.7 shows one of the ATC conditions from the measurement campaign. Both illustrate typical conditions.

Figure 4.6. Example of TTW scenario. Anchor and tag on opposite sides of a wall.

Figure 4.7. Tag and anchor in an ATC scenario.

Table 4.1. Configuration of DW1000 radios for measurement campaign.

Parameter	Channel 2	Channel 5
Center Frequency	3.9 GHz	6.5 GHz
Data rate	110 kbps	110 kbps
Pulse Repetition Frequency	64 MHz	16 MHz
Preamble Length	1024	1024
Preamble Code	9	3
SFD	Non-standard	Non-standard

4.4.2 Feature extraction

Two kinds of features are used to differentiate between ATC and TTW conditions: metrics which assess the quality of the received signal which are readily accessible via the DW1000's internal registers; and features extracted from the measured CIR that is logged in the DW1000's accumulator and can be read via serial peripheral interface (SPI) by the host micro-controller. Since the default two-way ranging algorithm running on the EVB1000 devices requires several messages to be exchanged between tag and anchor per ranging estimate, only the CIR from the last frame received at the tag during a two-way ranging exchange is logged. The following features are used.

Range: the two-way range between anchor and tag measured with the default Symmetric Double Sided Two-way Ranging (SDS-TWR) algorithm. As illustrated in Figure 4.2 and Figure 4.4, ranges estimated on Channel 2 and 5 are relatively similar in TTW conditions, but can differ up to several meters in ATC conditions.

Path Amplitudes $F1$, $F2$ and $F3$: the amplitudes of the paths of the measured impulse response in the accumulator. $F1$ is the magnitude of the detected first path. $F2$ and $F3$ are the magnitudes of the second and third paths after the first path, respectively. In general, these path amplitudes are expected to be larger in TTW scenarios, as shown in Figure 4.5.

First Path Power Level: the power level in the first detected path in dBm, given by:

$$FPPL = 10\log_{10}\left(\frac{F1^2 + F2^2 + F3^2}{N^2}\right) - A \tag{4.1}$$

where $F1$, $F2$ and $F3$ are the path amplitudes discussed above, N is the preamble accumulation count value and A is either 113.77 or 121.75, for a pulse repetition frequency (PRF) of 16 MHz or 64 MHz, respectively. $F1$, $F2$, $F3$ and N are directly read from the DW1000's internal registers. The power levels in TTW conditions are expected to be high, and significantly lower in ATC conditions, particularly in cases where the direct path is not detectable.

Received Power Level: the power level in the received signal level in dBm, given by:

$$RXPL = 10\log_{10}\left(\frac{C \times 2^{17}}{N^2}\right) - A \tag{4.2}$$

where C is the channel impulse response power, N is the preamble accumulation count value and A is either 113.77 or 121.75, for a PRF of 16 MHz or 64 MHz, respectively. C is read from the DW1000's internal registers.

Features are also extracted from the CIR. The DW1000 radio logs the channel impulse response in imaginary and real samples, which can be read from the device's registers for every received frame. The corresponding magnitude of the CIR is calculated from the real and imaginary samples as follows:

$$\left|h(t)\right| = \sqrt{h_i^2 + h_r^2} \tag{4.3}$$

where h_i are the imaginary samples and h_r are the real samples of the complex impulse response in the device's accumulator. Given the radio configuration in Table 4.1, the magnitude of the CIR calculated in (4.3) is 1016 samples long for Channel 2 and 992 samples long for Channel 5. Only the last 248 samples for magnitude of the CIR computed in (4.3) are used for feature extraction because the first 744 and 768 samples for Channel 2 and 5, respectively, precede the first path and contain no significant multipath information. The features described below are then extracted from $\left|h(t)\right|$ to characterize TTW and ATC conditions. These features capture the characteristics of CIRs illustrated in Figure 4.5.

The mean of $|h(t)|$, for instance, is expected to be larger for TTW conditions than for ATC conditions. The difference in shape between TTW and ATC CIRs is captured via kurtosis and skewness, which are statistical metrics that characterize how 'peaky' and symmetric a distribution is, respectively, and have been used for NLOS identification.

Mean and standard deviation: the mean and standard deviation of the magnitude samples obtained in (4.3).

Kurtosis:

$$\kappa = \frac{E\left[\left(|h(t)| - \mu_{|h|}\right)^4\right]}{\sigma^4} \tag{4.4}$$

where $\mu_{|h|}$ and σ are the mean and standard deviation of the CIR $|h(t)|$, respectively. Kurtosis describes how 'peaky' a distribution is.

Skewness:

$$S = \frac{E\left[\left(|h(t)| - \mu_{|h|}\right)^3\right]}{\sigma^3} \tag{4.5}$$

where $\mu_{|h|}$ and σ are the mean and standard deviation of the CIR $|h(t)|$, respectively. Skewness is an indicator of the asymmetry of a distribution.

Maximum Amplitude: the maximum amplitude (MA) of $|h(t)|$.

First to Maximum Path Delay: the difference in delay (nanoseconds) between the first path τ_F and the path with the maximum amplitude τ_M in $|h(t)|$, given by:

$$FMPD = \|\tau_M - \tau_F\| \tag{4.6}$$

For most TTW scenarios, it is expected that the $FMPD$ will be zero when the first path coincides with the maximum path, or a very small positive number otherwise. For ATC scenarios, particularly if the first path is not detectable, the $FMPD$ is expected to be larger since the maximum path does not coincide with the first path, as illustrated in Figure 4.5, where the difference between first and maximum path is about 25 nanoseconds for the ATC condition. To illustrate the difference in features between ATC and TTW, Figure 4.8 shows a histogram of $F2$ for Channels 2 and 5, and it is evident that the feature distributions for each class are statistically different and the two classes can easily be differentiated.

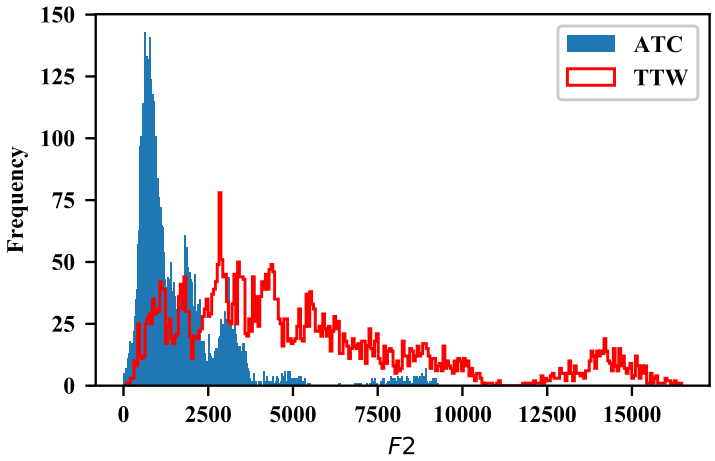

Figure 4.8. Histograms: comparison between the distribution of $F2$ for TTW and ATC conditions on Channel 5.

4.4.3 Classification

Several NLOS classification methods based on machine learning have been investigated. Since the focus of this work is on localization in sensor networks, classification methods that can be implemented on edge devices for two reasons are considered. Firstly, for large sensor networks, it is not practical to send extracted features from CIRs over the network to be centrally or remotely processed, therefore processing must be done on the device itself. Secondly, many use cases require real-time location, therefore NLOS classification should be executed on the device to minimize delays. Since edge devices are often resource-constrained, suitable machine learning classifiers include classifiers with low inference complexity such as linear classifiers which have simple decision functions that can be easily implemented in micro-controllers. To this end, the Naïve Bayes Classifier (NBC), Logistic Regression (LR) and Support Vector Machines (SVMs) are selected as classifiers. SVMs with radial

basis function (RBF) kernels are used for comparison with the linear classifiers mentioned above. It is emphasized that the goal here is not to use the most sophisticated algorithms for classification; it is to show that TTW and ATC can be accurately differentiated even if linear classifiers are used.

Naïve Bayes Classifier: the NBC is a probabilistic classifier based on Bayes' theorem. According to Bayes' theorem, the conditional probability is given by:

$$P(C_k|\boldsymbol{X}) = \frac{P(C_k)P(\boldsymbol{X}|C_k)}{P(\boldsymbol{X})} \tag{4.7}$$

where $\boldsymbol{X}$ is the input feature vector, C_k denotes a class, k is the class number, $P(C_k)$ is the prior probability of class C_k, and $P(\boldsymbol{X}|C_k)$ is the likelihood. The class predicted by the NBC is the class that corresponds to the maximum a posteriori (MAP) estimate computed over all classes:

$$\hat{y} = \underset{k\in\{1,\ldots,K\}}{\operatorname{argmax}}\ p(C_k)\prod_{i=1}^{n} p(x_i|C_k) \tag{4.8}$$

Although the NBC is not strictly a linear classifier, its decision function in (4.8) has similar complexity to decision functions for the linear classifiers mentioned below.

Logistic Regression: The Logistic Regression (LR) classifier is a linear classifier given by:

$$f(x) = \beta_0 + \beta_1 x_1 + \ldots + \beta_p x_p \tag{4.9}$$

where β_0 is the bias and x terms are the input features. Coefficients β_0 – β_p are estimated using maximum likelihood estimation (MLE). The probabilities are computed as:

$$P(C_k|\boldsymbol{X}) = \frac{1}{1+e^{f(x)}} \tag{4.10}$$

where the predicted class is the class that results in the larger of the probabilities calculated over the two classes. A positive class is predicted if $P(C_k|\boldsymbol{X})$ is larger than 0.5, otherwise the negative class is predicted.

Support Vector Machines: support vector machine classifiers attempt to find the separating hyperplane that maximizes the distance between support vectors. Using training data, the weights $\mathbf{w}$ are estimated using quadratic programming (QP) by minimizing the following objective function:

$$\begin{aligned} &\min_{\mathbf{w},b} \frac{1}{2}||\mathbf{w}||^2 \\ &\text{s.t.} \quad y_i(\mathbf{x}_i^T\mathbf{w}+b) \geq 1 \quad i=1,...,n \end{aligned} \tag{4.11}$$

where b is the bias. Once both $\mathbf{w}$ and bias b are estimated with training data, a prediction $y \in \{-1,1\}$ is made using the classifier as follows:

$$y = \text{sign}[\mathbf{w}^T\phi(\mathbf{x})+b] \tag{4.12}$$

where $\mathbf{x}$ denotes the input feature vector, y denotes the predicted label, and ϕ is a feature space transformation, e.g. radial basis function (RBF) in the case of the RBF kernel.

4.5 RESULTS AND DISCUSSION

To evaluate the results, the following metrics were used:

Classification Accuracy: sum of true positives and true negatives, divided by the total number of instances.

Precision: ratio of true positives to the sum of true and false positives.

Specificity: ratio of true negatives to the sum of true negatives and false positives.

Recall: ratio of true positives to the sum of true positives and false negatives.

F1 Score:

$$\mathbf{F1} = \frac{2 \cdot \mathbf{PR} \cdot \mathbf{RC}}{\mathbf{PR} + \mathbf{RC}} \tag{4.13}$$

where **PR** and **RC** denote the precision and recall respectively. Table 4.2 shows the classification results.

Table 4.2. Classification results (%).

Classifier	Feature Set	Accuracy	Precision	Specificity	Recall	F1 Score
NBC	$\mathbf{S_1}$	89.10	91.14	92.90	84.70	87.81
	$\mathbf{S_2}$	85.04	87.40	90.15	79.13	83.06
	$\mathbf{S_3}$	85.33	87.71	90.37	79.49	83.40
	$\mathbf{S_4} = \{F2_2, F3_2, F3_5, FPPL_2, \mu_5, \sigma_2, \sigma_5, \kappa_5, S_2\}$	89.39	91.92	93.58	84.53	88.07
LR	$\mathbf{S_1}$	99.80	99.65	99.69	99.91	99.78
	$\mathbf{S_2}$	94.26	94.20	95.03	93.37	93.78
	$\mathbf{S_3}$	98.44	97.73	98.00	98.94	98.33
	$\mathbf{S_4} = \{d_5, F2_5, F3_2, F3_5, \mu_2, \sigma_2, \sigma_5, \kappa_2, S_5\}$	99.67	99.56	99.62	99.72	99.65
SVM	$\mathbf{S_1}$	99.80	99.65	99.69	99.91	99.78
	$\mathbf{S_2}$	94.59	94.48	95.26	93.81	94.14
	$\mathbf{S_3}$	99.10	98.77	98.93	99.29	99.03
	$\mathbf{S_4} = \{d_5, F2_5, F3_2, F3_5, \mu_2, \sigma_2, \sigma_5, \kappa_2, S_5\}$	99.75	99.65	99.69	99.82	99.73
SVM-RBF	$\mathbf{S_1}$	99.99	99.99	99.99	99.99	99.99
	$\mathbf{S_2}$	99.18	99.64	99.69	98.59	99.11
	$\mathbf{S_3}$	99.67	99.73	99.77	99.56	99.65
	$\mathbf{S_4} = \{d_2, F3_2, F3_5, \mu_5, \kappa_5 FMPD_2, FMPD_5, \sigma_2, \sigma_5\}$	99.92	99.82	99.85	99.99	99.91

$\mathbf{S_1}$ refers to the set of all 24 features from Channels 2 and 5 combined; $\mathbf{S_2}$ refers to the set of 12 features from Channel 2, $\mathbf{S_3}$ refers to the set of 12 features from Channel 5, and $\mathbf{S_4}$ refers to the set with the best 9 features selected from $\mathbf{S_1}$. The features in $\mathbf{S_4}$ are selected using recursive feature elimination (RFE). Four classifiers were used: NBC, LR, SVM with a linear kernel and SVM with the RBF kernel. The subscripts 2 and 5 for the features in $\mathbf{S_4}$ denote Channel 2 and Channel 5, respectively. The NBC results are lower compared to other classifiers. This is due to the naive independence assumption and the fact that the likelihoods are not truly Gaussian. The results for the LR classifier are similar to the SVM with linear kernel. This is an expected result, since both are linear classifiers which typically have similar classification performance.

The results show that different channels yield different classification accuracies. In general, features extracted from Channel 5 result in better classification accuracy than features extracted from Channel 2. This can be attributed to the fact that Channel 5 has a higher center frequency (6.5 GHz), therefore the impact of ATC propagation is more noticeable in the CIRs, resulting in a higher contrast between TTW and ATC than in Channel 2. The fact that the classification results from the SVM with the RBF kernel are higher than the SVM with the linear kernel suggests that the features extracted from the dataset are not linearly separable. However, implementation of the decision function for a SVM with the RBF kernel on a resource-constrained device is more difficult than the simple decision function for a SVM with a linear kernel.

After feature selection by RFE, the performance of the LR classifier and SVM with linear kernel is very close to the performance of the SVM with RBF kernel. This indicates that high classification accuracy is possible with linear classifiers with low inference complexity, and can therefore be easily implemented in resource-constrained devices.

4.5.1 Application of NLOS classification in industrial environments

In the case of industrial environments specifically, there are several instances where detection of ATC conditions is important. A particular case are tunnels in underground mines, which are a challenging industrial scenario for ranging and localization due to the harsh propagation conditions. Most severe ranging errors in tunnels occur around corners, since signals do not penetrate rock strata and ranging in these scenarios occurs mostly through reflections. The inability to predict which route around

the corner of the tunnel the RF wave takes is what makes these ranging errors difficult to correct. However, systems used for collision avoidance only require ranging information between devices, e.g. vehicle-to-vehicle or vehicle-to-personnel, without any explicit location information relative to the mine. If no NLOS identification method is used, these ATC conditions go undetected and collisions can occur, since the system can report a much larger range due to ATC propagation, when in fact the two vehicles are much closer to each other and about to collide. When location information is also provided, such as in cases where mine-wide positioning systems are used for collision avoidance, a mine plan can be used in conjunction with the method studied in this chapter to mitigate ranging errors due to ATC conditions, similar to the method for TTW proposed in [80].

4.6 CONCLUSION

Classification of NLOS conditions into TTW and ATC was investigated in this chapter. A dataset was collected through a measurement campaign using IEEE 802.15.4a UWB devices in various TTW and ATC conditions. The results show that it is possible to distinguish these two conditions with high accuracy using linear classifiers, which enables implementation of these methods in resource-constrained devices for real-time classification. The usability of the method for collision avoidance in underground mining tunnels was also discussed. Although only collision avoidance was discussed, the method is applicable to other similar use cases. For future work, the measurement campaign will be extended to industrial scenarios and evaluated in conjunction with NLOS mitigation techniques. The classification method described in this chapter will also be implemented on microcontrollers for real-time classification.

4.7 CHAPTER SUMMARY

This chapter proposed a NLOS classification method to classify NLOS conditions into either TTW or ATC. The characteristics of the two types of NLOS conditions, and how they affect location accuracy, were discussed in detail. A measurement campaign illustrated the differences in these two types of NLOS conditions. Using data collected from the measurement campaign, it was shown that TTW and ATC conditions are identified with high classification accuracy, and that the use of channel statistics extracted from multiple channels leads to less complex NLOS classifiers.

Section 4.2 introduced and motivated the work in the chapter. Section 4.3 explained in detail the differences between TTW and ATC propagation, and how each type results in NLOS conditions with different characteristics, as observed by channel impulse responses and magnitude of NLOS biases. This section also discussed how ATC conditions arise often in industrial environments, and how important it is to identify NLOS conditions caused by ATC propagation so that an appropriate mitigation method can be applied. Section 4.4 described the experiments in detail. A measurement campaign to collect several channel impulse responses using IEEE 802.15.4a UWB devices in TTW and ATC conditions was conducted in two different buildings in an university campus. Feature extraction from the collected channel impulse responses to train classifiers was also described in detail. Section 4.5 discussed the results. It was shown that TTW and ATC NLOS conditions can be identified with high accuracy. It was also shown that using features from two channels results in less complex classifiers than using features from a single channel, therefore facilitating the implementation of the method in resource-constrained devices.

CHAPTER 5 RANGING ERROR MITIGATION FOR TTW NLOS CONDITIONS

5.1 CHAPTER OVERVIEW

This chapter proposes a method to mitigate NLOS conditions caused by through-the-wall propagation. A novel TOA TTW ranging model that relies on parameters from floor plans is proposed and experimentally evaluated. This model is extended for localization using a non-linear least squares estimator.

Section 5.2 introduces and motivates the work. The contributions in the chapter are given. Section 5.3 presents the conventional model for through-the-wall ranging and localization. Section 5.4 discusses the proposed method for TTW localization in detail. Section 5.5 describes the simulation setup to evaluate the proposed localization method and the simulation results for both static and mobile scenarios. Section 5.6 provides concluding remarks and suggestions for future work. Finally, a summary of the chapter is given in Section 5.7.

5.2 INTRODUCTION

Localization has been extensively researched in recent years, enabling improvements in location based services for various applications [3], including healthcare [75]. Different localization techniques have been investigated for various applications [86]. In the retail industry, localization has helped increase revenue by determining the location of customers and guiding them to specific products, resulting in an improved shopping experience and increased sales [87]. For accurate localization in industrial environments, several challenges exist [88]. In industry, localization has been used to improve logistics,

resulting in improved productivity and safety, where mitigation of NLOS conditions is important [14, 36, 81, 89]. Although many approaches for localization have been investigated, and high accuracy is possible in LOS conditions, accurate NLOS ranging/localization is still a challenge. In indoor scenarios, where the main obstructions are walls, location accuracy is adversely affected.

UWB is the state-of-the-art technology for wireless localization. The IEEE 802.15.4a standard supports ranging at the PHY level and commercial-off-the-shelf UWB devices have been shown to be very accurate and precise in measurement campaigns [90], with accuracy consistently better than 20 cm in LOS. However, in NLOS conditions, the accuracy quickly deteriorates, especially in the case where a reflected path is erroneously detected as the first path, resulting in errors in excess of 1 meter [90]. The NLOS condition results in a positive bias in the ranging measurement. In the first case, where RF waves traverse a wall, the permittivity of the wall causes the wave to change direction and reduce its propagation speed, resulting in a longer distance estimate at the receiver when the measured TOF is converted from time to distance [39], since it is assumed that RF waves travel at the speed of light throughout the propagation path. In the second case, when the direct communication path is completely blocked, a reflected path is detected as the direct path and again this results in a longer distance estimate since reflected paths are always longer than direct paths [39].

Several approaches have been proposed to address the NLOS problem. These include the use of machine learning [73] and the use of Kalman or Particles filters [57]. Although these methods yield good results, they have some limitations. The machine learning approach typically requires channel statistics to train NLOS error models. These statistics are collected from measurement campaigns which are cumbersome and labor intensive. Furthermore, the collected training data is usually site specific, therefore conducting the measurement campaign in one site and using the model in another site can often lead to poor results. The resulting location accuracy in this case is limited to the size of the training set and how well the collected data represents the variety of NLOS conditions in the respective site. Kalman filters typically require input from a secondary sensor, e.g. accelerometer, assume mobility and a starting position in LOS conditions. Such techniques are unsuitable for static wireless nodes, for instance, which have no mobility and do not transition from LOS to NLOS during the localization process. Therefore, a method to address these limitations should not require knowledge of the error statistics and work for static nodes as well.

This chapter focuses specifically on TTW NLOS ranging. The goal is to mitigate, or reduce, ranging

errors caused by TTW propagation in indoor environments. To this end, firstly, the conventional ranging model for TTW TOF from literature is simplified. Secondly, this model is used along with information from floor plans, i.e. wall thickness, to propose an approach that corrects ranging errors. Three assumptions are made: 1) the relative permittivity is approximately the same for all walls between anchors and tags; 2) the indoor positioning system in use is capable of room level location accuracy to ensure that the selected walls are the correct walls to obtain corresponding wall thickness from the floor plan; and 3) all range estimates are affected by noise and TTW NLOS conditions only, i.e. NLOS ranging errors are not a result of reflected or diffracted waves. These assumptions are feasible with UWB, therefore this work targets UWB. The contributions of this chapter are:

- A simplified model for TTW ranging as a function of the wall's relative permittivity and thickness, and experimental evaluation of the developed model,
- A method to retrieve information from floor plans to determine unknown parameters in the developed TTW ranging model,
- A localization method based on the developed TTW ranging model. The method is evaluated via simulations for various combinations of node positions, walls' locations and thickness, and the results shown that the bias in ranging estimates is significantly mitigated and that the estimated locations are more accurate than locations determined by NLOS ranges without mitigation.

This work is an extension of [91]. The work in [91] was a proof-of-concept using an iterative algorithm for localization. This work proposes a simplified ranging bias model as a function of the wall's relative permittivity and thickness, and evaluates the model experimentally. This simplified model enables localization to be formulated as an optimization problem instead, which is more efficient than the iterative approach. The proposed method is also further evaluated under varying noise conditions in both static and mobile scenarios, and it is shown that in all cases, the location estimates by the proposed method are more accurate than location estimates using NLOS ranges without mitigation.

5.3 BACKGROUND

5.3.1 Through-the-wall ranging

RF waves propagate in air at approximately the speed of light. When a RF wave traverses a wall, it is refracted, and the speed is reduced in proportion to the wall's refractive index. The propagation speed of a RF wave in a wall can be calculated by [39]:

$$V_w \approx \frac{c}{\sqrt{\varepsilon_r}} \tag{5.1}$$

where c is the speed of light in free space and ε_r is the wall's real relative permittivity. From (5.1), it is evident that the wave's speed decreases in a wall, therefore it takes the wave longer to traverse the wall - in comparison to free space - consequently increasing the wave's TOF. Figure 5.1 shows the ranging model to calculate the TOF from transmitter to receiver through a wall.

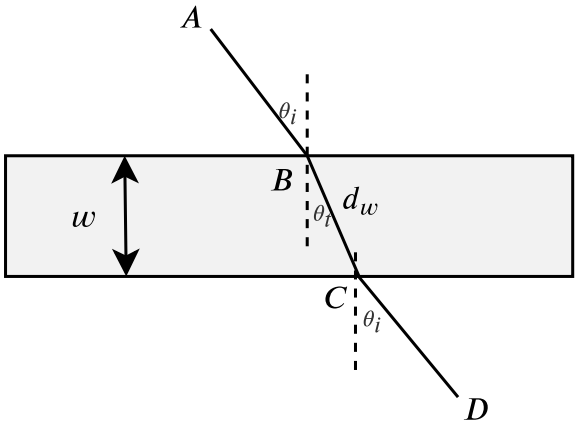

Figure 5.1. Through-the-wall ranging. Taken from [80], © 2020 IEEE.

The TOF from an anchor in location A to a tag in location D is given by:

$$\begin{aligned} t_{AD} &= t_{AB} + t_{BC} + t_{CD} \\ t_{AD} &= \frac{1}{c}\left(d_{AB} + d_w\sqrt{\varepsilon_r} + d_{CD}\right) \end{aligned} \tag{5.2}$$

where the t terms correspond to the TOF for the different sections of the propagation path shown in Figure 5.1, the d terms correspond to all the distances in the path A to D when converted from TOF to distance, d_w is the distance traversed by the wave in the wall, and w is the wall's thickness shown in Figure 5.1. The distance d_w is given by:

$$d_w = \frac{w}{\cos\theta_t} \tag{5.3}$$

where the transmission angle θ_t is related to the incidence angle θ_i by Snell's law:

$$n_1 \sin\theta_i = n_2 \sin\theta_t \tag{5.4}$$

where n_1 and n_2 and the refractive indices of air and the wall, respectively. Substituting (5.4) into (5.3), then (5.3) into (5.2) yields the NLOS range d_{AD}:

$$d_{AD} = d_{AB} + \frac{w\sqrt{\varepsilon_r}}{\cos(\sin^{-1}(\frac{\sin\theta_i}{\sqrt{\varepsilon_r}}))} + d_{CD} \tag{5.5}$$

The ranging bias caused by TTW propagation is then given by:

$$\begin{aligned} b &= d_{AD} - \|l_A - l_D\| \\ &= d_{AB} + \frac{w\sqrt{\varepsilon_r}}{\cos(\sin^{-1}(\frac{\sin\theta_i}{\sqrt{\varepsilon_r}}))} + d_{CD} - \|l_A - l_D\| \end{aligned} \tag{5.6}$$

where $\|l_A - l_D\|$ is the Euclidean distance between the anchor at A and tag at D. Since none of the true distances are known, none of the terms in (5.6) can be computed directly from a NLOS location estimate.

5.3.2 Localization

Localization using trilateration consists of finding a common point of intersection between three circles, where the radius for each circle is the distance from the respective anchor to a tag. A typical scenario for TTW localization is shown in Figure 5.2, where the tag's location (x,y) can be determined using trilateration by solving the following system of non-linear equations:

$$\begin{aligned}(x_1-x)^2+(y_1-y)^2&=d_1^2\\(x_2-x)^2+(y_2-y)^2&=d_2^2\\(x_3-x)^2+(y_3-y)^2&=d_3^2\end{aligned} \tag{5.7}$$

where (x_1,y_1), (x_2,y_2) and (x_3,y_3) are the known anchor locations and d_1, d_2 and d_3 are the measured ranges between anchors 1, 2 and 3 and the tag, respectively. This can be solved in the least squares sense by minimizing the following objective function:

$$\hat{x},\hat{y}=\min_{\boldsymbol{x},\boldsymbol{y}}\sum_{i=1}^{N}((x_i-x)^2+(y_i-y)^2-d_i^2)^2 \tag{5.8}$$

In the scenario illustrated in Figure 5.2, however, only NLOS ranges - as given by (5.5) - are known, therefore the ranging error in these ranges has to be mitigated to yield a LOS equivalent location when using trilateration. The next Section introduces a method to mitigate the bias present in NLOS range estimates.

5.4 PROPOSED METHOD

5.4.1 Simplification of through-the-wall ranging model

At normal incidence, i.e. $\theta_i=0$, the model for the bias b given by (5.6) reduces to:

$$b=w(\sqrt{\varepsilon_r}-1) \tag{5.9}$$

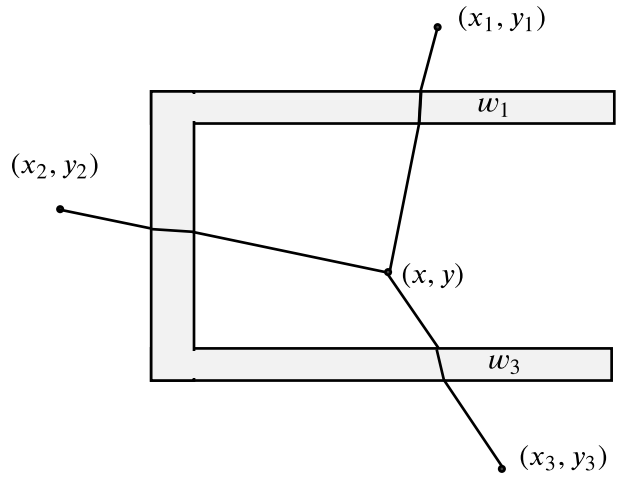

Figure 5.2. Through-the-wall localization. Taken from [80], © 2020 IEEE.

Since the model in (5.6) contains many parameters that cannot be determined without knowledge of the tag's true location, it is desirable to obtain a model similar to (5.9) which also applies to incidence angles $\theta_i > 0$. To obtain such a model, the following scenario with three anchors and one tag is simulated. The first anchor is placed at location $(0,0)$ and a tag is initially placed at location $P_I = (4, 1.5)$, and moved in a straight line in 20 cm increments up to location $P_F = (4,8)$. The incidence angle between anchor 1 and P_I is 25° and the incidence angle between anchor 1 and P_F is 68°. This simulation scenario is illustrated in Figure 5.3, where P_I denotes the starting point and P_F denotes the end point of the path the tag traverses.

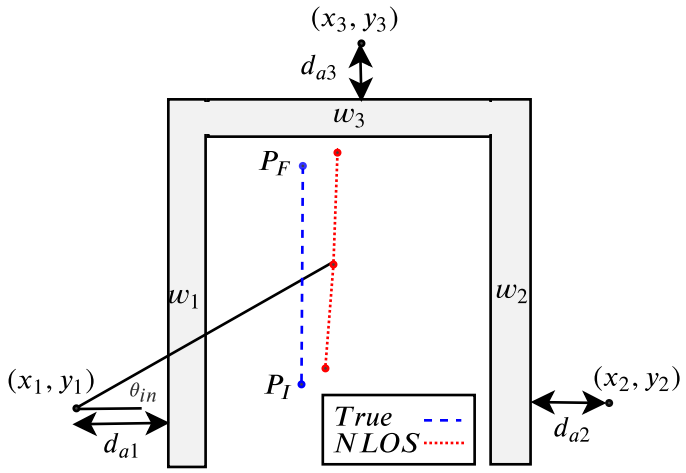

Figure 5.3. Simulation setup. Taken from [80], © 2020 IEEE.

For each location along the path, the true ranges are computed by calculating the Euclidean distances between the tag and anchors, and also calculating the NLOS ranges between the tag and the anchors using (5.5). Then, the bias for each anchor-tag pair is calculated using (5.6) since the true locations along the path are known, therefore all terms in (5.6) are also known. The NLOS location is calculated using (5.8) with the NLOS ranges as input. This scenario i simulated for different combinations of ε_r values of 3.0, 6.0 and 9.0, and wall thickness w of 0.25, 0.50 and 0.75 m for the three walls. These values represent realistic scenarios [92]. Values for wall thickness larger than 0.5 m can represent the addition of thicknesses from multiple walls to simulate cases where there is more than a single wall between tag and anchor. This is a valid approach given the assumption that ε_r is approximately the same for all walls. Using all the data obtained from the simulation, a model is fitted to the calculated bias by (5.6), as a function of w, ε_r and incidence angle θ_i using regression analysis. This model is given by:

$$b \approx w(\sqrt{\varepsilon_r} - 1) + 0.31 w \theta_i^2 \tag{5.10}$$

Compared to (5.9), the model in (5.10) has an additional term dependent on the wall thickness w and incidence angle θ_i. This term $0.31 w \theta_i^2$ accounts for the additional bias caused by incidence angles larger than zero. A comparison between the true biases calculated by (5.6) and the approximations calculated by (5.10) is shown in Figure 5.4, where the approximations are denoted by 'Setup 1' with values $\varepsilon_r = 3.0$ and $w = 0.25$ m, 'Setup 2' with values $\varepsilon_r = 6.0$ and $w = 0.50$ m, and 'Setup 3' with values $\varepsilon_r = 9.0$ and $w = 0.75$ m. It is seen that the biases determined by both models are very similar, with a maximum difference between the models less than 8 cm.

The model in (5.10), however, is based on θ_i which in practical scenarios is unknown since the tag's true location is unknown. In a case where the tag's NLOS location can be determined using NLOS ranges, the angle θ_{in} between an anchor and NLOS location of the tag is usually close to θ_i. To determine the relationship between θ_i and θ_{in}, NLOS locations determined using NLOS ranges are considered. With reference to Figure 5.3, the second anchor is placed at $(x_2, y_2) = (13, 0)$ and the third anchor at $(x_3, y_3) = (3, 10)$, and set the two respective wall thicknesses to 1 meter and ε_r= 10, to simulate conditions that can result in large biases. The same simulation as described previously is conducted, where the tag moves from P_I to P_F and the simulation is conducted for various values of ε_r and w for the wall between the tag and anchor 1. θ_{in} is determined as the angle between each NLOS

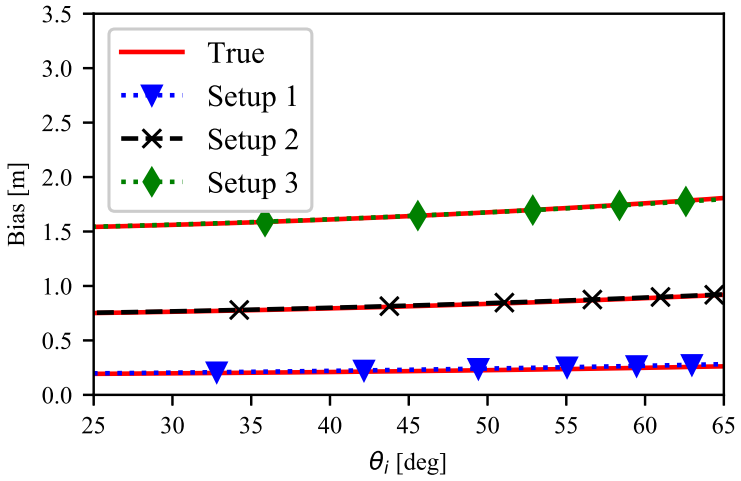

Figure 5.4. Simulated bias vs incidence angle for different values of w and ε_r. Taken from [80], © 2020 IEEE.

location and anchor 1, as illustrated in Figure 5.3. The scatter plot in Figure 5.5 shows the relationship between θ_i and θ_{in} for all simulations combined. The difference between θ_{in} and θ_i is mostly below 17 degrees.

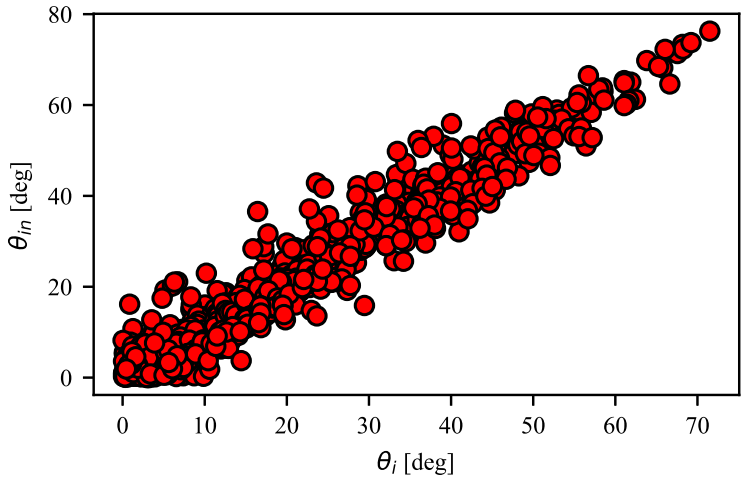

Figure 5.5. Incidence angles vs NLOS angles. Taken from [80], © 2020 IEEE.

Figure 5.6 shows the bias as a function of θ_{in}. The maximum difference between the biases predicted by the two models is less than 15 cm. Therefore, an equivalent bias model to (5.10) is given by:

$$b \approx w(\sqrt{\varepsilon_r} - 1) + 0.31 w \theta_{in}^2 \tag{5.11}$$

where θ_{in} is the NLOS angle between an anchor and the tag's NLOS location. Therefore, the NLOS range in terms of the true range and bias is given by:

$$d_{AD} \approx \|l_A - l_D\| + w(\sqrt{\varepsilon_r} - 1) + 0.31 w \theta_{in}^2 \tag{5.12}$$

To verify the bias and ranging models experimentally, a number of measurements were conducted using Decawave EVB1000 boards which are equipped with DW1000 UWB transceivers. These measurements were conducted for five concrete walls. Table 5.1 shows the configuration of the Decawave devices.

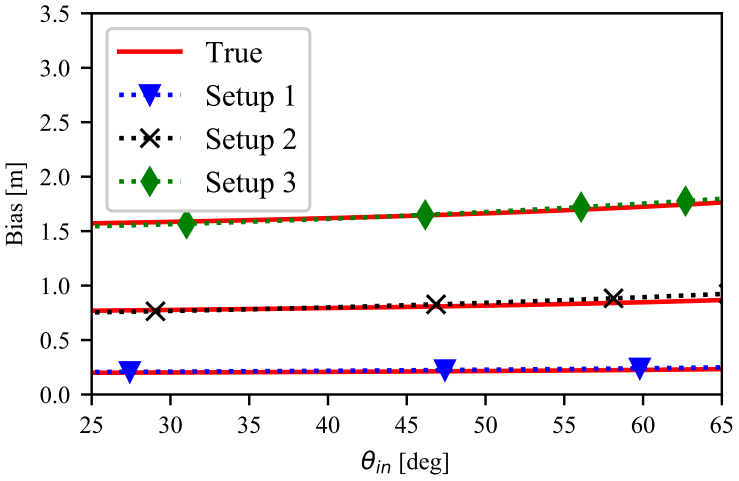

Figure 5.6. Simulated bias vs NLOS angle for different values of w and ε_r. Taken from [80], © 2020 IEEE.

Table 5.1. Configuration of UWB devices for measurement campaign.

Parameter	Value
Channel	2 (3.9 GHz)
Data rate	110 kbps
Pulse Repetition Frequency	64 MHz
Preamble Length	1024
Preamble Code	9
SFD	Non-standard

For each location, 150 ranging measurements were taken, and the NLOS range was computed as the average of these measurements. The true range was taken as the Euclidean distance between the tag

and anchor. For each experiment, one tag and one anchor were used. The measurement setup for one of the walls is discussed in detail to demonstrate the experimental procedure. Similar to the simulation, a tag was placed at an initial location $P_I = (3.54, 0.0)$ and moved along a straight path to location $P_F = (3,59, 4.76)$ in 50 cm increments, with 150 ranging measurements taken at each location. The anchor was placed at (0,0). The wall in this setup was 33 cm thick. This setup is illustrated in Figure 5.7, where the tag is shown in a corridor, and the anchor is located in a lecture hall, on the other side of the wall. The path P_I to P_F is therefore along the corridor.

Figure 5.7. TTW ranging experiment: a tag placed in a corridor (left) and an anchor placed in a lecture hall (right). Taken from [80], © 2020 IEEE.

For the initial location P_I, the tag is normally incident to the wall with $\theta_i = 0$. The bias at the initial location is calculated as 40 cm by subtracting the true range from the measured NLOS range. (5.9) is then used to compute ε_r, which is 4.89. For each location along the path P_I to P_F, the true range and measured NLOS range are logged. Since only one tag and one anchor are used for the measurements, there is only one NLOS range, when at least three ranges are required for localization. Therefore, simulated NLOS ranges from anchors 2 and 3 - as previously described in the simulation setup and illustrated in Figure 5.3 - are used in combination with the measured NLOS range to determine the NLOS angle θ_{in}. Figure 5.8 shows the measurements obtained for this example, along with the simulated ranges.

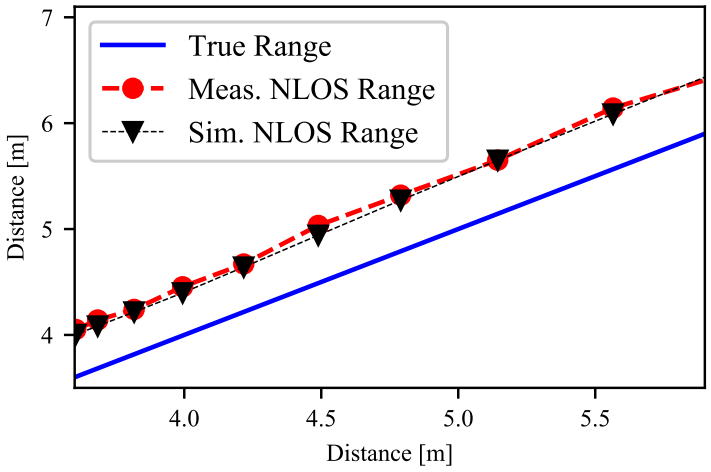

Figure 5.8. True vs measured and simulated NLOS ranges between anchor and tag for a wall with a thickness of 33 cm. Taken from [80], © 2020 IEEE.

The simulated line is generated by adding the bias calculated with (5.11) to the true distance to determine the NLOS range. It is evident that the measured and simulated NLOS ranges are very similar. Small differences can be caused by ranging noise which is only present in the ranges measured experimentally. Table 5.2 lists values for the simulated biases and the measured biases. The experiments conducted for the other four walls showed a similar relationship between simulated and measured NLOS ranges. Therefore, for the rest of the chapter, the bias model in (5.11) and TTW ranging model in (5.12) is adopted.

Table 5.2. Simulated vs measured biases.

Simulated [m]	0.40	0.40	0.40	0.46	0.51	0.52	0.54
Measured [m]	0.40	0.46	0.46	0.55	0.51	0.58	0.50

5.4.2 Retrieving w from floor plans

If floor plans of the site where the anchors and tags are deployed are available, the values for w_1, w_2 and w_3 for the wall thickness in Figure 5.2 can be extracted from floor plans. If the wall thickness is not available in floor plans, it can be measured manually. To use the proposed method, it is important to select the correct values for w. By using a wireless technology such as UWB that produces accurate and precise location estimates, it is possible to achieve room-level accuracy even in the presence of TTW NLOS conditions. Therefore, if the correct room where the tag is located is selected, the values

for w for said room can then be retrieved from the floor plan. In cases where multiple walls exist between anchor and tag, the wall thickness for all walls can be added, assuming that their relative permittivity is approximately the same.

In case a floor plan is not available, the thickness of walls in the site have to be measured manually and the wall locations have to be determined. The required labor to achieve this can be similar to fingerprint based systems that require building a map of fingerprints by taking site-specific measurements. However, most commercial and industrial venues typically have detailed floor plans available.

5.4.3 Calculation of NLOS angles

The calculation of the NLOS angles θ_{in} is as follows: the tag's location is estimated using NLOS ranges with (5.8) and the NLOS angles are then determined as illustrated in Figure 5.9.

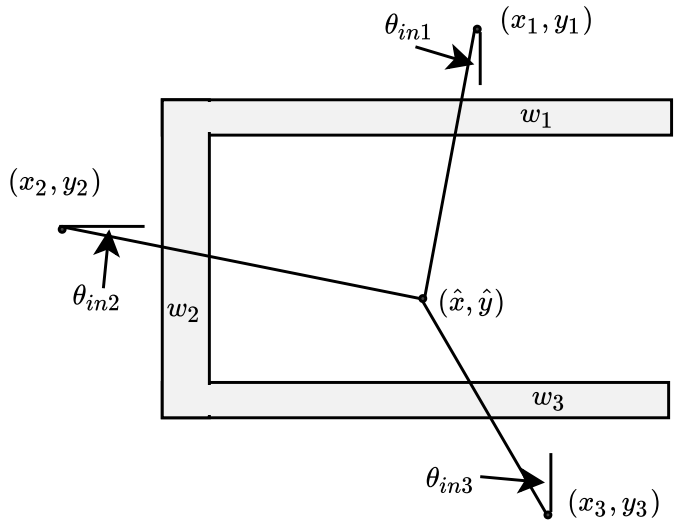

Figure 5.9. Illustration of NLOS angles θ_{in}.

5.4.4 Formulation: localization

In this section, localization using the developed TTW ranging and bias model is formulated as an optimization problem. Considering the simplified TTW ranging model in (5.12), the measured NLOS range $\hat{d}_i$ between a tag and anchor i is given by:

$$\begin{aligned}\hat{d}_i &= d_i + b_i + n_i \\ &= d_i + w_i(\sqrt{\varepsilon_r} - 1) + 0.31 w_i \theta_{in}^2 + n_i\end{aligned} \tag{5.13}$$

where d_i is the true range between anchor i and the tag, b_i is the bias corresponding to anchor i, n_i is Gaussian distributed noise with distribution $\mathcal{N}(\mu, \sigma^2)$, and the term $0.31 w_i \theta_{in}^2$ from (5.11) accounts for the additional bias caused by incidence angles larger than zero. Following from (5.13), the equivalent LOS range d_i is given by:

$$d_i = \hat{d}_i - w_i(\sqrt{\varepsilon_r} - 1) - 0.31 w_i \theta_{in}^2 - n_i \tag{5.14}$$

where $\hat{d}_i$ is the measured NLOS range between anchor i and the tag. The tag's 2D location can be computed using trilateration, which consists of finding a common point of intersection between three circles as given in (5.7). A location can then be determined by solving the following optimization problem:

$$\hat{x}, \hat{y}, \hat{\varepsilon}_r = \min_{\boldsymbol{x}, \boldsymbol{y}, \boldsymbol{\varepsilon_r}} \sum_{i=1}^{N} ((x_i - x)^2 + (y_i - y)^2 - d_i^2)^2 \tag{5.15}$$

where N is the number of anchors, i.e. three in the scenario described in Figure 5.2 and d_i is given by (5.14). In this work, three anchors are considered, as that is the minimum required to determine a LOS location. It is noted that the proposed approach can be extended to more anchors by modifying the value of N in the objective function and including the respective ranges and w terms for each additional anchor, since the simplified ranging model applies to each anchor-tag range estimate. The optimization problem in (5.15) is solved in the least squares sense with the Levenberg-Marquardt algorithm, and the resulting $(\hat{x}, \hat{y})$ is the equivalent LOS location. The mitigated ranges r_i are then given by:

$$r_i = \sqrt{(x_i - \hat{x})^2 + (y_i - \hat{y})^2} \tag{5.16}$$

where $(\hat{x}, \hat{y})$ is the location estimated by (5.15).

5.5 SIMULATIONS AND RESULTS

5.5.1 Simulation setup

To determine statistics for the ranging noise n, ranging measurements with two calibrated Decawave nodes were taken. The distance between the two nodes was measured for distances of 2 to 20 meters in LOS conditions, with 150 measurements taken for each distance. The mean for the ranging measurements was calculated for each distance. Maximum mean offsets (difference between the mean of the measured distances and true distance) of approximately over 20 cm were observed. This was possibly caused by the propagation environment and relative poses, i.e. antenna orientations of the nodes. These effects were also observed in [93]. The distribution of the observed mean offsets is shown in Figure 5.10, fitted with a Gaussian distribution given by $\mathcal{N}(0, 0.15^2)$. This ranging noise distribution was used for the simulations.

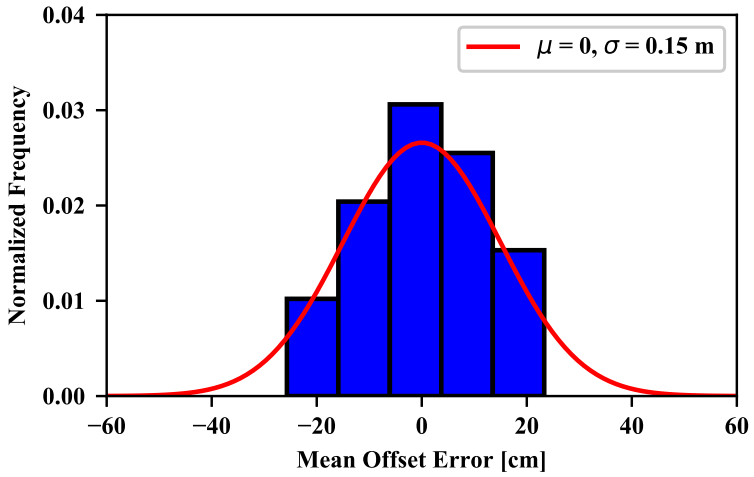

Figure 5.10. Distribution of mean offset errors. Taken from [80], © 2020 IEEE.

For the simulations, three anchors and one tag are used. Fixed wall locations are defined and a wall thickness between 0.2 and 1.0 m is generated for each wall from the distribution $\mathcal{U}(0.2, 1.0)$. The ε_r's for each wall are also generated from the distribution $\mathcal{U}(2.0, 10.0)$, which is a realistic range of values for walls [92]. Then, the x and y coordinates of each anchor are randomly generated such that they keep a similar geometrical arrangement relative to each other, as illustrated in Figure 5.2. This is done to maintain a good geometric dilution of precision (GDOP). For each tag location, the bias is calculated using (5.6) and the true range as the Euclidean distance between the tag and each anchor. The LOS range is computed by adding Gaussian distributed noise to the true range, and the NLOS range is

computed by adding the calculated bias to the LOS range. θ_{in} is computed as the angle between each anchor and NLOS location, which is determined using (5.8) with the NLOS ranges as input. Finally, the location with mitigated ranges is computed by (5.15). For each scenario, 150 tag locations are randomly generated within the region enclosed by the three anchors. This procedure is repeated for 20 times, where a different set of anchor locations, wall thicknesses and ε_r's are generated each time. This results in a total of 3000 trials. This is repeated for 4 different configurations. The reason for using four configurations is as follows. In a realistic scenario, the relative permittivity ε_r might not be exactly the same for all walls, and the wall thickness might not be exact when measured manually in instances where floor plans do not show it.

To evaluate the robustness of the proposed approach in such situations, a random deviation is introduced into both w and ε_r. For w, this is in the form of an uniform distribution given by $\mathcal{U}(0, 0.15)$ and for ε_r the values are selected such that the maximum difference between all three ε_r's is 3.0. This means that instead of being exactly the same for all three walls, the ε_r's for all three walls are within ± 3.0 of each other. The wall thickness can deviate from 0 to 15 cm, representing more realistic scenarios in the simulations. For configurations 1 and 3, it is assumed that the ranging noise has a distribution of $\mathcal{N}(0, 0.15^2)$ and for configurations 2 and 4, it is assumed that the ranging noise has a distribution of $\mathcal{N}(0, 0.25^2)$. The reason for the increase in σ in configurations 2 and 4 is to evaluate the robustness of the proposed approach with larger ranging noise. The details of all four configurations are listed in Table 5.3. Results for all simulations are discussed below.

Table 5.3. Configurations to test robustness of proposed method.

Config	**Ranging noise μ σ**	**ε_r max difference**	**w min, max**
1	0, 0.15	0	0, 0
2	0, 0.25	0	0, 0
3	0, 0.15	3.0	0, 0.15
4	0, 0.25	3.0	0, 0.15

5.5.2 Ranging errors

Three different types of ranging errors are considered: errors in LOS conditions, which are typically caused by noise only; NLOS ranging errors caused by TTW propagation; and mitigated ranging errors,

which are the final ranging errors after NLOS mitigation using the proposed method. The ranging error is given by:

$$e = \hat{d}_k - d_i \tag{5.17}$$

where k denotes either LOS, NLOS or mitigated, and d_i denotes the true range. Note that although the distribution of the noise in (5.13) is known, the actual values are not known, therefore the error e in (5.17) includes both the bias b and noise n. As previously described, various scenarios were simulated to evaluate the proposed method. The results were determined for four different configurations C1 to C4.

The histograms in Figure 5.11 and 5.12 show the distribution of NLOS vs LOS and NLOS vs mitigated ranging errors for all four configurations combined. The LOS errors are included so that they can be compared to the mitigated ranging errors. It is observed in the histograms that the mitigated ranging errors are very close to the LOS ranging errors. Table 5.4 shows the mean μ and standard deviation σ for all ranging errors for each configuration listed in Table 5.3. The mitigated ranging errors have very similar statistics to LOS errors, showing that the proposed method is able to correct NLOS ranging errors significantly. In particular, the mean for mitigated ranging errors in all configurations is close to zero, indicating that the original NLOS bias has been removed.

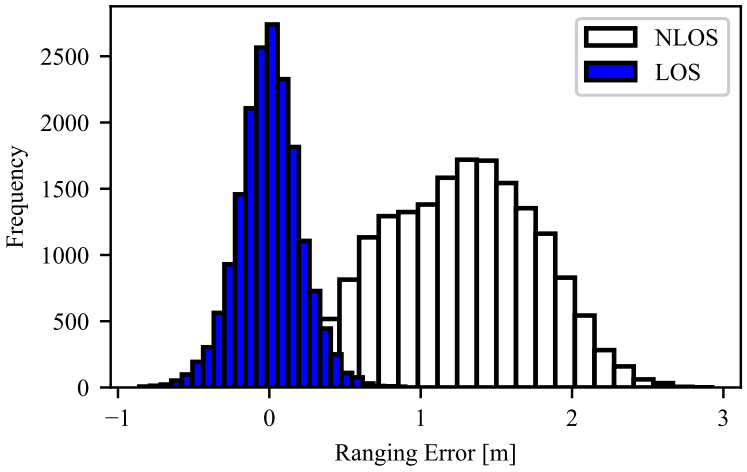

Figure 5.11. Distribution of LOS ranging errors vs NLOS ranging errors. Taken from [80], © 2020 IEEE.

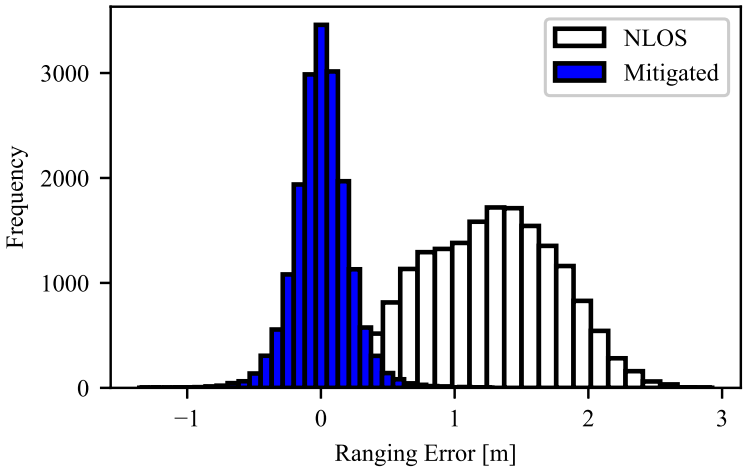

Figure 5.12. Distribution of ranging errors mitigated by the proposed approach vs NLOS ranging errors. Taken from [80], © 2020 IEEE.

Table 5.4. Ranging error statistics.

	μ [m]	σ [m]
No mitigation (NLOS)	0.969	0.54
LOS C1	0.004	0.13
LOS C2	0.003	0.24
LOS C3	-0.002	0.14
LOS C4	0.002	0.25
After mitigation C1	0.004	0.15
After mitigation C2	0.006	0.24
After mitigation C3	-0.001	0.19
After mitigation C4	0.022	0.26

Furthermore, the standard deviations for mitigated ranging errors in all configurations are smaller than the NLOS case. Therefore, the method is shown to be robust even with the random deviations introduced in w and ε_r listed in Table 5.3.

5.5.3 Location errors

To determine the improvement in location accuracy, location errors between the true location (x,y) and the location $(\hat{x},\hat{y})$ estimated by NLOS ranges are compared against location errors between the true location (x,y) and the location $(\hat{x},\hat{y})$ estimated by mitigated ranges. In both cases, the location error E is given by:

$$E = \sqrt{(x-\hat{x})^2 + (y-\hat{y})^2} \tag{5.18}$$

where $(\hat{x},\hat{y})$ is the estimated location either by NLOS ranges or mitigated ranges. Mean location error (MLE) and Root Mean Square Error (RMSE) are also considered. The MLE is given by:

$$MLE = \frac{\sum_{n=1}^{N} \sqrt{(x-\hat{x}_n)^2 + (y-\hat{y}_n)^2}}{N} \tag{5.19}$$

where N is the number of ranging measurements. The RMSE is given by:

$$RMSE = \sqrt{\frac{1}{N}\sum_{n=1}^{N}\left[(x-\hat{x}_n)^2 + (y-\hat{y}_n)^2\right]} \tag{5.20}$$

Figure 5.13 shows the cumulative distribution function (CDF) for location errors for the LOS, NLOS and mitigated cases. It is evident that the location estimates for mitigated ranges are much closer to LOS location estimates than NLOS. Overall, location accuracy is significantly improved in comparison to location estimates from NLOS ranges. It is also observed that mitigated location errors are very close to LOS location errors, showing the effectiveness of the proposed method at improving location accuracy. MLE and RMSE are shown in Table 5.5, and is is observed that the MLE and RMSE for the mitigated case are also close to the LOS case.

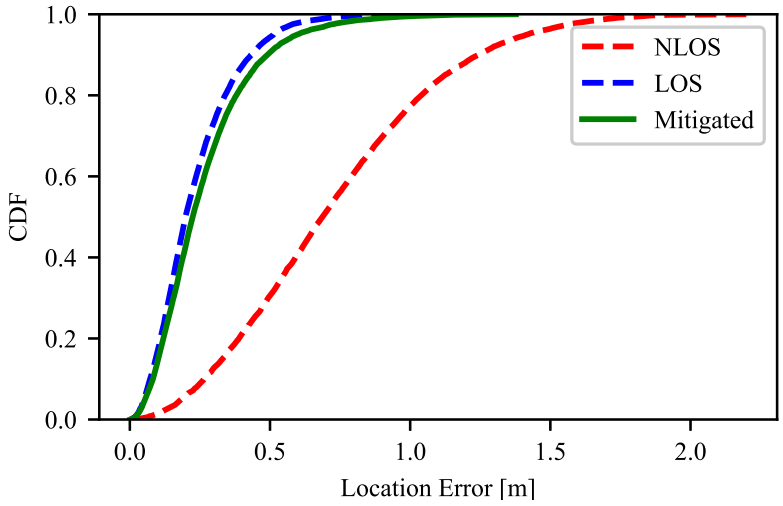

Figure 5.13. Cumulative distribution function for location errors. Taken from [80], © 2020 IEEE.

Table 5.5. Location errors: MLE and RMSE.

	MLE [m]	**RMSE [m]**	**Improvement**
No mitigation (NLOS)	0.60	0.68	-
LOS C1	0.18	0.20	71%
LOS C2	0.29	0.33	52%
LOS C3	0.17	0.20	71%
LOS C4	0.29	0.34	50%
After mitigation C1	0.18	0.21	69%
After mitigation C2	0.29	0.34	51%
After mitigation C3	0.25	0.29	58%
After mitigation C4	0.34	0.40	42%

5.5.4 Location errors in mobile scenarios

The results for the location accuracy discussed above are from static scenarios. Since location estimates can also be used for tracking and navigation, it is of interest to determine the performance of the proposed method in mobile scenarios. To this end, the performance of the proposed method was evaluated by simulating a mobile tag along a predefined path surrounded by walls. In the simulation, the topology of the three fixed anchors is similar to the topology illustrated in Figure 5.2 used in the simulations for static scenarios. As the tag moves along the path, the location estimates are determined

using (5.15). The path, i.e. ground truth, in this example resembles the shape of an ellipse as shown in Figure 5.14. Figure 5.14 shows the simulation results, where the ground truth, NLOS location estimates, and location estimates after ranges have been mitigated. The simulation setup for this scenario is described in Table 5.6.

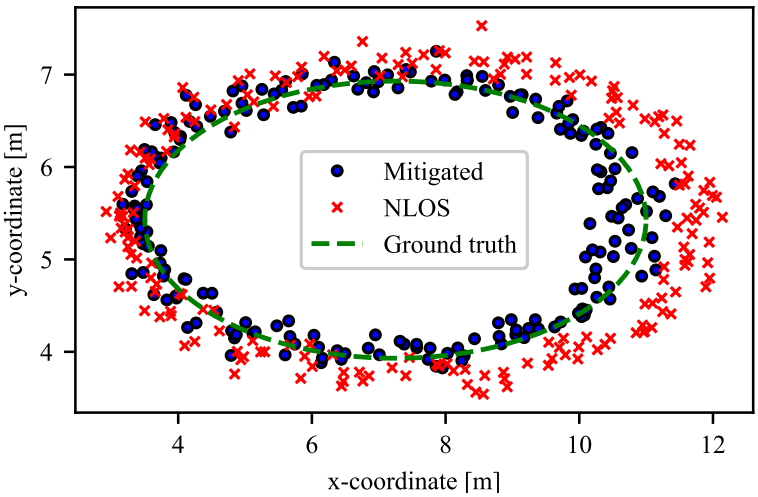

Figure 5.14. True path vs location estimates with NLOS and Mitigated ranges. Taken from [80], © 2020 IEEE.

Table 5.6. Simulation setup for mobile scenario.

Parameter	Value
(x_1, y_1)	(9, 11)
(x_2, y_2)	(0, 6)
(x_3, y_3)	(10, 0)
Venue dimensions	6.0 m by 12.0 m
w_1, w_2, w_3	0.47 m, 0.27 m, 0.32 m
ε_{r1}, ε_{r2}, ε_{r3}	6.0, 9.0, 7.5
Distribution of ranging noise n	$\mathcal{N}(0.0, 0.15^2)$

Table 5.7 shows the RMSE results over the simulated path with the improvement in terms of percentage. Since the LOS case is used as a benchmark, it is noted that the base NLOS result would need to improve by 67% to achieve parity with the LOS case. The base NLOS result is improved by 53%, which is a large step in the direction of having a result equivalent to LOS.

Table 5.7. RMSE results for mobile scenario.

	LOS	**NLOS**	**Mitigated**	**Improvement**
RMSE [m]	0.19	0.58	0.27	53%

5.6 CONCLUSION

This chapter proposed a method to mitigate ranging errors caused by TTW NLOS conditions in indoor environments. The proposed method relies on a simplified TTW ranging model that expresses known NLOS ranges in terms of wall thickness and relative permittivity. NLOS ranges together with the ranging model are then used to find the equivalent LOS location using trilateration. It was shown that the proposed method produces significantly more accurate location estimates than location estimates using NLOS ranges. For future work, it is of interest to investigate the more general case where the wall thickness is not known and the relative permittivity is not assumed to be the same for all walls. It is also of interest to evaluate the localization component of the proposed method experimentally using UWB COTS nodes.

5.7 CHAPTER SUMMARY

This chapter proposed a NLOS mitigation method for NLOS conditions caused by through-the-wall propagation. The method was evaluated experimentally and the results show that it outperforms localization using a LLS estimator (without any mitigation) significantly with regards to location accuracy. Section 5.2 introduced and motivated the work. The context of the work was explained and the importance of mitigating NLOS biases caused by TTW NLOS conditions was highlighted. Section 5.3 presented conventional models for through-the-wall ranging and localization. Characteristics of TTW NLOS conditions were discussed in detail. Section 5.4 discussed the proposed method for TTW localization in detail. Firstly, a novel simplified model for TTW TOA ranging was proposed and experimentally evaluated. Secondly, the integration of the ranging model into localization was described. It was also described how wall thickness is obtained from floor plans and used in the ranging model. Compared to other TTW localization methods in literature, this method does not assume normal incidence for refracted signals nor that all walls have the same thickness. Section 5.5 described the simulation setup to evaluate the proposed localization method and the simulation results for both

static and mobile scenarios. The results showed that NLOS conditions caused by TTW propagation can be significantly mitigated, with resulting location accuracies close to equivalent LOS conditions. Section 5.6 concluded the work and interesting possibilities for future work were highlighted.

CHAPTER 6 MITIGATION OF RANDOM NON-LINE-OF-SIGHT LOCATION ERRORS

6.1 CHAPTER OVERVIEW

This chapter proposes a localization method for NLOS conditions. The proposed method relies on geometric constraints imposed by the positive biases introduced in TOA ranging by NLOS conditions. These geometric constraints are leveraged to determine a node's location in NLOS conditions, resulting in higher location accuracy than using LLSE for localization.

Three different cases are considered: NLOS conditions are identifiable; NLOS conditions are identifiable and LOS ranges between nodes are also available; NLOS ranges are not identifiable. For the first two cases, the results show that the proposed method significantly outperforms the LLSE approach. For the third case, it is shown that the method results in similar location accuracy to a state-of-the-art SDP based localization algorithm, but it is more computationally efficient.

Section 6.2 introduces and motivates the work, and lists the contributions. Section 6.3 proposes a localization method for the three different cases mentioned above. In Section 6.4, the proposed method is evaluated via simulation for the three different cases described in Section 6.3. Concluding remarks are provided in Section 6.5. Finally, a summary of the chapter is given in Section 6.6.

6.2 INTRODUCTION

Accurate localization is an enabler of many applications. Services in smart cities [3] and industries like healthcare [75] have improved their productivity and efficiency through the use of localization. Due to the demand, many localization techniques have been proposed to meet different requirements. The state-of-the-art in wireless localization is UWB localization, standardized by IEEE 802.15.4a [38]. Compared to other RF based localization techniques, UWB is superior in terms of accuracy and precision. This is due to the fact that it uses very short pulses for communication, which allow reliable detection of the first path, even in the presence of multipath, resulting in very accurate ranges which in turn result in accurate location estimates.

This high accuracy and precision, however, is typically observed in LOS conditions only. In NLOS conditions, the direct path is attenuated, and is either detectable or non-detectable. In the first case, the signal traverses an obstruction and therefore the TOF increases. In the second case, a multipath component is detected erroneously as the direct path. Both cases are discussed in detail in Section 2.3.2. In both cases, a positive bias in the ranging measurement is observed when the measured TOF is converted from time to distance. If the NLOS condition is caused by a wall or a similar obstruction, the magnitude of the bias is related to the size of the obstruction and its relative permittivity [39], and biases in this case typically range from a few decimeters to around a meter. In the second case, if a multipah component is erroneously detected as the first path, this can lead to large ranging biases, which have been shown to range from one to several meters in experiments conducted with COTS UWB radios [90]. Hence, to obtain accurate location estimates in these conditions, ranging biases have to be mitigated.

Several approaches to address this problem have been proposed in literature. These include the use of machine learning [65], [84] and other methods which assume that error statistics are known [39]. Optimization based techniques have also been proposed by formulating the localization as a linear [52], quadratic [94] or semi-definite program [11]. Techniques using floor plans have also been proposed [95]. The method proposed in this chapter takes a different approach. In a scenario where all anchors are properly deployed around the sensing area, it is common that at least one LOS anchor is available. We consider the specific case where, at any given time, a sensor node has one LOS link to an anchor and all its other links to the remaining anchors are NLOS. Such scenarios can occur in industrial environments, for instance, where moving vehicles and other machinery can temporarily block the

LOS signal path at random times [36]. However, since these scenarios involve moving obstructions that are often not predictable, the use of maps or floor plans is not practical. Secondly, collecting error statistics for each type of obstruction is also not practical, as obstructions can differ in material and size significantly, and are also dependent on the environment. Therefore, the ranging bias caused by these obstructions can be considered a random ranging bias. It is also of interest to investigate the case where multiple sensor nodes only have one LOS link to any anchor and can also determine the LOS ranges between them, i.e. inter-node ranges, and how these scenarios can be exploited to further improve location accuracy. Another scenario of interest, which can occur in very harsh dynamic environments, is the case where all ranges are NLOS. The contributions of this chapter are:

- A method to mitigate random ranging biases in scenarios where a tag can range with multiple anchors but only one anchor is LOS, all anchors are NLOS, or a random number of anchors are NLOS,
- Evaluation of the proposed method via simulations, for a variety of node locations and number of anchors under random NLOS ranging biases, that show that in comparison to location estimates using NLOS ranges without mitigation, the proposed method improves location accuracy significantly,
- The results show that location accuracy can be further improved if LOS ranges between nodes are also used in the localization step of the proposed method,
- The results show that in the case where the NLOS ranges are not identifiable and a random number of ranges are NLOS, the proposed algorithm outperforms SDP-based localization in terms of execution time.

6.3 PROPOSED METHODS

The first scenario considered in this chapter is the case where NLOS ranges can be identified. If at least three anchors are LOS, then the tag's location is estimated using these anchors only. If only two anchors are LOS, there are two possible tag locations since there are two intersection points. The intersection point that is closest to the circle defined by a third anchor is selected as the location. The other two possibilities are the case where only one anchor is LOS and the case where all anchors are NLOS.

6.3.1 Localization with NLOS identification

A node's location can be estimated in the least squares sense by minimizing the following objective function:

$$\hat{x},\hat{y} = \min_{x,y} \sum_{i=1}^{N} ((x_i - x)^2 + (y_i - y)^2 - \hat{d}_i^2)^2 \tag{6.1}$$

where the distance measurement $\hat{d}_i$ includes noise n_i and a positive bias b_i due to NLOS, and N is the number of anchors. This bias has to be removed, or mitigated, to produce an equivalent LOS range r_i, which is given by:

$$r_i = \hat{d}_i - b_i \tag{6.2}$$

In the presence of NLOS biases, the LOS location can be computed in terms of the equivalent LOS ranges as follows:

$$(x_i - x)^2 + (y_i - y)^2 = (\hat{d}_i - b_i)^2, i = 1,...,N \tag{6.3}$$

where the measured NLOS range $\hat{d}_i$ is replaced with the equivalent LOS ranges. For the purpose of explaining the approach, let us assume $N = 5$ and that the node has a LOS link to anchor 1, i.e. $b_1 = 0$, and NLOS links to the remaining anchors. Then, the system of equations to solve for the equivalent LOS location $[x,y]^T$ is:

$$\begin{aligned}
(x_1 - x)^2 + (y_1 - y)^2 &= \hat{d}_1^2 \\
(x_2 - x)^2 + (y_2 - y)^2 &= (\hat{d}_2 - b_2)^2 \\
(x_3 - x)^2 + (y_3 - y)^2 &= (\hat{d}_3 - b_3)^2 \\
(x_4 - x)^2 + (y_4 - y)^2 &= (\hat{d}_4 - b_4)^2 \\
(x_5 - x)^2 + (y_5 - y)^2 &= (\hat{d}_5 - b_5)^2
\end{aligned} \tag{6.4}$$

where the range between the tag and anchor 1 is LOS and the ranges between the tag and anchors 2 to 5 are NLOS. The system in (6.4) is an underdetermined system with $N+1$ unknowns and N equations. Therefore, there is no unique solution when directly solving for $[x, y, b_2, b_3, b_4, b_5]^T$.

Assuming there is no ranging noise and anchor 1 is LOS, the true location of the node lies along the circumference of the circle with center (x_1, y_1) and radius $\hat{d}_1$, where $\hat{d}_1$ is the measured distance between anchor 1 and the node. The radii of the circles defined by the NLOS anchors constrain the set of possible node locations to the arc between points A and B shown in Figure 6.1, where $(x_1, y_1) = (0,0)$. We define the region between points A and B the feasible region, where all xy points along the arc are possible solutions to the node's true location in (6.4). The values that the biases take across the feasible region are illustrated in Figure 6.2.

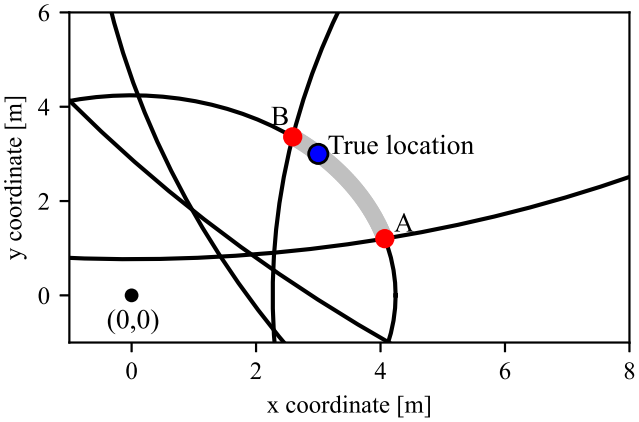

Figure 6.1. Illustration of feasible region.

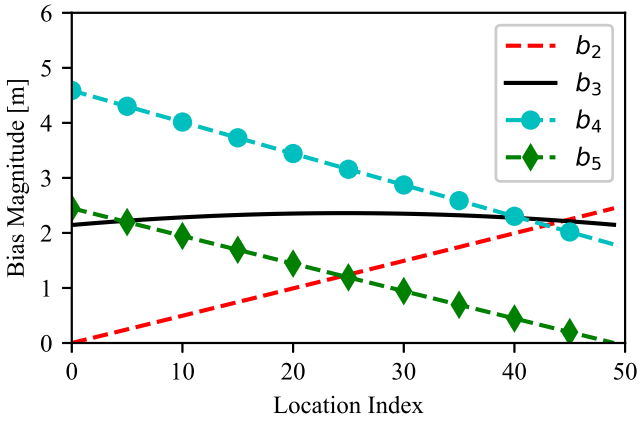

Figure 6.2. Bias values for possible locations along the feasible region.

Given this scenario, a possible approach is to select the midpoint of the arc bounded by points A and B as the node's location. To achieve this, the following procedure is followed. Let p_A and p_B denote the boundary points of the feasible region as illustrated in Figure 6.3.

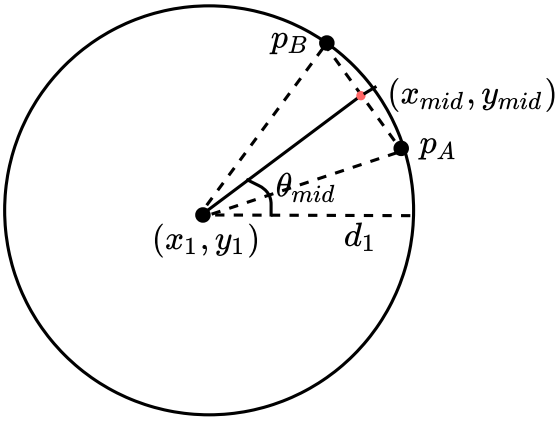

Figure 6.3. Illustration of localization with NLOS identification.

The boundary points of the feasible region are determined as follows. All $2(N-1)$ intersection points between the circle defined by the LOS anchor and the circle defined by each NLOS anchor are determined. An intersection point p which is either at the start or at the end of the feasible region, satisfies the following condition for all NLOS anchors:

$$\sqrt{(x_i - x_p)^2 + (y_i - y_p)^2} < \hat{d}_i \tag{6.5}$$

where i denotes the i-th NLOS anchor, $\hat{d}_i$ is the measured NLOS range between the node and the i-th NLOS anchor, and x_p and y_p are the x and y coordinates of intersection point p. Among all computed intersection points, the two points p_A and p_B that satisfy the criteria in (6.5) are selected as boundary points, and the feasible region is defined by the arc enclosed by p_A and p_B. To find the midpoint of this arc, the midpoint (x_{mid}, y_{mid}) of the line from point p_A and p_B is computed. Then, the angle θ_{mid} of the midpoint illustrated in Figure 6.3, is computed as:

$$\theta_{mid} = \frac{\theta_A + \theta_B}{2} \tag{6.6}$$

where θ_A is the angle to point p_A and θ_B is the angle to point p_B. Finally, the x and y coordinates for the node's location are computed as the midpoint of the arc from p_A to p_B:

$$(x,y) = (d_1 \sin\theta_{mid}, d_1 \cos\theta_{mid}) \tag{6.7}$$

6.3.2 Localization with NLOS identification: cooperative approach

Assuming N anchors and two nodes i and j (with at least one LOS link to an anchor each) and LOS range r_{ij} between the nodes, the location of a node is determined as follows. Following the approach described in Section 6.3.1, points p_A and p_B for the feasible region are determined. However, instead of finding the midpoint of points p_A and p_B, a set of possible locations along the feasible region is generated as follows. Firstly, angle θ_A between the LOS anchor's location and p_A, and angle θ_B between the LOS anchor's location and p_B, are calculated. Since all possible locations of node i lie in the feasible region, the angle θ_l for any possible location l is bounded by $\theta_A < \theta_l < \theta_B$.

With a starting value of θ_A, θ_l is incremented by θ_Δ until $\theta_l = \theta_B$. For each increment, the potential location (x_l, y_l) is the center for a circle with radius given by the LOS range between source nodes i and j, i.e. range r_{ij}.

Points p_A and p_B for source node j are also calculated, and a bounding box is placed around the feasible region of node j. This is illustrated in Figure 6.4 where the bounding box which contains the feasible region for source node j is shown. Since the LOS range between the two source nodes is known, only locations within the respective feasible regions that have a distance between them which is equal to the LOS range between the two source nodes are relevant. Therefore, for each possible location l, a circle with center (x_l, y_l) and radius r_{ij} is defined.

For each potential location l, we check if the circle with center (x_l, y_l) and radius r_{ij} has intersection points with the circle defined by the anchor with a LOS link to anchor j. If there are intersection points, it is then checked if those intersection points are within the bounding box which encloses the feasible region in the LOS anchor for source node j. If yes, the (x_l, y_l) location is inserted into vector $\bar{l}$. This procedure is repeated until $\theta_l = \theta_B$. Finally, the location of node i is found by computing the centroid

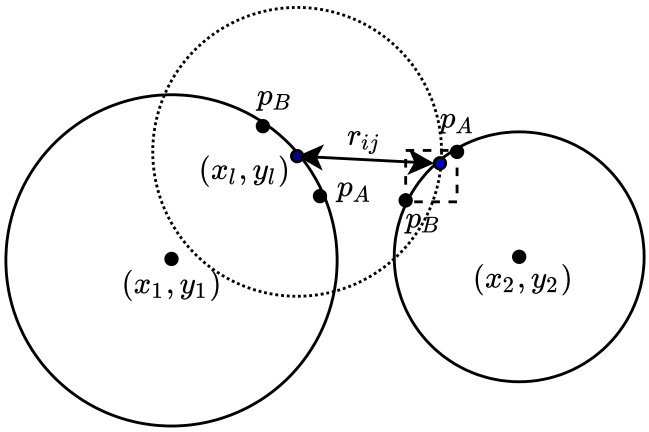

Figure 6.4. Illustration of one step for cooperative localization.

of the locations in vector $\bar{l}$. Algorithm 1 describes this procedure. In Algorithm 1, the location of node i is estimated and node j is used as an auxiliary node. The anchor with LOS to node j is represented by circle C_j, where the center of C_j is the anchor's location and the radius is the LOS range d_j between the anchor and node j.

6.3.3 Localization without NLOS identification

The case where NLOS ranges are not identifiable is also important. In this case, it is assumed that all ranges are NLOS since the LOS/NLOS status is unknown. There are at most $\binom{N}{2}$ pairwise combinations of N anchors, where each pair has none, one or two intersection points. Firstly, all M intersection points are determined. Table 6.1 shows the worst-case number of combinations that must be done for 3 to 8 anchors. Secondly, all intersection points (x_p, y_p) that satisfy (6.5) are selected.

Table 6.1. Number of pairwise combinations.

Number of Anchors	3	4	5	6	7	8
Number of Combinations	3	6	10	15	21	28

The calculation in (6.5) is done for every intersection point for N anchors, i.e. in the worst-case scenario, there are $M \times \binom{N}{2}$ computations. Finally, the tag's location is estimated by computing the centroid of the selected intersection points:

Algorithm 1 Proposed algorithm for cooperative localization.

Result: $[\hat{x}, \hat{y}]$

Determine all intersection points for node i. Repeat for node j

Find the two boundary points p_A and p_B that satisfy (6.5) for node i. Repeat for node j

Compute θ_A and θ_B for node i

Init $\theta_l = \theta_A$ and set $\theta_\triangle = 0.01$. Init vector $\bar{l}$ to empty

while $\theta_l < \theta_B$ **do**

Find location $l = (x_l, y_l)$ on feasible region of node i with angle θ_l

Define circle C_l with center $l = (x_l, y_l)$ and radius d_{ij}

Determine the two intersection points p_{lj} between C_l and C_j

if *any* p_{lj} *is in node* j*'s bounding box* **then**

Append location $l = (x_l, y_l)$ to vector $\bar{l}$

end

$\theta_l = \theta_l + \theta_\triangle$

end

Compute location of node i as the centroid of the locations in vector $\bar{l}$

$$(\hat{x}, \hat{y}) = \left(\frac{1}{m} \sum_{k=1}^{m} x_p^k, \frac{1}{m} \sum_{k=1}^{m} y_p^k \right) \tag{6.8}$$

where m is the number of intersection points that satisfy (6.5), k is the index of the intersection point, and x_p and y_p are the x and y coordinates of these points, respectively.

There is one exception when no intersection points that satisfy (6.5) are found. In this case, the radii of all circles can be incremented by the standard deviation of the ranging noise, such that the overlap between circles is increased and the possibility of finding intersection points exists. This case can occur if some anchors are LOS - when the ranging noise is negative - such that no overlaps between the circles defined by the radii of the anchors exist. Alternatively, in cases where there are more than three anchors, different subsets of anchors can be considered until a subset with intersection points is found. However, in the dataset used in the simulations, less than 10% of the location estimates did not have any intersection points that satisfied (6.5).

6.4 RESULTS AND DISCUSSION

6.4.1 Simulations

To evaluate the proposed algorithm, simulations were conducted. The parameters for the simulations are listed in Table 6.2. The anchors have fixed locations listed in Table 6.2.

Table 6.2. Simulation setup.

Parameter	Value
Anchors 1-3 coordinates	$(0,0),(0,10),(10,10)$
Anchors 4-6 coordinates	$(10,0),(10,5),(5,10)$
Anchors 7-8 coordinates	$(0,5),(5,0)$
$\theta_{\triangle}$	0.01
Bias b distribution	$\mathcal{U}(0.4, 3.5)$
Ranging noise n distribution	$\mathcal{N}(0.0, 0.2^2)$
Number of runs N	2000

The x and y coordinates for the node to be located are randomly generated with distribution $\mathcal{U}(0.0, 20.0)$, each bias is generated with distribution $\mathcal{U}(0.4, 3.5)$, and zero-mean Gaussian noise is generated with distribution $\mathcal{N}(0.0, 0.2^2)$. The biases are estimated using the proposed algorithm for each node location. The NLOS ranges are subtracted by the estimated biases, i.e. mitigated, and then used to determine the node's equivalent LOS location using (6.1). This procedure is done for 2000 random node locations for each anchor configuration, i.e. 3 - 8 NLOS anchors, resulting in a total of 12000 samples. The parameters in Table 6.2 were selected based on experiments conducted in [12] and [90] using commercial-off-the-shelf UWB devices. For ranges measured experimentally, the standard deviation was observed to be small - typically less than 5 cm - but to account for the mean offset errors mentioned in [12] and effects from harsh environments, we set the ranging noise standard deviation to a more realistic 20 cm. We assume that the ranges between the node and anchors are determined using TWR, which does not require synchronization between the node and anchors. All simulations were conducted in Python. The objective function in (6.1) was minimized using SciPy's **optimize** package with the Levenberg-Marquardt algorithm.

6.4.2 Bias estimation with NLOS identification

After mitigation, it is of interest to determine how close the estimated biases are to the true biases. Figure 6.5 shows the difference between the estimated and true biases for 100 of the 2000 samples for the simulation scenario with 4 anchors, i.e. 1 LOS and 3 NLOS anchors. Figure 6.6 shows the same for 8 anchors, i.e. 1 LOS and 7 NLOS anchors. Note that these results are for the case where only one anchor is LOS, and for the bias that changes the least over the estimation window, e.g. b_2 in Figure 6.2). It is observed that in the case of 7 NLOS anchors, the estimated biases are very close to the true biases. This is due to the fact that a higher number of NLOS anchors can result in a smaller feasible region, resulting in more accurate estimation of the biases. Table 6.3 lists the bias estimation error statistics for different numbers of NLOS anchors. It is seen that 95%, i.e. 2σ, of bias estimates are within ± 1 meter of the true value in the case of 3 NLOS anchors and within ± 67 cm of the true value in the case of 7 NLOS anchors. Large estimation errors are only observed for a small fraction of observations, as most estimated biases are relatively close to the true bias, especially in cases with more anchors. These results show that the bias can be accurately estimated, particularly for the case of 7 NLOS anchors and 1 LOS anchor.

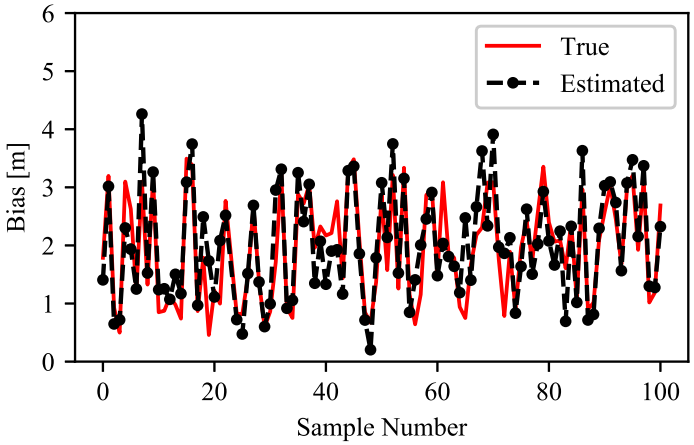

Figure 6.5. True bias vs estimated bias for 3 NLOS anchors.

6.4.3 Location accuracy with NLOS identification

It is also of interest to determine the impact of the proposed method on location accuracy. To this end, we use two metrics to compare localization using the NLOS ranges without any mitigation and localization using ranges after mitigation by the proposed method. The two metrics are location error

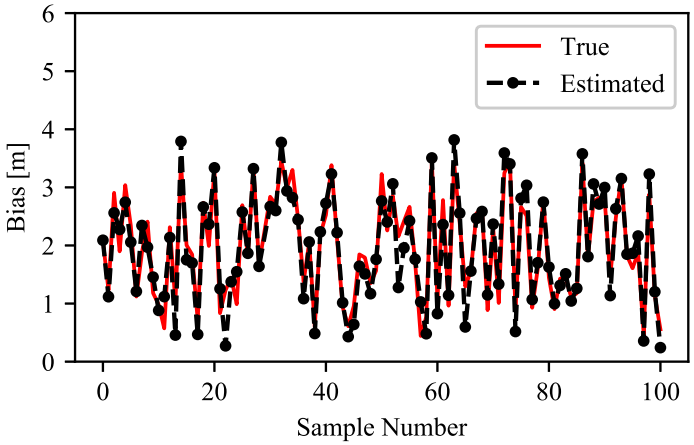

Figure 6.6. True bias vs estimated bias for 7 NLOS anchors.

Table 6.3. Bias estimation error.

Number of NLOS Anchors	μ [m]	σ [m]	2σ [m]
3	0.08	0.49	0.90
5	0.11	0.41	0.78
7	0.02	0.34	0.67

and root mean square error (RMSE). Location error is defined as the Euclidean distance between the true location (x,y) and the estimated location $(\hat{x},\hat{y})$:

$$e = \sqrt{(\hat{x}-x)^2+(\hat{y}-y)^2} \tag{6.9}$$

The RMSE is given by:

$$RMSE = \sqrt{\frac{1}{N}\sum_{n=1}^{N}\left[(\hat{x}_n-x)^2+(\hat{y}_n-y)^2\right]} \tag{6.10}$$

where N = 2000 for these simulations. A cumulative distribution function (CDF) of the location errors is shown in Figure 6.7 for various anchors, where MITI denotes mitigated, and 3, 5 and 7 are the number of NLOS anchors.

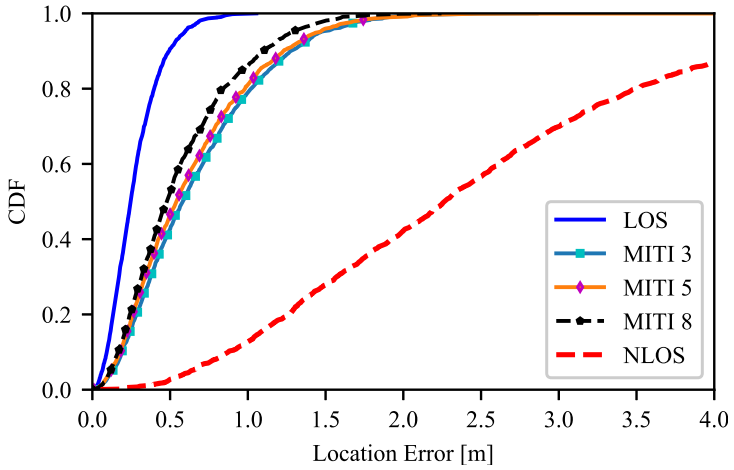

Figure 6.7. CDF for location errors for various anchors.

It is evident that as the number of anchors increases, the location error decreases. This is due to the fact that as the number of anchors increases, the bias estimation errors decrease, therefore the location estimates become more accurate. The RMSE for different numbers of anchors is shown in Figure 6.8. It is seen that as the number of anchors increases, the mitigated location errors decrease, as expected.

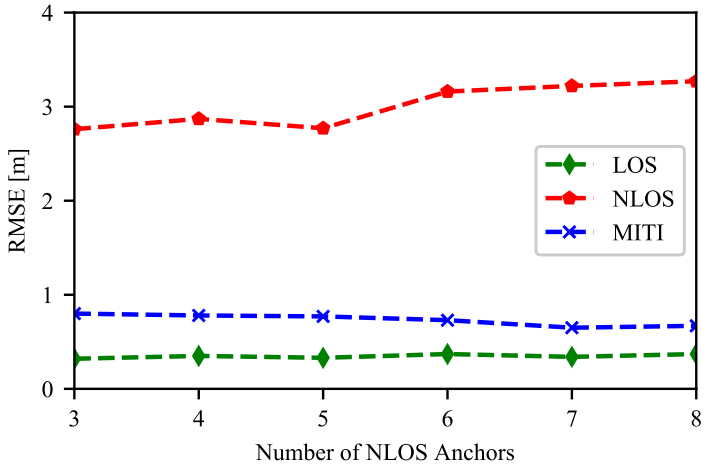

Figure 6.8. Location RMSE.

6.4.4 Location accuracy with NLOS identification: cooperative approach

The same simulation setup is used for the cooperative approach, but in this case we simulate $K = 3$ nodes instead of one node only. Random locations, ranging noise and biases are generated for all K nodes as described in the previous subsection. One of the nodes is randomly selected, defined as node

i and the results are extracted for that node as described in Algorithm 1. Table 6.4 shows the statistics for the bias estimation errors in the case where a node can determine its location to the anchors and has LOS ranges to 2 other nodes.

Table 6.4. Bias estimation error: cooperative approach.

Number of NLOS Anchors	μ [m]	σ [m]	2σ [m]
3	0.06	0.40	0.79
5	0.08	0.34	0.68
7	0.02	0.31	0.59

It is seen that, in comparison to the non-cooperative results in Table 6.3, the bias estimation errors have less variance, showing that the biases are further mitigated by the proposed method. The CDF for location errors for the cooperative case is shown in Figure 6.9.

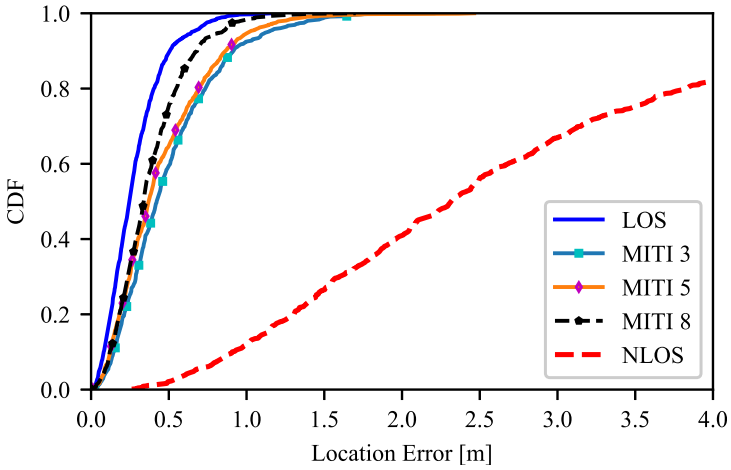

Figure 6.9. CDF for location errors for various anchors using the cooperative approach.

Compared to the CDF in Figure 6.7, it is evident that the location accuracy in the cooperative case is improved. The root mean-square location errors between the non-cooperative (NON-COOP) and cooperative (COOP) approach for 3 to 7 NLOS anchors are also compared in Figure 6.10. It is observed that the RMSE for the cooperative case is better than the non-cooperative case, and is very close to the LOS case with 7 NLOS anchors. Overall, the results show that the location accuracy using the cooperative approach is higher than the non-cooperative approach.

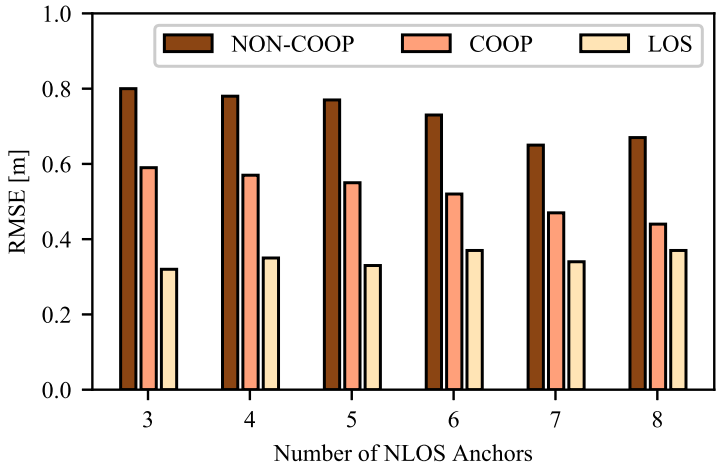

Figure 6.10. RMSE: Non-cooperative vs cooperative approach.

6.4.5 Location accuracy without NLOS identification

The algorithm described in Section 6.3.3 is evaluated for 2000 location estimates using 8 anchors with at least one NLOS range. The simulation setup described in Section 6.4.1 is also used here. The bias distribution is changed to $\mathcal{U}(2.0, 6.0)$ such that it is comparable to the setup described in [55]. The results are compared to a SDP-based algorithm for TOA localization proposed in [55], which was shown to outperform Least Median Squares, QP and Huber estimators. The node's location $\mathbf{x}$ in [55] is found by solving the following convex optimization problem:

$$\begin{aligned} &\min_{\mathbf{x},z,h_i,c_i} \sum_{i\in\mathcal{A}} v_i(r_i^2 - h_i - c_i)^2 + \delta \sum_{i\in\mathcal{A}} c_i^2 \\ &\text{s.t.} \quad h_i = \begin{bmatrix} \mathbf{y_i} \\ -1 \end{bmatrix}^T \begin{bmatrix} \mathbf{I}_2 & \mathbf{x} \\ \mathbf{x}^T & z \end{bmatrix} \begin{bmatrix} \mathbf{y_i} \\ -1 \end{bmatrix}, \\ &\qquad \begin{bmatrix} \mathbf{I}_2 & (\mathbf{y}_i - \mathbf{x}) \\ (\mathbf{y}_i - \mathbf{x}) & r_i^2 + u_i \end{bmatrix}^T \succeq \mathbf{0}_3, \\ &\qquad \begin{bmatrix} \mathbf{I}_2 & \mathbf{x} \\ \mathbf{x}^T & z \end{bmatrix} \succeq \mathbf{0}_3, \; c_i \geq 0 \end{aligned} \tag{6.11}$$

where i is the number of anchors, v_i is a weight vector, and r_i are the measured ranges between the

tag and anchor i. The problem in (6.11) was implemented using CVXPY with the MOSEK solver on Python 3.6.6. Similar to the work in [55], the constant δ was set to 0.1. Table 6.5 shows the RMSE of the proposed algorithm compared to the SDP algorithm.

Table 6.5. RMSE for LLSE, SDP and proposed method.

σ [m]	LLSE [m]	SDP [m]	MITI [m]
0.1	3.10	1.69	1.61
0.2	3.12	1.69	1.73
0.3	3.11	1.77	1.78
0.4	3.17	1.87	1.87
0.5	3.24	1.90	1.96

The simulations are run for values of σ 0.1, 0.2, 0.3 and 0.5 (in meters) to see how robust the proposed method is to ranging noise. The LLSE column refers location estimates obtained with the closed form LLS estimator in (2.10) without any NLOS mitigation. The comparison was carried out for different values of σ to evaluate the robustness of the proposed algorithm. MITI refers to the proposed method. Figure 6.11 shows the CDF for ranging noise with a σ of 0.5 for eight anchors. The number of NLOS ranges is randomly generated (from an uniform distribution) with values between 1 and 8 for all samples.

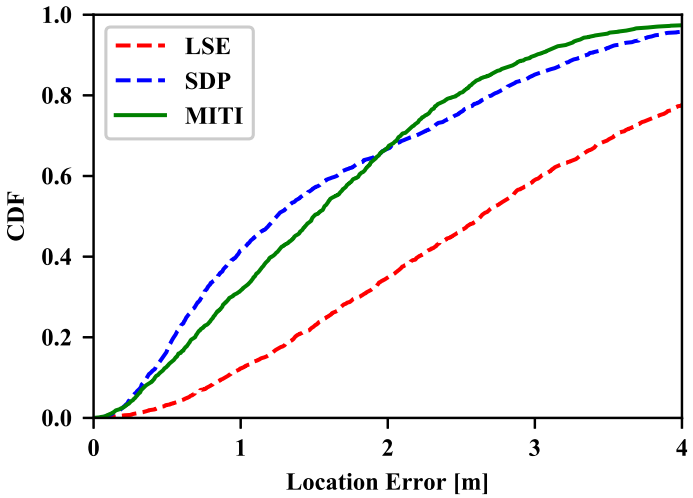

Figure 6.11. CDF with location errors for LLSE, SDP and proposed method (MITI).

The average execution times in milliseconds are shown in Table 6.6. These were measured over all 2000 location estimates for a σ of 0.5 using a timer from the timeit package in Python 3.6, by

Table 6.6. Execution times in milliseconds.

Approach	Implementation	Time [ms]
LLSE	Python using Numpy	2.72
SDP	Python CXVPY with MOSEK solver	187.2
MITI	Python using Numpy	28.53

timestamping the start of calculation with the command start = timer(), timestamping the end of the computation with end = timer() at the end of the execution, and subtracting the two timestamps to obtain the elapsed time. For the SDP solver in CVXPY, the timestamps were placed just before and just after the function prob.solve(solver=cp.MOSEK, verbose=False). These execution times were measured on a computer with an Intel Celeron N4300 (dual core) processor with 4GB RAM and a solid-state drive running Windows 10. It is evident that the proposed algorithm is over five times faster than the SDP algorithm and it has similar location accuracy. The proposed algorithm has the following advantages: it does not require any specialized solver and it relies only on computation of square roots, therefore it executes faster than the state-of-the-art SDP approach. Another advantage of this algorithm is that different sections of it can be optimized for implementation in resource-constrained devices, while for the SDP approach it is not trivial to do so since optimization expertise is required.

6.5 CONCLUSION

This chapter proposed a method for localization in NLOS conditions. The proposed method was evaluated via simulations and it was shown that the method increases location accuracy in scenarios with limited LOS where NLOS ranges are identifiable. The proposed method was extended to a cooperative approach, which was shown to further improve location accuracy. Finally, a method to deal with the case where NLOS is not identifiable was also proposed, and shown to have similar location accuracy while outperforming a SDP-based approach in terms of execution time.

6.6 CHAPTER SUMMARY

This chapter proposed a localization method for scenarios with NLOS conditions caused by random NLOS biases. The method was evaluated for the case where NLOS conditions are identifiable and

the case where NLOS conditions are not identifiable. For the latter case, the results showed that the proposed method outperforms SDP based localization.

Section 6.2 introduced and motivated the work. The context of the work was explained, and the importance of mitigating NLOS ranges caused by random NLOS conditions was highlighted. In Section 6.3, novel localization methods for NLOS conditions were developed. Three variants were developed: mitigation with NLOS identification, cooperative mitigation with NLOS mitigation and mitigation without NLOS identification. The proposed methods do not rely on knowledge of channel statistics, nor distribution of NLOS ranges, for mitigation and they can be used for random NLOS conditions. In Section 6.4, the proposed method is evaluated (via simulations) for the three different variants described in Section 6.3. The results showed that the first and second variants outperform the conventional LLS estimator in terms of location accuracy. The third variant resulted in location accuracy similar to a state-of-the-art SDP based localization algorithm, and outperformed it in terms of execution time. The conclusion to the chapter is given in Section 6.5.

CHAPTER 7 CONCLUSION

7.1 SUMMARY

Accurate localization is required for many applications across various domains. Several challenges to achieve accurate localization exist, including identification and mitigation of NLOS conditions. NLOS conditions degrade location accuracy and can affect several applications, particularly in industrial environments. To apply NLOS identification and mitigation methods effectively in IR-UWB sensor networks, several requirements must be met. These methods should be of low complexity; they should be applicable to both static and mobile scenarios; they should use limited site-specific training data; and they should ideally not rely on knowledge of the distribution of range measurements. Most identification and mitigation methods in literature do not address all these requirements cohesively. In many cases, methods provide higher location accuracy at the expense of increased computational or time complexity.

The main objective of this thesis was to improve the location accuracy of IR-UWB sensor networks in NLOS conditions. This thesis investigated the use of NLOS identification and mitigation for IR-UWB sensor networks. Approaches for NLOS identification and mitigation that focus on these aspects - location accuracy, location update rate and complexity - were proposed. Two approaches for NLOS identification and two approaches for NLOS mitigation in sensor networks were proposed. The results are supported by measurement campaigns conducted with IEEE 802.15.4a compliant IR-UWB devices. With regards to the research hypotheses, the results of this study show that:

1. The use of channel statistics from multiple UWB channels results in less complex NLOS classifiers than classifiers that rely on a single channel.

2. Using distance residuals, NLOS location estimates can be detected with high accuracy without relying on multiple range measurements nor channel statistics.

3. NLOS mitigation can be done without knowledge of channel statistics, multiple range measurements nor mobility. In cases where a floor plan is available, information from the floor plan can be leveraged for mitigation of NLOS conditions caused by TTW propagation. In cases where a floor plan is not available, mitigation can be done by considering geometric constraints that arise in NLOS localization due to the positive biases.

4. Node-to-node LOS ranges further improve mitigation of NLOS conditions compared to approaches which only consider node-to-anchor ranges.

7.2 CONTRIBUTIONS

A comprehensive review of the state-of-the-art in NLOS identification and mitigation is presented in Chapter 2. This review is presented from a perspective of IR-UWB sensor networks. Challenges particular to harsh industrial environments - which often present more issues than conventional indoor environments such as residential and office environments - are discussed in detail.

A NLOS identification method that does not rely on channel statistics nor range measurement statistics is proposed in Chapter 3. The method relies on a classifier trained with distance residuals (instead of channel statistics) from LOS and NLOS conditions. Since residuals are calculated at the localization level, and are therefore agnostic to the wireless standard used in the PHY layer, this approach is not limited to UWB localization. Since distance residuals are calculated at the localization level, individual NLOS channel identification is not performed. The proposed method addresses this limitation by supporting identification of individual NLOS ranges for cases where certain criteria are met.

A NLOS classification method to classify NLOS conditions into TTW or ATC is proposed in Chapter 4. Both types of NLOS conditions occur often in indoor localization and their identification is crucial to the application of specific mitigation methods for each type of condition. This method relies on channel statistics extracted from two UWB channels: one channel in the low-band (3244–4742 MHz) and one channel in the high-band (5944–10234 MHz). In general, channel statistics from the channel

in the high-band result in higher classification accuracy. When channel statistics from both channels are combined, the high classification accuracy is achieved with less channel statistics, leading to less complex classifiers. Although this method requires channel statistics, the results are collected from two sites, but are not biased towards any of the sites. The results are supported by measurement campaigns.

A mitigation method for TTW NLOS conditions based on a novel TTW TOA ranging model and information from floor plans is proposed in Chapter 5. This TTW TOA ranging model has less parameters than the conventional TTW TOA ranging model, and does not rely on the knowledge of incidence angles or other parameters that require a detailed characterization of the environment. The model is experimentally evaluated, and integrated into localization using a NLLS estimator. All results show that NLOS conditions caused by TTW are significantly mitigated with the proposed method, yet the knowledge of channel statistics and models for the NLOS errors, are not required. The results are supported by measurement campaigns.

Three variants of a NLOS mitigation method that does not rely on floor plans nor channel statistics are proposed in Chapter 6. This method relies on geometric constraints, that arise due to the fact that the biases created by NLOS conditions are by definition positive, to estimate a more accurate location in comparison to a LLS estimator. The method is evaluated for the case where NLOS ranges are not identifiable and the case where they are identifiable. The first case is compared to state-of-the-art SDP based localization, and it is found that it results in similar location accuracy, but its execution time is much faster, making it more suitable for applications that require a fast update rate. Secondly, the proposed method does not require any specialized optimization solvers that are challenging to implement in resource-constrained devices. For the latter case, the method is extended to leverage node-to-node LOS range to further constrain the region where the estimated location lies, leading to a more accurate location estimation than the non-cooperative method.

7.3 FURTHER RESEARCH

Evaluation and linearization of the TTW mitigation method in sensor nodes: the method in Chapter 4 relies on a TOA ranging model that requires an algorithm for non-linear least squares like LM. An interesting direction for future work is the linearization of the objective function in (5.15) such

that a closed form solution similar to the one in (2.10) is developed. In its current form, the expression in (5.15) requires an initial estimate of the location. If the expression in (5.15) linearized, then no initial location estimate is required.

Benchmarking proposed methods on resource constrained devices: it is of interest to compare the complexity of the method proposed in Chapter 3 with the other NLOS identification methods proposed in this thesis. The NLOS identification methods proposed in Chapter 4 should perform well in resource-constrained devices because of the simple linear decision functions, but this has to be verified experimentally. Although the mitigation algorithms proposed in Chapter 6 were shown to outperform the state-of-the-art SDP algorithm in terms of execution time, these measurements were taken an x86 based computer. These should be evaluated on resource-constrained devices. The work in [12] used the Forces Pro solver for SDP localization, while the algorithms proposed in Chapter 6 do not require any specialized solver. More recently, there has been an increasing focus on TDOA based localization and UWB devices now support TDOA based localization. The methods proposed in this thesis are TOA based, therefore it is of interest to extend the proposed methods to TDOA based localization.

Integrated evaluation of proposed methods: although the NLOS identification methods in Chapters 3 and 4 were developed independently of the mitigation methods presented in Chapters 5 and 6, they are related. The mitigation method in Chapter 5 assumes identification of TTW NLOS conditions, while the technique to identify TTW NLOS conditions is evaluated independently in Chapter 4. These two methods can be integrated and evaluated. The technique introduced in Chapter 3 can be used to select LOS anchors to improve the limited location accuracy in scenarios with many LOS anchors by identifying sets of LOS anchors and using those in the location estimate for the method proposed in Chapter 6. It is expected that this identification technique will work well in scenarios with many LOS ranges, and improve the limited location accuracy compared to SDP with many LOS anchors.

REFERENCES

[1] S. Vatansever and I. Butun, "A broad overview of GPS fundamentals: Now and future," in *Proceedings of the 2017 IEEE 7th Annual Computing and Communication Workshop and Conference (CCWC)*, Las Vegas, USA, 2017, pp. 1–6.

[2] A. Yassin *et al.*, "Recent advances in indoor localization: A survey on theoretical approaches and applications," *IEEE Communications Surveys & Tutorials*, vol. 19, no. 2, pp. 1327–1346, 2nd Quarter 2017.

[3] M. Usman, M. R. Asghar, I. S. Ansari, F. Granelli, and K. A. Qaraqe, "Technologies and solutions for location-based services in smart cities: Past, present, and future," *IEEE Access*, vol. 6, pp. 22 240–22 248, 2018.

[4] Markets and Markets, "Indoor Location Market - Global Forecast to 2025," 2019. Accessed: Oct. 10, 2020. [Online]. Available: https://www.marketsandmarkets.com/Market-Reports/indoor-location-market-989.html

[5] N. Bulusu, J. Heidemann, and D. Estrin, "GPS-less low-cost outdoor localization for very small devices," *IEEE Personal Communications*, vol. 7, no. 5, pp. 28–34, Oct. 2000.

[6] N. Patwari, J. N. Ash, S. Kyperountas, A. O. Hero, R. L. Moses, and N. S. Correal, "Locating the nodes: cooperative localization in wireless sensor networks," *IEEE Signal Processing Magazine*, vol. 22, no. 4, pp. 54–69, July 2005.

[7] E. Karapistoli, F. Pavlidou, I. Gragopoulos, and I. Tsetsinas, "An overview of the IEEE 802.15.4a standard," *IEEE Communications Magazine*, vol. 48, no. 1, pp. 47–53, Jan. 2010.

[8] C. McElroy, D. Neirynck, and M. McLaughlin, "Comparison of wireless clock synchronization algorithms for indoor location systems," in *Proceedings of the 2014 IEEE International Conference on Communications (ICC)*, Sydney, Australia, 2014, pp. 157–162.

[9] I. Guvenc and C. Chong, "A survey on TOA based wireless localization and NLOS mitigation techniques," *IEEE Communications Surveys & Tutorials*, vol. 11, no. 3, pp. 107–124, 3rd Quarter 2009.

[10] Y. P. J. Khodjaev and A. Saeed Malik, "Survey of NLOS identification and error mitigation problems in UWB-based positioning algorithms for dense environments," *Annals of Telecommunications*, vol. 65, no. 5, pp. 301–311, Aug. 2010.

[11] H. Chen, G. Wang, Z. Wang, H. C. So, and H. V. Poor, "Non-line-of-sight node localization based on semi-definite programming in wireless sensor networks," *IEEE Transactions on Wireless Communications*, vol. 11, no. 1, pp. 108–116, Jan. 2012.

[12] P. N. Beuchat, H. Hesse, A. Domahidi, and J. Lygeros, "Enabling optimization-based localization for IoT devices," *IEEE Internet of Things Journal*, vol. 6, no. 3, pp. 5639–5650, June 2019.

[13] K. Bregar and M. Mohorčič, "Improving indoor localization using convolutional neural networks on computationally restricted devices," *IEEE Access*, vol. 6, pp. 17 429–17 441, 2018.

[14] B. Silva, Z. Pang, J. Åkerberg, J. Neander, and G. P. Hancke, "Positioning infrastructure for industrial automation systems based on UWB wireless communication," in *Proceedings of the 40th Annual Conference of the IEEE Industrial Electronics Society (IECON)*, Dallas, USA, 2014, pp. 3919–3925.

[15] S. Kuutti, S. Fallah, K. Katsaros, M. Dianati, F. Mccullough, and A. Mouzakitis, "A survey of the state-of-the-art localization techniques and their potentials for autonomous vehicle applications," *IEEE Internet of Things Journal*, vol. 5, no. 2, pp. 829–846, April 2018.

[16] A. Shahi, J. West, and C. Haas, "Onsite 3D marking for construction activity tracking," *Automation in Construction*, vol. 30, no. 1, pp. 136–143, Mar. 2013.

[17] F. Kirsch, R. Miesen, and M. Vossiek, "Precise local-positioning for autonomous situation awareness in the internet of things," in *Proceedings of the 2014 IEEE MTT-S International Microwave Symposium (IMS2014)*, Tampa, USA, 2014, pp. 1–4.

[18] R. S. Kulikov, A. A. Chugunov, D. V. Tsaregorodcev, N. I. Petukhov, and I. R. Indrikov, "Two-dimension positioning solution of high accuracy navigation and orientation for service robots," in *Proceedings of the 2019 International Youth Conference on Radio Electronics, Electrical and Power Engineering (REEPE)*, Moscow, Russia, 2019, pp. 1–4.

[19] W. Wang, Z. Zeng, W. Ding, H. Yu, and H. Rose, "Concept and validation of a large-scale human-machine safety system based on real-time UWB indoor localization," in *Proceedings of the 2019 IEEE/RSJ International Conference on Intelligent Robots and Systems (IROS)*, Macau, China, 2019, pp. 201–207.

[20] K. Nienhaus, M. Hahn, and R. Winkel, "Wireless sensing applications in the mining and minerals industry," in *Proceedings of the 2009 IEEE MTT-S International Microwave Workshop on Wireless Sensing, Local Positioning, and RFID*, Cavtat, Croatia, 2009, pp. 1–4.

[21] V. Djaja-Josko and J. Kolakowski, "UWB positioning system for elderly persons monitoring," in *Proceedings of the 2015 23rd Telecommunications Forum Telfor (TELFOR)*, Belgrade, Serbia, 2015, pp. 169–172.

[22] A. Barua, C. Dong, F. Al-Turjman, and X. Yang, "Edge computing-based localization technique to detecting behavior of dementia," *IEEE Access*, vol. 8, pp. 82 108–82 119, 2020.

[23] A. Basiri *et al.*, "Indoor location based services challenges, requirements and usability of current solutions," *Computer Science Review*, vol. 24, no. 1, pp. 1–12, May 2017.

[24] L. Thrybom, J. Neander, E. Hansen, and K. Landernas, "Future challenges of positioning in underground mines," *IFAC-PapersOnLine*, vol. 48, no. 10, pp. 222–226, June 2015.

[25] L. Thrybom, M. Gidlund, J. Neander, and K. Landernas, "Key requirements for successful deployment of positioning applications in industrial automation," in *Proceedings of the International Conference on Indoor Positioning and Indoor Navigation (IPIN)*, Montbeliard, France, 2013, pp. 1–4.

[26] A. A. M. Saleh and R. Valenzuela, "A statistical model for indoor multipath propagation," *IEEE Journal on Selected Areas in Communications*, vol. 5, no. 2, pp. 128–137, Feb. 1987.

[27] J. Karedal, S. Wyne, P. Almers, F. Tufvesson, and A. F. Molisch, "A measurement-based statistical model for industrial ultra-wideband channels," *IEEE Transactions on Wireless Communications*, vol. 6, no. 8, pp. 3028–3037, Aug. 2007.

[28] J. Ferrer-Coll, P. Ängskog, H. Shabai, J. Chilo, and P. Stenumgaard, "Analysis of wireless communications in underground tunnels for industrial use," in *Proceedings of the 38th Annual Conference of the IEEE Industrial Electronics Society (IECON)*, Montreal, Canada, 2012, pp. 3216–3220.

[29] A. Chehri, P. Fortier, and P. Tardif, "Characterization of the ultra-wideband channel in confined environments with diffracting rough surfaces," *Wireless Personal Communications*, vol. 62, no. 4, pp. 859–877, Aug. 2012.

[30] V. Sipal, B. Allen, and D. Edwards, "Impact of antennas on practical UWB signals," in *Proceedings of the 7th European Conference on Antennas and Propagation (EuCAP)*, Gothenburg, Sweden, 2013, pp. 545–548.

[31] E. Tanghe, D. P. Gaillot, M. Liénard, L. Martens, and W. Joseph, "Experimental analysis of dense multipath components in an industrial environment," *IEEE Transactions on Antennas and Propagation*, vol. 62, no. 7, pp. 3797–3805, July 2014.

[32] J. F. Coll, J. Chilo, and B. Slimane, "Radio-frequency electromagnetic characterization in factory infrastructures," *IEEE Transactions on Electromagnetic Compatibility*, vol. 54, no. 3, pp. 708–711, June 2012.

[33] C. Nerguizian, C. Despins, and S. Affes, "Geolocation in mines with an impulse response fingerprinting technique and neural networks," *IEEE Transactions on Wireless Communications*, vol. 5, no. 3, pp. 603–611, Mar. 2006.

[34] I. Guvenc, C. Chong, and F. Watanabe, "NLOS identification and mitigation for UWB localization systems," in *Proceedings of the 2007 IEEE Wireless Communications and Networking Conference*, Kowloon, China, 2007, pp. 1571–1576.

[35] Decawave. *DW1000 Datasheet*. (2016). Accessed: Oct. 10, 2020. [Online]. Available: https://www.decawave.com/sites/default/files/resources/dw1000-datasheet-v2.09.pdf

[36] B. Silva and G. P. Hancke, "IR-UWB-based non-line-of-sight identification in harsh environments: Principles and challenges," *IEEE Transactions on Industrial Informatics*, vol. 12, no. 3, pp. 1188–1195, June 2016.

[37] M. Di Benedetto, T. Kaiser, A. Molish, I. Oppermann, C. Politano, and D. Porcino, *UWB Communication Systems: A Comprehensive Overview*, 1st ed. Hindawi Publishing Corporation, 2006.

[38] IEEE 802.15.4a, "Part 15.4: Wireless medium access control (MAC) and physical layer (PHY) specifications for low-rate wireless personal area networks (LRWPANs)," *IEEE Std 802.15.4a-2007*, pp. 1–210, Aug 2007.

[39] D. Dardari, A. Conti, U. Ferner, A. Giorgetti, and M. Z. Win, "Ranging with ultrawide bandwidth signals in multipath environments," *Proceedings of the IEEE*, vol. 97, no. 2, pp. 404–426, Feb. 2009.

[40] Q. Ngo, P. Roussel, B. Denby, and G. Dreyfus, "Correcting non-line-of-sight path length estimation for ultra-wideband indoor localization," in *Proceedings of the 2015 International Conference on Location and GNSS (ICL-GNSS)*, June 2015, pp. 1–6.

[41] P. Pagani, F. Talom, P. Pajusco, and B. Uguen, *Ultra-Wideband Radio Propagation Channels: A Practical Approach*, 1st ed. Wiley, 2008.

[42] A. Beck, P. Stoica, and J. Li, "Exact and approximate solutions of source localization problems," *IEEE Transactions on Signal Processing*, vol. 56, no. 5, pp. 1770–1778, May 2008.

[43] W. Dargie and C. Poellabauer, *Fundamentals of Wireless Sensor Networks: Theory and Practice*, 1st ed. Wiley, 2010.

[44] D. W. Marquardt, "An algorithm for least-squares estimation of nonlinear parameters," *Journal of the Society for Industrial and Applied Mathematics*, vol. 11, no. 2, pp. 431–441, July 1963.

[45] Y. Lin, D. O'Malley, and V. Vesselinov, "A computationally efficient parallel Levenberg-Marquardt algorithm for highly parameterized inverse model analyses," *Water Resources Research*, vol. 52, no. 9, pp. 6948–6977, Sept. 2016.

[46] Pi-Chun Chen, "A non-line-of-sight error mitigation algorithm in location estimation," in *Proceedings of WCNC. 1999 IEEE Wireless Communications and Networking Conference (Cat. No.99TH8466)*, New Orleans, USA, 1999, pp. 316–320.

[47] L. Jiao, J. Xing, and F. Y. Li, "Performance comparison of residual related algorithms for ToA positioning in wireless terrestrial and sensor networks," in *Proceedings of the 2009 1st International Conference on Wireless Communication, Vehicular Technology, Information Theory and Aerospace & Electronic Systems Technology*, Aalborg, Denmark, 2009, pp. 278–283.

[48] D. Liu, M. Lee, C. Pun, and H. Liu, "Analysis of wireless localization in nonline-of-sight conditions," *IEEE Transactions on Vehicular Technology*, vol. 62, no. 4, pp. 1484–1492, May 2013.

[49] M. P. Wylie and J. Holtzman, "The non-line of sight problem in mobile location estimation," in *Proceedings of ICUPC - 5th International Conference on Universal Personal Communications*, Cambridge, USA, 1996, pp. 827–831.

[50] J. Borras, P. Hatrack, and N. B. Mandayam, "Decision theoretic framework for NLOS identification," in *Proceedings of VTC '98. 48th IEEE Vehicular Technology Conference. Pathway to Global Wireless Revolution (Cat. No.98CH36151)*, Ottawa, Canada, 1998, pp. 1583–1587.

[51] B. J. Silva and G. P. Hancke, "Characterization of non-line of sight paths using 802.15.4a," in *Proceedings of the 2017 IEEE International Conference on Industrial Technology (ICIT)*, Toronto, Canada, 2017, pp. 1436–1440.

[52] S. Venkatesh and R. M. Buehrer, "NLOS mitigation using linear programming in ultrawideband location-aware networks," *IEEE Transactions on Vehicular Technology*, vol. 56, no. 5, pp. 3182–3198, Sept. 2007.

[53] K. Yu and Y. J. Guo, "Improved positioning algorithms for nonline-of-sight environments," *IEEE Transactions on Vehicular Technology*, vol. 57, no. 4, pp. 2342–2353, July 2008.

[54] G. Wang, H. Chen, Y. Li, and N. Ansari, "NLOS error mitigation for TOA-based localization via convex relaxation," *IEEE Transactions on Wireless Communications*, vol. 13, no. 8, pp. 4119–4131, Aug. 2014.

[55] R. M. Vaghefi, J. Schloemann, and R. M. Buehrer, "NLOS mitigation in TOA-based localization using semidefinite programming," in *Proceedings of the 2013 10th Workshop on Positioning, Navigation and Communication (WPNC)*, Dresden, Germany, 2013, pp. 1–6.

[56] Z. Su, G. Shao, and H. Liu, "A soft-minimum method for NLOS error mitigation in TOA systems," in *Proceedings of the 2016 IEEE 84th Vehicular Technology Conference (VTC-Fall)*, Montreal, Canada, 2016, pp. 1–4.

[57] J. M. Huerta, J. Vidal, A. Giremus, and J. Tourneret, "Joint particle filter and UKF position tracking in severe non-line-of-sight situations," *IEEE Journal of Selected Topics in Signal Processing*, vol. 3, no. 5, pp. 874–888, Oct. 2009.

[58] Chin-Der Wann and Chih-Sheng Hsueh, "NLOS mitigation with biased kalman filters for range estimation in UWB systems," in *Proceedings of TENCON 2007 - 2007 IEEE Region 10 Conference*, Taipei, Taiwan, 2007, pp. 1–4.

[59] X. Zhou, A. Jin, and Q. Meng, "NLOS error mitigation in mobile location based on modified extended kalman filter," in *Proceedings of the 2012 IEEE Wireless Communications and Networking*

Conference (WCNC), Paris, France, 2012, pp. 2451–2456.

[60] S. Yousefi, X. Chang, and B. Champagne, "Mobile localization in non-line-of-sight using constrained square-root unscented kalman filter," *IEEE Transactions on Vehicular Technology*, vol. 64, no. 5, pp. 2071–2083, May 2015.

[61] C. Gentile, "Using the kurtosis measure to identify clusters in wireless channel impulse responses," *IEEE Transactions on Antennas and Propagation*, vol. 61, no. 6, pp. 3392–3395, June 2013.

[62] S. Maranò, W. M. Gifford, H. Wymeersch, and M. Z. Win, "NLOS identification and mitigation for localization based on UWB experimental data," *IEEE Journal on Selected Areas in Communications*, vol. 28, no. 7, pp. 1026–1035, Sept. 2010.

[63] S. Venkatesh and R. M. Buehrer, "Non-line-of-sight identification in ultra-wideband systems based on received signal statistics," *IET Microwaves, Antennas & Propagation*, vol. 1, no. 6, pp. 1120–1130, Dec. 2007.

[64] Z. Xiao, H. Wen, A. Markham, N. Trigoni, P. Blunsom, and J. Frolik, "Non-line-of-sight identification and mitigation using received signal strength," *IEEE Transactions on Wireless Communications*, vol. 14, no. 3, pp. 1689–1702, Mar. 2015.

[65] H. Wymeersch, S. Marano, W. M. Gifford, and M. Z. Win, "A machine learning approach to ranging error mitigation for UWB localization," *IEEE Transactions on Communications*, vol. 60, no. 6, pp. 1719–1728, June 2012.

[66] M. Heidari, N. A. Alsindi, and K. Pahlavan, "UDP identification and error mitigation in toa-based indoor localization systems using neural network architecture," *IEEE Transactions on Wireless Communications*, vol. 8, no. 7, pp. 3597–3607, July 2009.

[67] V. Savic, E. G. Larsson, J. Ferrer-Coll, and P. Stenumgaard, "Kernel methods for accurate UWB-based ranging with reduced complexity," *IEEE Transactions on Wireless Communications*, vol. 15, no. 3, pp. 1783–1793, Mar. 2016.

[68] M. Ramadan, V. Sark, J. Gutierrez, and E. Grass, "NLOS identification for indoor localization using random forest algorithm," in *Proceedings of WSA 2018 22nd International ITG Workshop on Smart Antennas*, Bochum, Germany, March 2018, pp. 1–5.

[69] Y. Zhu, W. Xia, F. Yan, and L. Shen, "NLOS identification via AdaBoost for wireless network localization," *IEEE Communications Letters*, vol. 23, no. 12, pp. 2234–2237, Dec. 2019.

[70] M. Stahlke, S. Kram, C. Mutschler, and T. Mahr, "NLOS detection using UWB channel impulse responses and convolutional neural networks," in *Proceedings of the 2020 International Conference on Localization and GNSS (ICL-GNSS)*, Tampere, Finland, 2020, pp. 1–6.

[71] J. Fan and A. S. Awan, "Non-line-of-sight identification based on unsupervised machine learning in ultra wideband systems," *IEEE Access*, vol. 7, pp. 32 464–32 471, 2019.

[72] Z. Miao, L. Zhao, W. Yuan, and F. Jin, "Application of one-class classification in NLOS identification of UWB positioning," in *Proceedings of the 2016 International Conference on Information System and Artificial Intelligence (ISAI)*, Hong Kong, China, 2016, pp. 318–322.

[73] T. Van Nguyen, Y. Jeong, H. Shin, and M. Z. Win, "Machine learning for wideband localization," *IEEE Journal on Selected Areas in Communications*, vol. 33, no. 7, pp. 1357–1380, July 2015.

[74] S. K. Meghani, M. Asif, F. Awin, and K. Tepe, "Empirical based ranging error mitigation in IR-UWB: A fuzzy approach," *IEEE Access*, vol. 7, pp. 33 686–33 697, Mar. 2019.

[75] B. Cheng, L. Cui, W. Jia, W. Zhao, and G. P. Hancke, "Multiple regions of interest coverage in camera sensor networks for tele-intensive care units," *IEEE Transactions on Industrial Informatics*, vol. 12, no. 6, pp. 2331–2341, Dec. 2016.

[76] S. V. Sibanyoni, D. T. Ramotsoela, B. J. Silva, and G. P. Hancke, "A 2-D acoustic source localization system for drones in search and rescue missions," *IEEE Sensors Journal*, vol. 19, no. 1, pp. 332–341, Jan. 2019.

[77] U. M. Qureshi, G. P. Hancke, T. Gebremichael, U. Jennehag, S. Forsström, and M. Gidlund, "Survey of proximity based authentication mechanisms for the industrial internet of things," in *Proceedings of the 44th Annual Conference of the IEEE Industrial Electronics Society (IECON)*, Washington DC, USA, 2018, pp. 5246–5251.

[78] U. M. Qureshi, Z. Umair, Y. Duan, and G. P. Hancke, "Analysis of bluetooth low energy (BLE) based indoor localization system with multiple transmission power levels," in *Proceedings of the 2018 IEEE 27th International Symposium on Industrial Electronics (ISIE)*, Cairns, Australia, 2018, pp. 1302–1307.

[79] U. M. Qureshi, Z. Umair, and G. P. Hancke, "Evaluating the implications of varying bluetooth low energy (BLE) transmission power levels on wireless indoor localization accuracy and precision," *Sensors*, vol. 19, no. 15, July 2019, Art. no. 3282.

[80] B. J. Silva and G. P. Hancke, "Ranging error mitigation for through-the-wall non-line-of-sight conditions," *IEEE Transactions on Industrial Informatics*, vol. 16, no. 11, pp. 6903–6911, Nov. 2020.

[81] B. Silva, R. Dos Santos, and G. P. Hancke, "Towards non-line-of-sight ranging error mitigation in industrial wireless sensor networks," in *Proceedings of the 42nd Annual Conference of the IEEE Industrial Electronics Society (IECON)*, Florence, Italy, 2016, pp. 5687–5692.

[82] B. J. Silva and G. P. Hancke, "Non-line-of-sight identification without channel statistics," in *Proceedings of the 46th Annual Conference of the IEEE Industrial Electronics Society (IECON)*, Singapore, 2020, pp. 4489–4493.

[83] L. Zwirello, M. Janson, C. Ascher, U. Schwesinger, G. F. Trommer, and T. Zwick, "Localization in industrial halls via ultra-wideband signals," in *Proceedings of the 2010 7th Workshop on Positioning, Navigation and Communication*, Dresden, Germany, 2010, pp. 144–149.

[84] V. Savic, J. Ferrer-Coll, P. Ängskog, J. Chilo, P. Stenumgaard, and E. G. Larsson, "Measurement analysis and channel modeling for TOA-based ranging in tunnels," *IEEE Transactions on Wireless Communications*, vol. 14, no. 1, pp. 456–467, Jan. 2015.

[85] J. Ferrer Coll, J. Dolz Martin de Ojeda, P. Stenumgaard, S. Marzal Romeu, and J. Chilo, "Industrial indoor environment characterization - propagation models," in *Proceedings of the 10th International Symposium on Electromagnetic Compatibility*, York, UK, 2011, pp. 245–249.

[86] A. Abu-Mahfouz and G. P. Hancke, "Localised information fusion techniques for location discovery in wireless sensor networks," *International Journal of Sensor Networks*, vol. 26, no. 1, pp. 12–25, Jan. 2018.

[87] K. Pahlavan, P. Krishnamurthy, and Y. Geng, "Localization challenges for the emergence of the smart world," *IEEE Access*, vol. 3, pp. 3058–3067, 2015.

[88] B. J. Silva and G. P. Hancke, "Practical challenges of IR-UWB based ranging in harsh industrial environments," in *Proceedings of the 13th IEEE International Conference on Industrial Informatics (INDIN)*, Cambridge, UK, July 2015, pp. 618–623.

[89] D. Wu, D. Chatzigeorgiou, K. Youcef-Toumi, and R. Ben-Mansour, "Node localization in robotic sensor networks for pipeline inspection," *IEEE Transactions on Industrial Informatics*, vol. 12, no. 2, pp. 809–819, April 2016.

[90] A. R. Jiménez Ruiz and F. Seco Granja, "Comparing Ubisense, BeSpoon, and Decawave UWB location systems: indoor performance analysis," *IEEE Transactions on Instrumentation and Measurement*, vol. 66, no. 8, pp. 2106–2117, Aug. 2017.

[91] B. J. Silva and G. P. Hancke, "An approach to improve location accuracy in non-line-of-sight scenarios using floor plans," in *Proceedings of the 17th IEEE International Conference on Industrial Informatics (INDIN)*, Helsinki, Finland, July 2019, pp. 1715–1718.

[92] C. Thajudeen, A. Hoorfar, F. Ahmad, and T. Dogaru, "Measured complex permittivity of walls with different hydration levels and the effect on power estimation of TWRI target returns," *Progress In Electromagnetics Research B*, vol. 30, pp. 177–199, May 2011.

[93] A. Ledergerber and R. D'andrea, "Calibrating away inaccuracies in ultra wideband range measurements: A maximum likelihood approach," *IEEE Access*, vol. 6, pp. 78 719–78 730, 2018.

[94] S. Wu, S. Zhang, and D. Huang, "A TOA-based localization algorithm with simultaneous NLOS mitigation and synchronization error elimination," *IEEE Sensors Letters*, vol. 3, no. 3, pp. 1–4, Mar. 2019.

[95] N. Rajagopal, P. Lazik, N. Pereira, S. Chayapathy, B. Sinopoli, and A. Rowe, "Enhancing indoor smartphone location acquisition using floor plans," in *Proceedings of the 17th ACM/IEEE International Conference on Information Processing in Sensor Networks (IPSN)*, Porto, Portugal, April 2018, pp. 278–289.